PEOPLE'S DEMOCRATIC REPUBLIC OF ALGERIA
MINISTRY OF HIGHER EDUCATION AND SCIENTIFIC RESEARCH
UNIVERSITY OF ECHAHID HAMMA LAKHDAR - EL OUED

Faculty of Technology
Department of Electrical Engineering

Doctoral Thesis

Submitted by:

AHFOUDA Abdelkarim

In order to obtain the **LMD DOCTORATE** degree in:
Electrotechnics

Option: Electrical Machines

Entitled

Integration of Z-Source Converter in Active Harmonic Filtering

Defended on 12/12/2024, before the jury composed of:

Mr. Talal Guia	MCA	Univ. of El Oued	president
Mr. Youcef BEKAKRA	professor	Univ. of El Oued	supervisor
Mr. laid ZELLOUMA	professor	Univ. of El Oued	co-supervisor
Mr. Kamel SRAIRI	professor	Univ. of Biskra	examiner
Mr. Mohamed Toufik BENCHOUIA	professor	Univ. of Biskra	examiner
Mr. Ali KHECHEKHOUCHE	MCA	Univ. of El Oued	examiner

University year 2023/2024

Thesis prepared in the Laboratory for the Exploitation and Development of Saharan Energy Resources

REPUBLIQUE ALGERIENNE DEMOCRATIQUE ET POPULAIRE
MINIISTERE DE L'ENSEIGNEMENT SUPERIEUR ET DE LA RECHERCHE SCIENTIFIQUE
UNIVERSITE ECHAHID HAMMA LAKHDAR - EL OUED

Faculté de Technologie
Département de Génie Electrique

Thèse de Doctorat

Présentée par :

AHFOUDA Abdelkarim

En vue de l'obtention du diplôme de DOCTORAT LMD en :

Electrotechnique

Option: Machines Electriques

Intitulé

Intégration des convertisseurs Z-source dans les filtres actifs des harmoniques

Soutenue le 12/ 12/ 2024, devant le jury composé:

Mr. Talal Guia	MCA	Université d'El Oued	Président
Mr. Youcef BEKAKRA	Professeur	Université d'El Oued	Rapporteur
Mr. laid ZELLOUMA	Professeur	Université d'El Oued	Co-Rapporteur
Mr. Kamel SRAIRI	Professeur	Université de Biskra	Examinateur
Mr. Mohamed Toufik BENCHOUIA	Professeur	Université de Biskra	Examinateur
Mr. Ali KHECHEKHOUCHE	MCA	Université d'El Oued	Examinateur

Année Universitaire 2023/2024

Mémoire préparé au sein du Laboratoire d'Exploitation et de Valorisation des Ressources Energétiques Sahariennes

ACKNOWLEDGMENT

First and foremost, I extend my sincere gratitude to my Merciful **GOD**, whose unwavering support, patience, and strength enabled me to successfully complete this thesis.

I am deeply thankful to my academic advisors, **Prof. Youcef BEKAKRA** and **Prof. Laid ZELLOUMA**, for their invaluable guidance and enlightening ideas throughout the course of my research.

I would like to express my appreciation to **Prof. Ahmed IBRAHIM**, **Dr. Djaafar TOUMI**, **Dr. Bouzid MENSOURI**, and **Dr. Ouahid BOUAKAZ** for their assistance during the implementation of the experimental setup.

I am grateful to the members of the examination committee: **Prof. [Name], Prof. [Name], and Dr. [Name]**, for their constructive criticism, recommendations, and for making my defense an enriching experience.

Special thanks are extended to the Power Electronics Group in the Department of Electrical and Computer Engineering for their collaborative efforts in overcoming various challenges during the research.

I also wish to acknowledge my parents, siblings, and my dear wife for their unwavering love, encouragement, and support throughout this journey, especially during both the highs and lows.

Contents

List of Tables

List of Figures

GENERAL INTRODUCTION

In an ideal three-phase system, voltage and current are waves of constant frequency and amplitude. On the other hand, the phase current generated by a nonlinear load connected to an ideal three-phase power network through a transmission network is not sinusoidal, but consists of a superposition of several harmonics and inter-harmonics. By definition, harmonics are a periodic sinusoidal component and its frequency is an integer multiple of the fundamental frequency, while harmonics refer to any signal element whose frequency is not a multiple of the fundamental frequency. Distorted current causes distribution system voltage distortion [1].

There are many non-linear elements that cause power distortion such as power converters, electronic consumables, electric arc furnaces and discharge lamps, etc. In addition, transformers and motors can also cause power distortion, because they are not characteristically ideal. Although nonlinear loads have been around for decades, not only high power industrial equipment but also low power electrical equipment. Although low-power applications do not cause noticeable distortion, such as the electric arc furnace, multiple low-power devices operating simultaneously can cause quite serious problems [2].

Distorted voltages and currents have a number of harmful effects, such as creating resonances between the inductor and capacitance in the supply network, and overcurrent and overvoltage in motors and generators. In transformers, the distorted current cause’s mechanical and thermal vibrations, which lead to thermal and mechanical effects that degrade the insulation. Distortion also reduces the accuracy of various measuring instruments and degrades the operating characteristics of power system protection. In addition, communication systems and electronic consumers may be disrupted or damaged [3].

Passive filters are commonly used to reduce distortion from harmonic currents in industrial power systems, but their performance depends on the system impedance and the harmonic currents of nonlinear loads, making them ineffective in some situations in certain conditions. and create opportunities for harmonic propagation in the power system [4].

To overcome these disadvantages, positive energy filters have been introduced. They introduce harmonic voltage or current of appropriate amplitude and phase angle into the system and compensate for the harmonics of non-linear loads [5].

Many configurations of active filters have been introduced in the literature. The filters that best meet today's industry constraints are parallel-operated filters, series-series filters, or series-parallel combinations. In the case of non-linear source current, a parallel filter is the best solution to reduce low and medium power noise. Active filtering is most beneficial when fast response is required under dynamic loads. On the other hand, it is important to note that the performance of active filters is deeply linked to the algorithm for detecting harmonic references as well as the method used to track these references [5][6].

The first chapter is dedicated to the presentation of disturbances in the power supply networks in current and voltage in connection with non-linear loads, as well as the origin of these disturbances and their consequences in electrical systems. Then the techniques and methods for decontamination of electrical networks are presented.

The second chapter is dedicated to the study of the three-phase parallel active filter, we will show the different constituent elements of the filter, the different control circuits of the DC bus voltage and the monitoring circuit of the reference harmonic currents.

In the third chapter, we present the most widely used strategies for detecting harmonic currents, such as: the instantaneous active and reactive power method, the synchronous reference method, notch filter method and the filter-based method Multivariable. Detailed analytical study of each of these methods is presented to evaluate the performance of each algorithm.

The fourth chapter will be devoted to the study and controlňof a two-level and multi-level Z source inverter.

Finally, in chapter five, we integrate Z-source inverter into active harmonic filters

Chapter I :

General information on electrical network disturbances

I.1 Introduction

Electric power systems and grids represent intricate and dynamic networks. They are susceptible to unexpected or sudden fluctuations in currents and voltages, primarily caused by a variety of linear and non-linear loads. Additionally, various types of grid disturbances, including accidents, can further exacerbate these fluctuations [7]. The widespread adoption of power semiconductors in industrial and domestic applications has led to the contamination of electric grids with harmonic currents and voltages. These harmonics adversely affect the normal operation of most grid-connected devices, resulting in significant economic losses. Numerous classic and modern solutions have been proposed in the literature to address harmonic problems. This chapter will explore the harmonic issue as one of the most common power quality concerns. Subsequently, various modern and traditional solutions will be discussed.

I.2 Power Systems Distortion and Problems

Within power systems, various voltage and current challenges may arise. The primary voltage issues encompass short-duration variations, voltage interruptions, frequency fluctuations, voltage dips, and harmonics. Harmonics, in particular, constitute the predominant concern regarding power system currents.

I.2.1 Voltage Variation for Short Duration

Short-duration voltage variations occur due to malfunctions in certain systems or simultaneous starting of numerous electrical loads. These anomalies can lead to fluctuations in voltage amplitude, including increases or decreases, or even complete voltage cancellation within a brief timeframe [7]. An increase in voltage is characterized by a deviation ranging from 10% to 90% of the nominal voltage, as specified in the IEEE 1159-1995 standard. This deviation can persist from half a cycle to one minute. Similarly, as per the same reference, voltage increase is defined when the voltage amplitude reaches approximately 110% to 180% of its nominal value.

I.2.2 Voltage Interruption

Voltage cut-off occurs when the voltage of the load drops to less than 10% of its nominal value for a brief period lasting less than one minute. Voltage interruption may result from faults within the electrical system, malfunctions in connected equipment, or inadequate control systems. The primary defining feature of voltage interruption is the duration over which it occurs.

I.2.3 Frequency Variations

Under normal circumstances, the frequency of the distribution grid should fall within the range of 50±1 Hz. Frequency variations in the grid may manifest for customers utilizing auxiliary electric sources such as solar systems or thermal stations. These deviations are infrequent and typically occur under exceptional conditions, such as turbine malfunctions.

I.2.4 Unbalance in Three Phase Systems

When the currents and voltages in a three-phase system do not possess identical amplitudes or when the phase angle between any two phases deviates from 120°, the system is considered unbalanced. Ideally, a three-phase system should be balanced with equal loads across all phases. However, in reality, loads vary, and distribution grid issues may further complicate matters.

I.2.5 Voltage Dips (Sags)

Voltage dips manifest as periodic disturbances, arising naturally from transistor switching and the start-up of large loads such as motors, elevators, lighting systems, heaters, and the like. These occurrences can adversely affect the operation of protection equipment.

I.2.6 Harmonics

Power systems are engineered to operate at standard frequencies of either 50 or 60 Hz. Nevertheless, certain types of loads generate currents and voltages with frequencies that are integer multiples of the fundamental frequency, resulting in harmonic distortion—a form of electrical pollution. Harmonic distortion manifests as additional frequency components in the waveform. In power systems, two main types of harmonics are encountered [8]:

Synchronous harmonics: These harmonics comprise sinusoidal waveforms with frequencies that are integer multiples of the fundamental frequency. The multiplication factor is commonly referred to as the harmonic number. Synchronous harmonics can be further categorized into:

- ✓ Sub-harmonics: Occur when the harmonic frequency is less than the fundamental frequency.
- ✓ Super harmonics: Occur when the harmonic frequency exceeds the fundamental frequency.

Harmonics, akin to overtones in music, refer to integer multiples of an instrument's fundamental or natural frequency, generated by a succession of standing waves of increasing order. Similarly, in power circuits, nonlinear loads produce harmonic currents that are integer multiples of the supply's fundamental frequency. The proliferation of solid-state power electronics has significantly augmented both the quantity and magnitude of these loads. The notion of harmonics was introduced in the early 19th century by Joseph Fourier, who demonstrated that all periodic non-sinusoidal signals can be expressed as an infinite sum or series of sinusoids with discontinuous frequencies, as indicated by Equation (I-1).

$$i(t) = I_0 + \sum_{h=-\infty}^{a} I_h \cos(h\omega t + \varphi_h) \tag{I-1}$$

The component I_0 within the Fourier series represents the direct component, while the initial term of the summation with index h=1 corresponds to the fundamental frequency of the signal. The remaining components of the series are referred to as harmonics within the h range. Illustrated in Figure is the waveform containing the third harmonic (h=3). Within the three-phase electrical grid, the primary harmonic components consist of harmonics within the ranges of (6*h±1) [9].

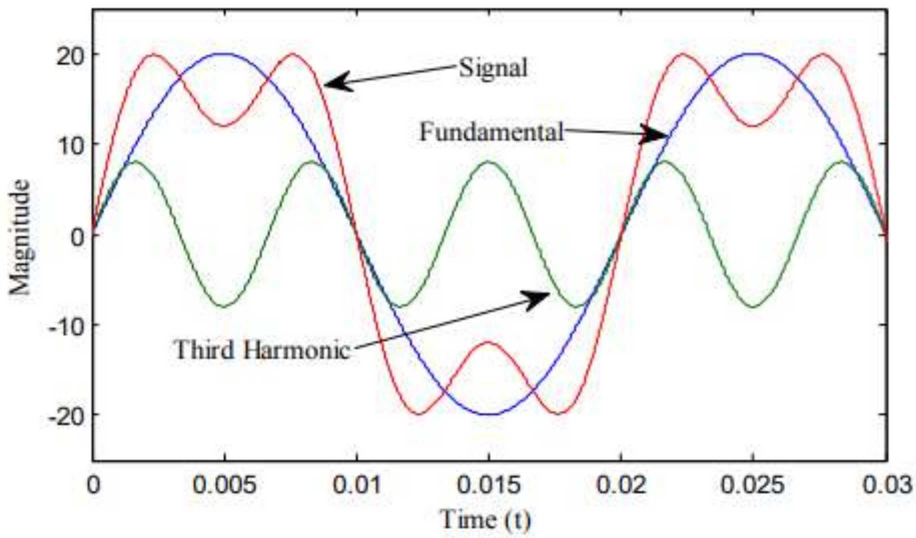

Figure I.1 Harmonic content of a signal and its fundamental.

The exciting current of transformers, arc furnaces, rectifiers, and various other loads can introduce harmonics into utility lines. To regulate the impact of these harmonics, most utilities adhere to the permissible harmonic current levels outlined in the IEEE 519 standard.

I.2.6.1 Total Harmonic Distortion (THD)

The total harmonic distortion (THD) of a signal quantifies the harmonic distortion within current or voltage. It is computed as the ratio of the sum of the powers of all harmonic components to the power of the fundamental frequency. Harmonic distortion arises from the inclusion of waveforms at frequencies that are multiples of the fundamental frequency.

$$THD(\%) = \frac{\sqrt{\sum_{i=2}^{a} x_i^2}}{|x_1|} \tag{I-2}$$

The Total Harmonic Distortion (THD) serves as a valuable metric in numerous applications and stands as the most widely utilized harmonic index. Nonetheless, it possesses a limitation in that it does not effectively indicate the voltage stress on a capacitor, as this is associated with the peak value of the voltage waveform [10].

I.2.6.2 Distortion Factor

The distortion factor F_d is expressed as the ratio of the RMS value of the fundamental to that of the signal. It is mathematically defined as:

$$F_d = \frac{I_{L1}}{I_{rms}} \tag{I-3}$$

When the current is purely sinusoidal, the distortion factor is equal to unity, but it diminishes as distortion becomes evident.

I.2.6.3 Crest Factor

The crest factor of a signal, denoted as Fc, is specified by Equation (I-4):

$$F_c = \frac{crest\ value}{effective\ value} \tag{I-4}$$

In sinusoidal waves, the crest factor equals 1.41. However, it can reach a value of 5 in instances of highly distorted waves

I.2.6.4 Effects of Harmonics

Harmonic currents entering the utility feeder can lead to various issues. These currents might become trapped by power factor correction capacitors, causing overloads or triggering resonant over-voltages. Furthermore, they have the potential to distort the feeder voltage sufficiently to disrupt the operation of computers, telephone lines, motors, and power supplies, and in severe cases, even result in transformer failures due to eddy current losses. To address this, harmonic currents can be mitigated by installing series LC filters tuned to the offending frequencies. These filters should be designed to exhibit low impedance at the resonant frequency compared to the source impedance at that frequency. However, there's a caveat. If a filter is installed with a series resonance at the 7th harmonic, it will also create a parallel resonance with the utility at a lower frequency when the source inductance is combined with the filter inductance. Should this parallel resonance coincide with or closely align with the 5th harmonic, it could lead to the previously described resonant over-currents. Additionally, the installation of series resonant traps inevitably introduces parallel resonances at frequencies below the trap frequencies. To mitigate these risks, it is recommended to install multiple resonant traps, starting with the lowest harmonic frequency of concern and then proceeding sequentially to higher-frequency harmonics. If these traps are switched, they should be activated in sequence, beginning with the lowest frequency trap, and deactivated in sequence, commencing with the highest frequency trap [11].

The threshold for voltage or current distortion is dictated by the susceptibility of loads (including power sources), which are impacted by the distorted parameters. Among various types of equipment, heating appliances exhibit the lowest sensitivity. Conversely, the most sensitive equipment comprises electronic devices designed under the assumption of nearly ideal sinusoidal fundamental frequency voltage or current waveforms. Electric motors represent a common load type positioned between these two extremes.

I.2.6.5 Power Factor

Power factor refers to the ratio of real power to volt-amperes and represents the cosine of the phase angle between voltage and current in an AC circuit. These parameters are precisely defined in systems characterized by sinusoidal voltages and currents. Improving power factor entails the addition of capacitors to the power line, which draw a leading current and supply lagging *VArs* to the system. Power factor correction capacitors can be toggled as required to uphold *VAr* and voltage control [11].

In the case of a sinusoidal signal, the power factor is determined by the quotient of active power divided by apparent power. Typically, parameters for electrical equipment are provided based on nominal voltage and current. A low power factor may suggest inefficient utilization of these devices. Apparent power can be defined as:

$$S = V_{rms}.I_{rms} = V_{rms}.\sqrt{\frac{1}{T}\int_0^T i_L^2 dt} \quad \text{(I-5)}$$

The active power P can be given by the relation:

$$P = V_{rms}.I_{L1}.\cos(\alpha 1) \quad \text{(I-6)}$$

The reactive power Q is defined by:

$$Q = V_{rms}.I_{L1}.\sin(\alpha 1) \quad \text{(I-7)}$$

The power factor in this case can be given by Eqn.(I-8).

$$P.F = \frac{P}{S} = \frac{P}{\sqrt{P^2 + Q^2}} \quad \text{(I-8)}$$

In the case where there is harmonics, a supplementary power called the distorted power D appears. This power can be given by the relation (I-9).

$$D = V_{rms} \cdot \sqrt{\sum_{n=2}^{\alpha} I_{Ln}^2} \quad \text{(I-9)}$$

The apparent power can then be expressed as:

$$S = \sqrt{P^2 + Q^2 + D^2} \quad \text{(I-10)}$$

From eqn. (I-10), we can notice that the power factor decreases because of the existence of harmonics in addition to the reactive power consumption [12]. The Fresnel diagram of the power is given in Figure I.2.

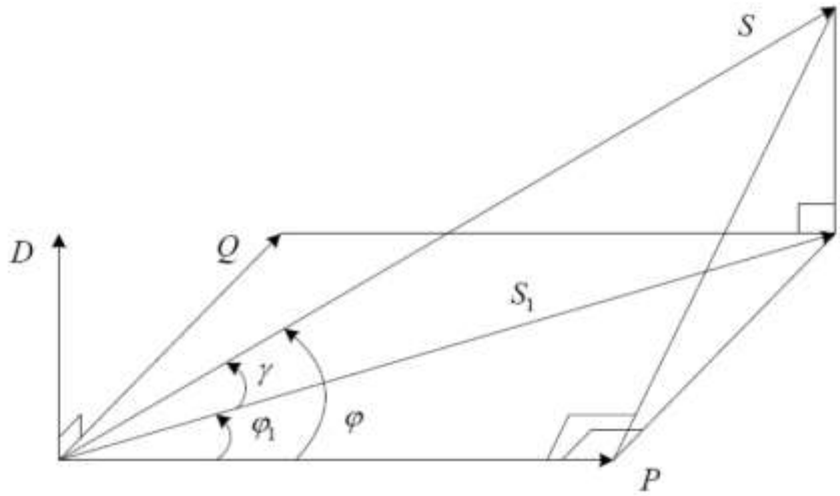

Figure I.2 Fresnel representation of the power [13].

φ: *The phase between active power P and apparent power S.*
$\varphi 1$: *The phase between active power P and apparent power S1.*
γ: *The phase between apparent power in a linear system and that in a non-linear system.*

I.3 Harmonic Currents Sources

The primary source of harmonics arises from the introduction of harmonic currents by non-linear loads. Among these loads, diode bridges stand out as prominent contributors in power applications due to their inherent non-linear characteristics, which do not require control and offer longevity at a low cost [9]. Additionally, numerous other loads contribute to harmonic generation, including [10][14]:

- ✓ Industrial equipments (welding machines, arc furnaces, induction furnaces, rectifiers).
- ✓ Offices equipments (computers, photocopiers,…etc.).
- ✓ Domestic devices (TVs, micro-wave furnaces, neon lightening,…etc.).
- ✓ Power inverters.
- ✓ Power transformers when working in the saturation zone also are considered as non-linear loads that produce harmonics.

The operation of non-linear loads results in the generation of harmonic currents, which subsequently propagate throughout the electrical grid. As these harmonic currents traverse the feeding impedances, such as transformers and the grid itself, they induce harmonic voltages within these feeders. It's important to note that the impedance of conductors increases with the frequencies of the currents they carry, resulting in different impedances for each range of current harmonics. Consequently, harmonic currents within a specific range, denoted as h, engender harmonic voltages across the impedance. Consequently, all loads connected to the same point will experience the same perturbed voltage [14]. The per-phase equivalent circuit of a non-linear load connected to the grid is illustrated in Figure I.3.

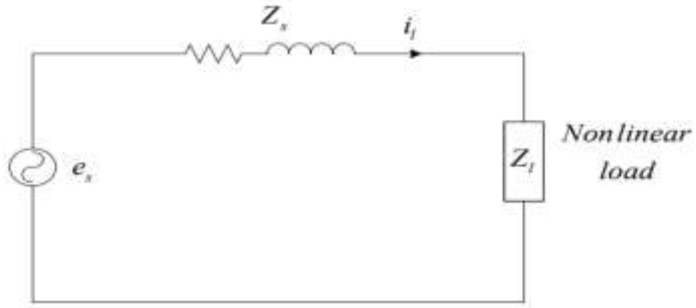

Figure I.3 Equivalent circuit per phase of a non-linear load connected to the grid [12].

The spread of harmonic currents from different loads can be represented as in Figure I.4.

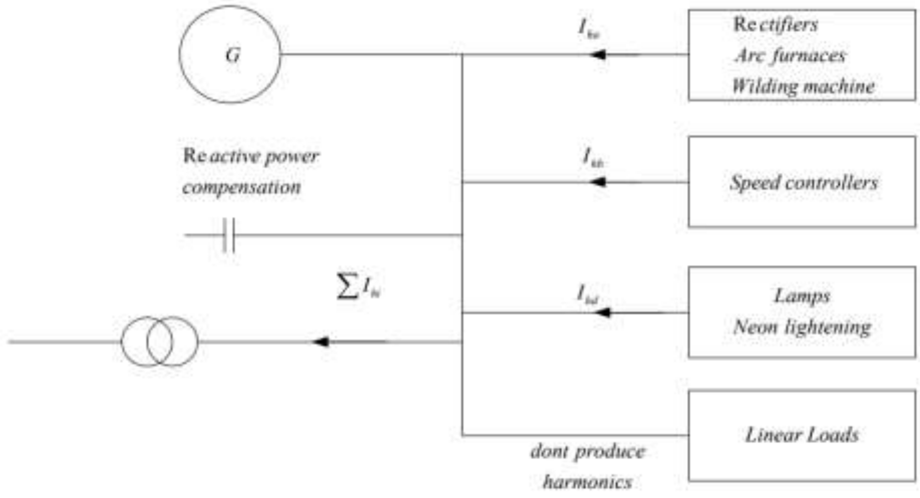

Figure I.4 Spread of harmonic currents into the grid [14].

I.4 Economic effects of harmonics

- ✓ Premature aging of materials which forces its replacement, in addition to an initial over sizing of these materials.
- ✓ The overloading of the grid which implies to increase the nominal power and to oversize the installations, causing more and more losses.
- ✓ The current distortions cause sudden triggers and the stop of production equipments.

The expenditure incurred due to material costs, energy consumption, and production inefficiencies significantly impairs the competitive edge and operational efficiency of manufacturing facilities and corporations.

I.5 Solutions for the Harmonics

Addressing the filtration of grid currents and voltage presents a fundamental challenge for both distributors and consumers alike. This is primarily due to the disparate application of harmonic emission regulations across various countries, prompting manufacturers of electrical devices to engineer products that comply with international standards' conditions and thresholds. In response, electric utility companies employ diverse filtering equipment and actively support research endeavors aimed at identifying novel, efficient solutions to power quality issues. Additionally, consumers sometimes opt to install reactive power and harmonic compensation units to enhance power factor and mitigate energy consumption costs.

A plethora of traditional and contemporary approaches for harmonics mitigation and power quality enhancement have been proposed in academic literature. While some focus on load optimization to minimize harmonic emissions, others advocate for the adoption of external filtering devices to curtail the propagation of harmonics within the grid [15].

I.5.1 In-Line Reactors

The implementation of an in-line reactor or choke represents a straightforward remedy for managing harmonic distortion arising from adjustable speed drives. This solution entails the integration of a relatively modest reactor or choke at the drive's input. The induction offered by this component impedes rapid capacitor charging, compelling the drive to draw current over an extended duration. Consequently, this mitigates current magnitude with considerably reduced harmonic content, all while maintaining consistent energy delivery [16].

I.5.2 Transformers with Passive Coupling

Certain configurations of triangle zigzag coupling in transformers enable the suppression of third-order harmonics and their multiples. However, the trade-off for employing these coupling schemes is an increase in source impedance, consequently leading to heightened voltage harmonic distortion [9][16].

I.5.3 Passive Filters [9]

The most commonly utilized method for harmonic reduction is the passive filter, known for its relatively lower cost compared to alternative techniques. This approach involves tuning inductors, capacitors, and the load resistance to regulate harmonics. However, passive filters can introduce complications to power systems. Essentially, they are engineered to divert harmonics away from lines or obstruct their passage through specific system components by aligning elements to resonate at targeted frequencies. These filters are pre-set and fine-tuned based on the impedance of their connection points, rendering them unable to instantly adapt to load variations. Consequently, alterations in load impedance can unexpectedly modify their cutoff frequency, potentially leading to resonance with other system elements.

I.5.3.1 Resonant Filter

The resonant passive filter illustrated in Figure I.5 comprises an inductor connected in series with a capacitor, the values of which are determined based on the targeted harmonic frequencies for elimination. This filter is characterized by low impedance at the specified harmonics and sufficient impedance at the fundamental frequency. Consequently, a separate filter is required for each harmonic range slated for elimination [12]. The equivalent circuit of this resonant filter, incorporating the harmonic source and grid impedance, is depicted in Figure I.6.

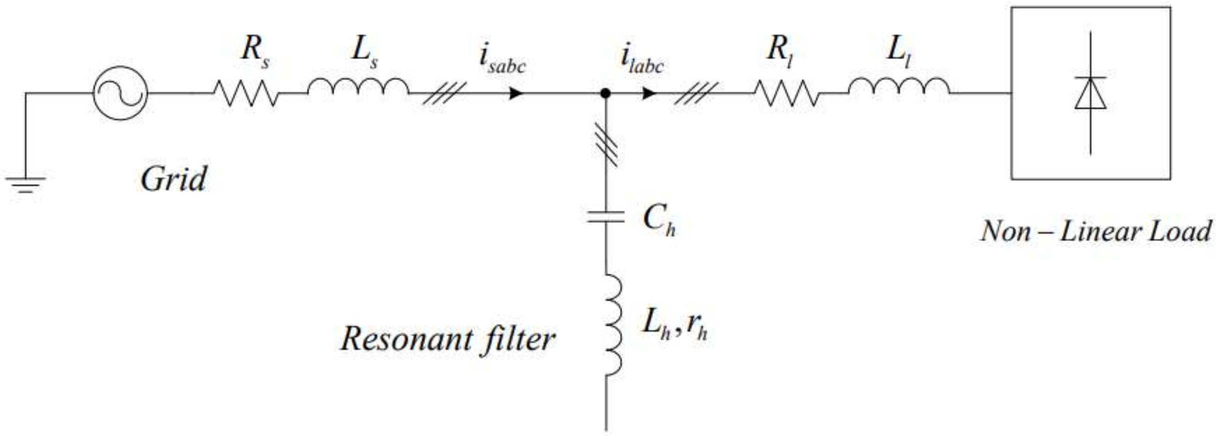

Figure I.5 Resonant filter in parallel with non-linear load [12].

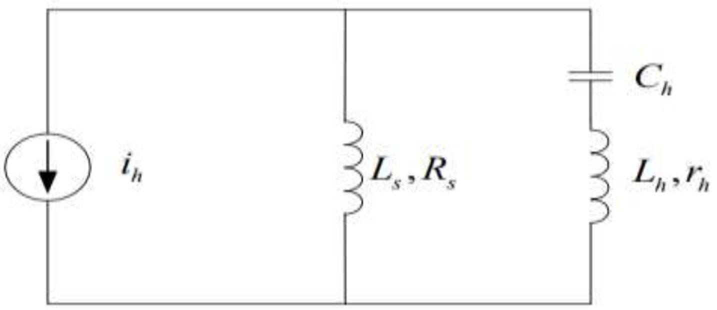

Figure I.6 Harmonic equivalent circuit of passive filter with the grid impedance [12][17].

I.5.3.2 Amortized Filter or High Pass Filter of Second Order

The second-order high-pass filter depicted in Figure I.7 is composed of passive elements RLC. This filter is designed to attenuate harmonics across a broad frequency spectrum. Typically, it is employed for the suppression of high-order harmonics that are significantly distant from the system's fundamental frequency.

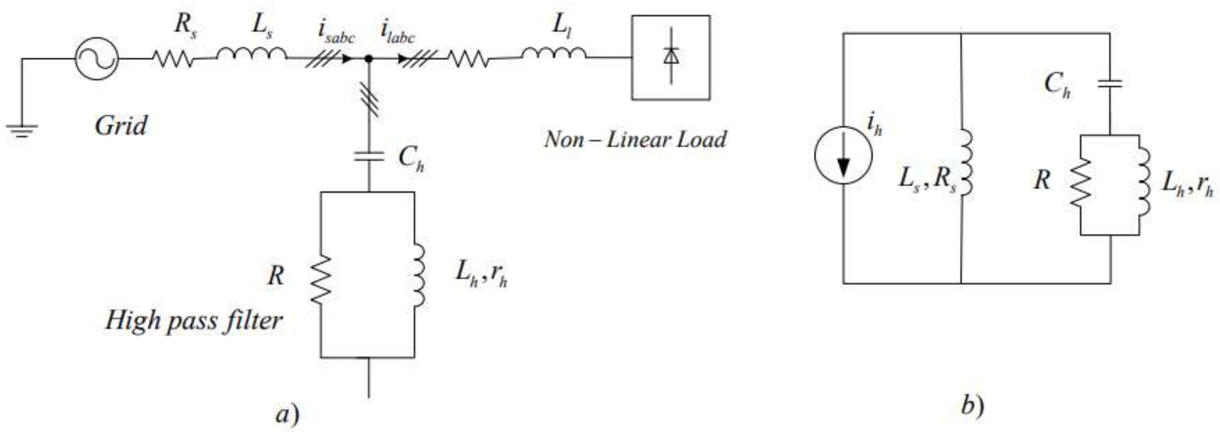

Figure I.7 a) Diagram of the high pass filter. b) Equivalent circuit of the HPF.

I.5.3.3 Resonant Amortized Filter

These filter assemblies consist of resonant filters tailored to specific harmonic frequencies, linked in parallel with a high-pass filter to target the higher harmonics. The configuration of connecting resonant filters for the 5^{th} and 7^{th} harmonics with a high-pass filter is illustrated in Figure I.8.

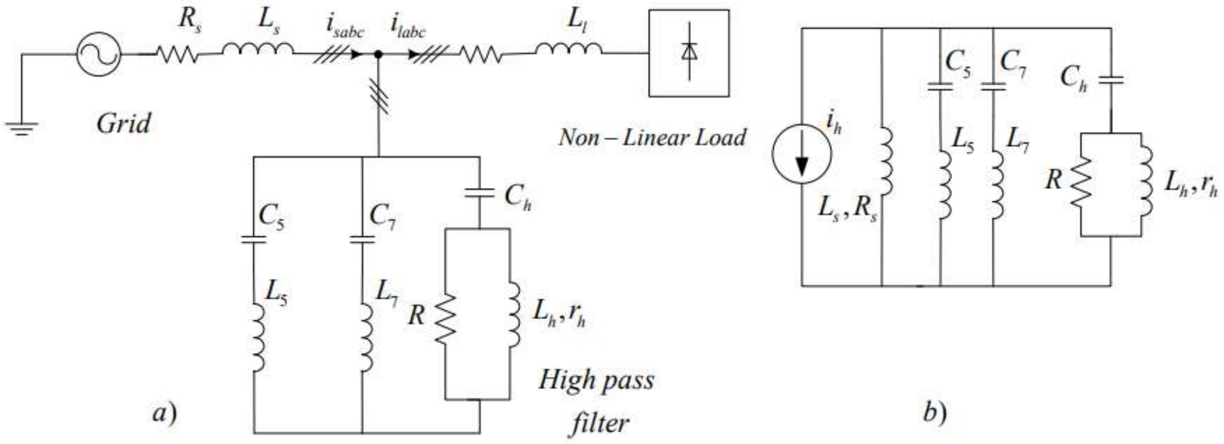

Figure I.8 a) Diagram of the connection of amortized resonant filters. b) Equivalent circuit diagram. [17]

Conventional methods commonly employed for mitigating harmonics and correcting power factor typically involve the integration of passive filters connected in parallel to intercept harmonic currents. These filters typically consist of either second-order resonant filters or amortized high-pass filters. While these solutions are straightforward and commonly implemented, they are also associated with significant drawbacks [12]:

- ✓ Designing a filter necessitates a basic understanding of the electric grid's configuration.
- ✓ The sizing of the filter relies on both the harmonic spectrum and the impedance of the grid.
- ✓ Voltage harmonics can result in the generation of certain current harmonics by passive filters, which are then injected into the grid.
- ✓ Changes in the source frequency impact the compensation characteristics of passive filters. In power systems, we typically account for significant frequency variations, often around 0.5 Hz.
- ✓ Any alterations to the grid, such as restructuring or the addition of new clients, can influence the compatibility of the passive filter. Therefore, any changes made to the grid must be accompanied by corresponding adjustments to the passive filter.
- ✓ There exists a potential for resonance to occur between the grid and the passive filters at particular frequencies. To address this issue, the quality factor of the filter is decreased, resulting in increased consumption of active power.
- ✓ These circuits exhibit capacitance at the fundamental frequency and are regarded as sources of reactive power.

These challenges render the application of passive filters problematic and ineffective in numerous scenarios. Given the dynamic nature of grid parameters and the variability of harmonic spectra, constructing passive filters tailored solely to specified harmonics proves insufficient for eliminating grid harmonics.

I.6 Modern Solutions for Harmonics Problems

Novel approaches have been suggested as effective remedies for eradicating electric grid harmonics, aiming to overcome the drawbacks associated with traditional methods such as passive filters [1]. Among these solutions, two predominant categories have emerged as the most commonly utilized:

- ✓ Active filters, whether implemented in series, parallel, or a combination of both within a Unified Power Quality Conditioner (UPQC).
- ✓ Hybrid filters, incorporating both active and passive filter elements simultaneously.

I.6.1 Active Power Filters

The primary role of active power filters (APFs) is to produce harmonic currents or voltages in such a way that the grid current or voltage maintains a sinusoidal waveform. These APFs can be connected to the grid either in series (Series APF) or in shunt (SAPF) to compensate for voltage or current harmonics, respectively. Alternatively, they can be combined with passive filters to form hybrid filters (HAPF).
Active filters represent a relatively recent advancement in harmonic elimination technology. Operating on power electronic principles, they typically come at a higher cost compared to passive filters. However, they offer significant advantages, notably; they do not resonate with the power system and operate independently of system impedance characteristics. This independence makes them suitable for challenging scenarios where passive filters fail due to resonance issues and where they do not interfere with other elements within the power system [16].

Active filters offer numerous advantages over traditional methods for harmonic compensation, including [9]:

- ✓ Flexibility to adjust to load variations.
- ✓ Capability for selective compensation of harmonics.
- ✓ Capacity limitations in power compensation.
- ✓ Potential for compensating reactive power.

I.6.1.1 Series Active Power Filter (series APF)

The objective of the series Active Power Filter (APF) is to alter the impedance of the grid at a local level. Functioning as a harmonic voltage source, it counteracts voltage disturbances originating from the grid or those induced by the flow of harmonic currents through the grid impedance. Nevertheless, series APFs are incapable of compensating for the harmonic currents generated by the loads themselves.

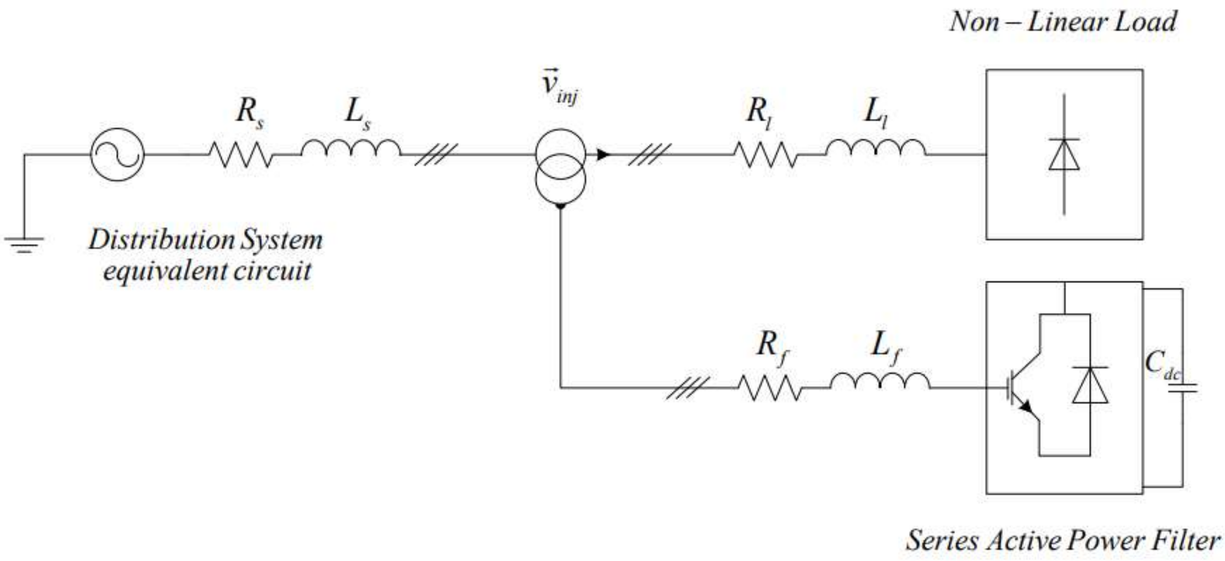

Figure I.9 Series active power filter connected to the grid [1].

I.6.1.2 Shunt Active Power Filter (SAPF)

Shunt Active Power Filters (SAPFs) are linked in parallel with the loads generating harmonics. Their role is to promptly inject harmonic currents, thereby offsetting those absorbed by the non-linear loads. This action aims to restore the grid current to a sinusoidal waveform.

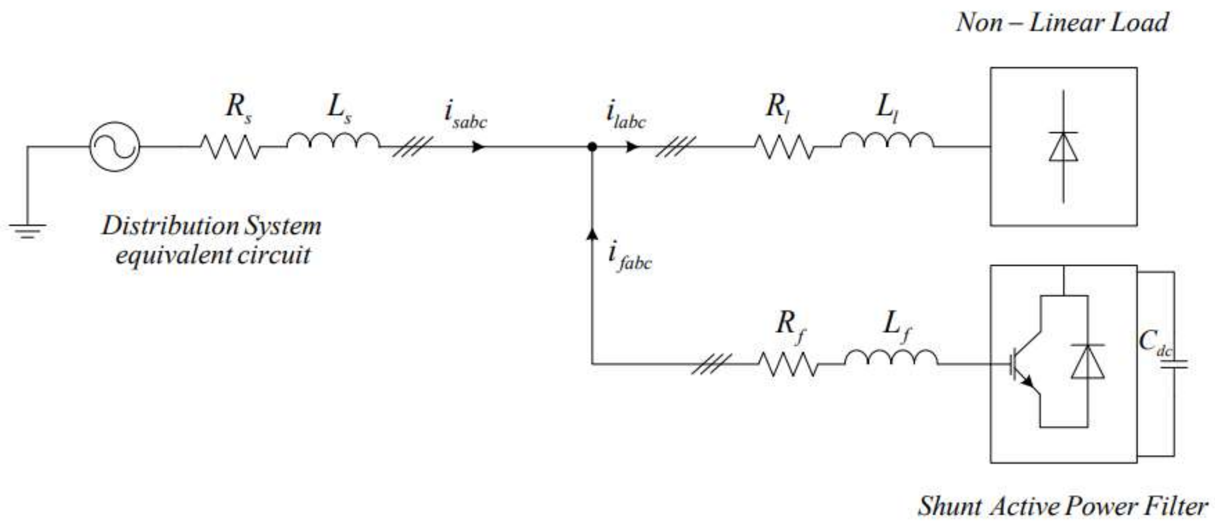

Figure I.10 Shunt APF connected in parallel with non-linear load [1].

I.6.1.3 Combination of Parallel and Series APF (UPQC)

Figure I.11 illustrates the integration of two Active Power Filters (APFs) in parallel and series configurations, also known as a Unified Power Quality Conditioner (UPQC). This arrangement amalgamates the benefits of both series and parallel APF types, enabling the concurrent attainment of sinusoidal source current and voltage [1].

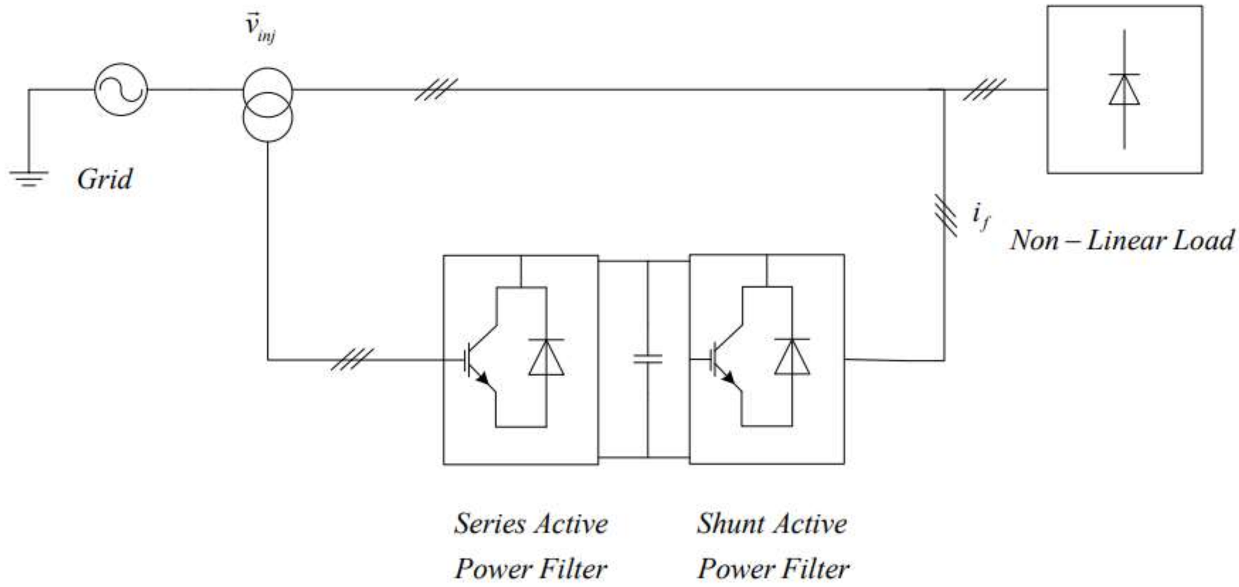

Figure I.11 Unified Power Quality Conditioner's Diagram [1].

I.6.2 Hybrid Filters

The hybrid filter represents a filter topology that combines the advantages of both passive and active filters. Due to this integration, it is regarded as the optimal solution for mitigating harmonic currents within the grid. The primary catalyst for the adoption of hybrid filters is the advancement in power semiconductor technology, exemplified by devices like MOSFETs and IGBTs. Moreover, from an economic standpoint, hybrid power filters offer the advantage of reducing the cost associated with Active Power Filters (APFs) [18].

Hybrid power filters can be categorized based on several factors, including the number of elements employed in the topology, the type of system being treated (such as single-phase, three-phase three-leg, or four-leg systems), and the type of inverter utilized (whether it is a current source inverter or a voltage source inverter) [1].

I.6.2.1 Series Association of Active Filter with Passive Filter

In this configuration, the active filter is linked in parallel with the passive filter, with both connected in shunt with the load, as illustrated in Figure I.12. The passive filters address specific harmonic bands, while the active filter compensates for the remaining grid harmonics.

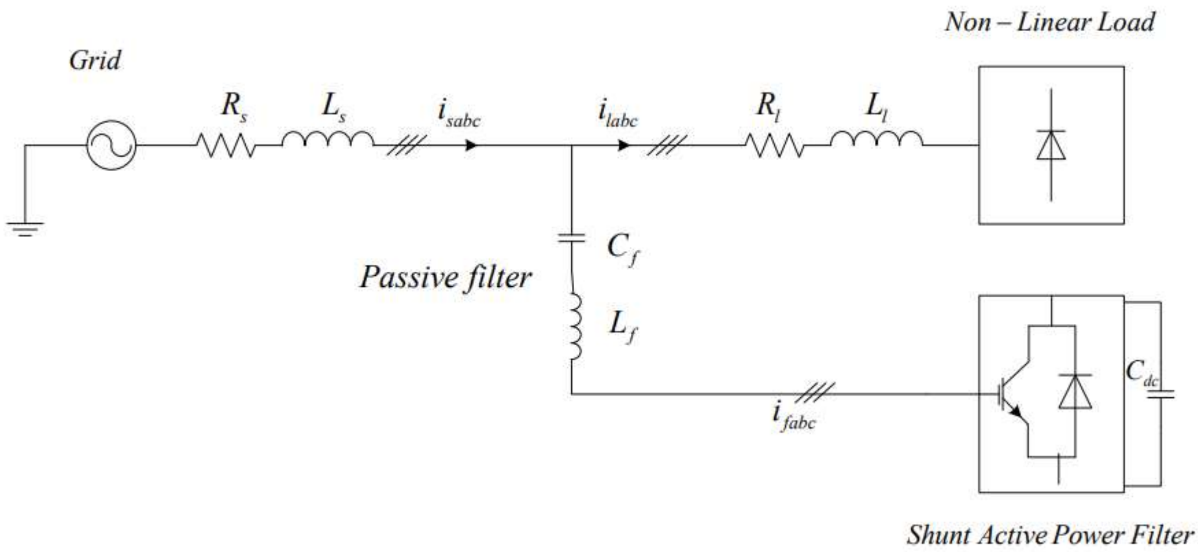

Figure I.12 Series association of SAPF and passive filter [12].

I.6.2.2 Parallel Association of SAPF with Passive Filters

In this topology, the active filter is connected in parallel with the passive filter. Both of them are shunted with the load as shown in Figure I.13. The passive filters compensate certain harmonic ranges, while the active filter compensates the rest of the grid harmonics.

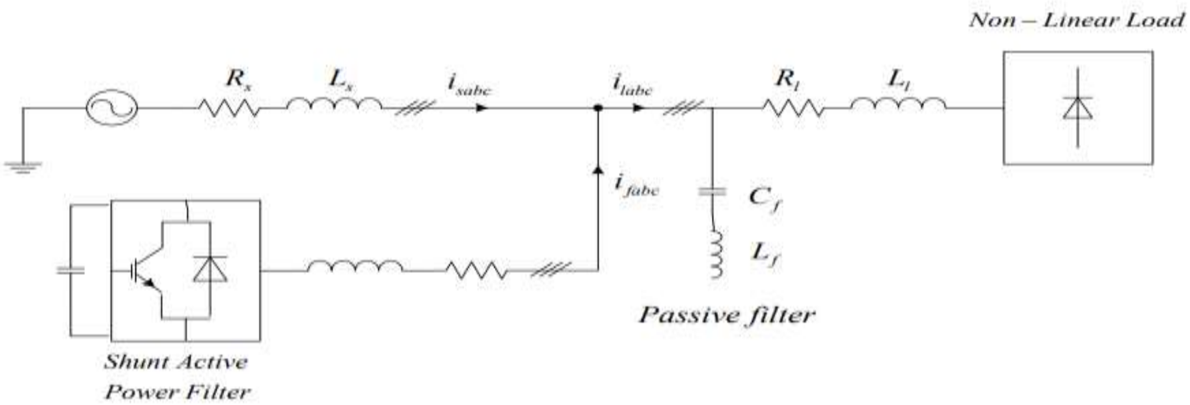

Figure I.13 Parallel association of SAPF and passive filters [12].

I.6.2.3 Series Active Filter with Passive Filter

The arrangement depicted in Figure I.13 mitigates the potential for anti-resonance between the components of the passive filter and the grid impedance. Here, the series active filter acts as a resistance against harmonic currents, directing them towards the passive filter while preserving the integrity of the fundamental frequency [1].

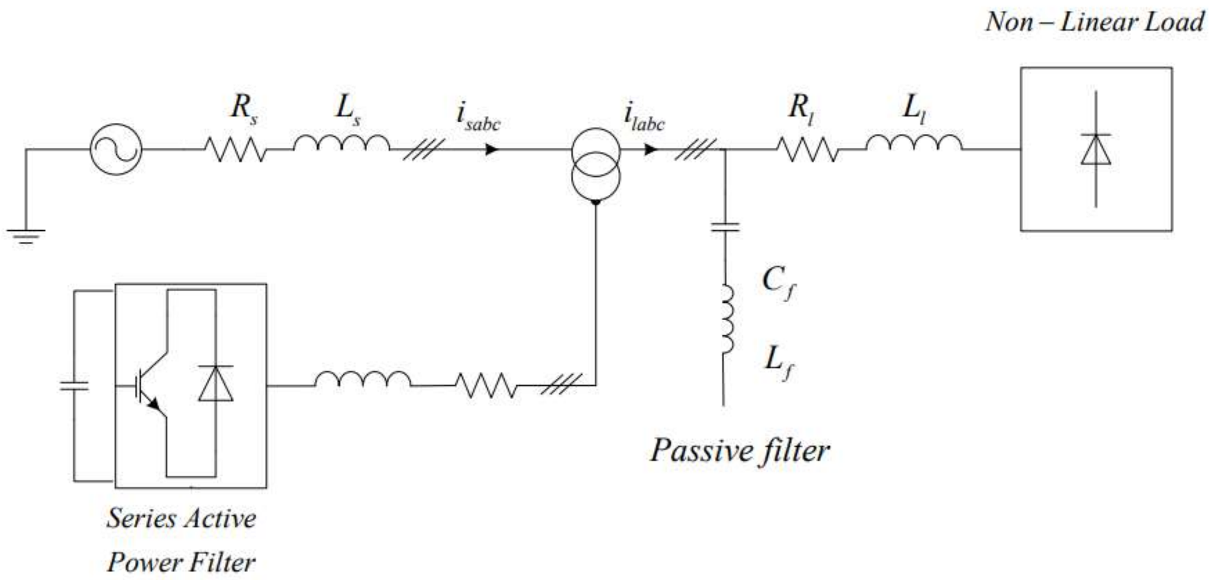

Figure I.14 : Series active power filter with passive filter [1].

I.7 Non-Linear Loads

When the current drawn by electrical equipment diverges from the voltage applied across it, the equipment is deemed to exhibit a nonlinear relationship between input voltage and current [12] [14] . Any equipment incorporating rectification falls into the category of nonlinear loads. These loads produce voltage and current harmonics, which can detrimentally affect equipment designed for linear operation. Transformers responsible for supplying power to industrial settings experience increased heat losses when connected to harmonic-generating sources (nonlinear loads).

I.7.1 Modeling of the Non-Linear Load (Diode Bridge with Inductive Load)

The non-linear load consists of a three-phase bridge rectifier linked to the grid via a line inductor $(L_l,\ R_l)$, supplying power to an inductive load $(R_{dc},\ L_{dc})$, depicted in Figure I.15.

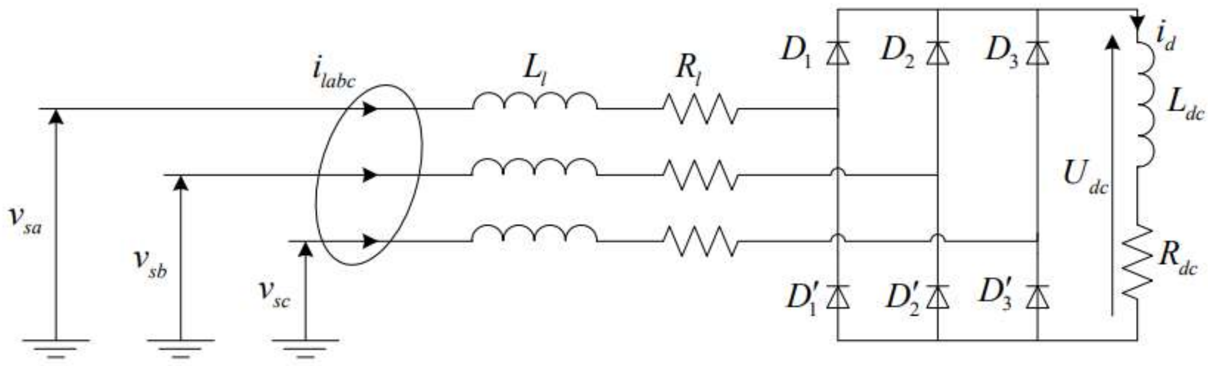

Figure I.15 Diode bridge rectifier with RL load.

To simplify matters, we assume the rectifier to be ideal. Two diodes on the same leg of the rectifier cannot be in the same state simultaneously. If D_1 is conducting, one of the diodes, either D_5 or D_6, must also be conducting. It is established that D_1 conducts when the voltage v_{sa} exceeds both v_{sb} vsb and v_{sc}, or:

$$v_{sa} = Max(V_{sj}) \;; \qquad j = 1,2,3 \tag{I-11}$$

The same condition is applied on the other diodes and we find:

$$\begin{aligned} &D_i \; passesif \; v_{si} = Max(V_{sj}) \;; \quad i, j = 1,2,3 \\ &D_{i+3} passesif \; v_{si} = Min(V_{sj}) \;; \quad i, j = 1,2,3 \end{aligned} \tag{I-12}$$

The output voltage is given then by:

$$U_{dc} = Max(V_{sj}) - Min(v_{sj}); \qquad j = 1,2,3 \tag{I-13}$$

From where we can calculate the average of the output voltage, it is given by:

$$\bar{U}_{dc} = \frac{3\sqrt{3}}{\pi} v_{peak} = \frac{3\sqrt{3}}{\pi}\sqrt{2}v = 1.654\sqrt{2}v \tag{I-14}$$

Figure I.16 shows the output voltage of the three phase diode rectifier and the line voltage on the PCC.

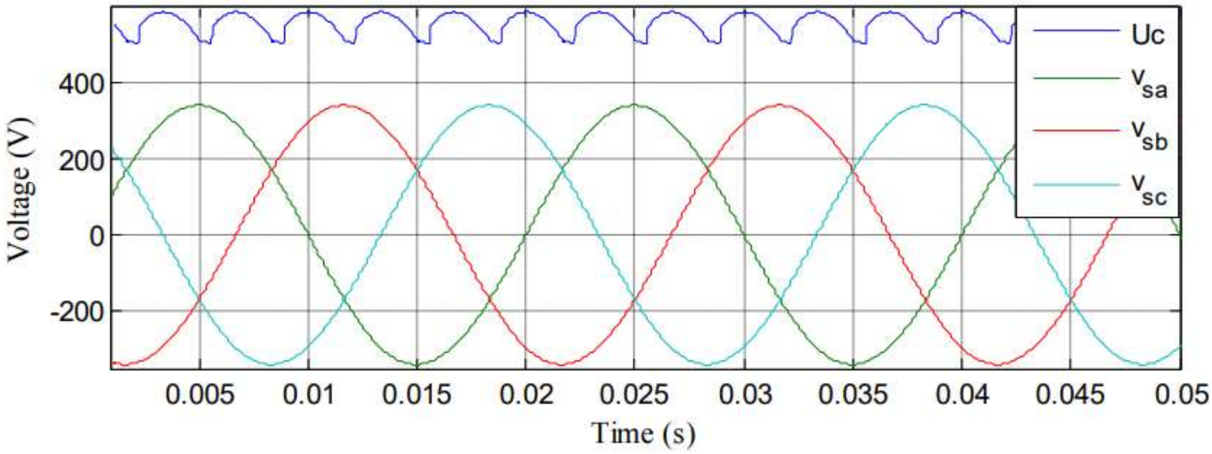

Figure I.16 Input and output voltage of three phase bridge rectifier.

I.8 Shunt Active Power Filter

The concept of utilizing active power filters to address harmonic issues and provide reactive power compensation was introduced over two decades ago [19]. It has demonstrated its capability to regulate grid currents and enhance power quality. The theories and applications of active power filters have gained popularity and garnered significant attention. Unlike passive harmonic filters, which are susceptible to component degradation and resonance issues, active power filters offer a promising solution for both reactive power compensation and harmonic current elimination. As previously mentioned, the Shunt Active Power Filter (SAPF) is connected in parallel with the nonlinear load, effectively acting as another controlled nonlinear load. To the grid, the system comprising the nonlinear load and the SAPF appears as a linear load connected to the Point of Common Coupling (PCC). When compensating reactive power, this load appears resistive; otherwise, it may appear as either an inductive or capacitive linear load.

The typical configuration of the Shunt Active Power Filter (SAPF) consists of either a two-level, three-level, or multilevel voltage source inverter, along with a DC power storage capacitor, input low pass filter, and the corresponding control circuitry. The construction and control principles of the SAPF will be addressed in the subsequent chapter of this study.

I.9 Conclusion

The goal of this chapter is to establish a collection of information about the most common problems in electrical networks. First, we have listed different types of faults in general such as short-time voltage variations, voltage interruptions, frequency variations and finally faults related to current and power imbalances. Pressure stress by showing the consequences of an imbalance.

Then, we turned to problems of harmonics, the object of this work, we studied their origin and their consequences for electrical installations, some standards for waves Harmonic has been presented along with decontamination techniques and methods of network supply .

Then, we moved on to the presentation of passive filters as well as the different configurations of these filters the operating principle of active filters is demonstrated with a presentation of active filter classification methods in the literature.

Chapter II :

Parallel Active Filter, Control Principle and Sizing

II.1 Introduction

The depollution of the electrical grid and the maintenance of a desired voltage at the connection point regardless of the current absorbed by the non-linear load are ensured through various control structures of active filtering. As previously mentioned, the filtering structure by parallel voltage inverter with the non-linear load is the most prevalent solution in industrial installations, known as the parallel active filter (PAF) of voltage type [2].

The parallel active filter is therefore the prudent choice we consider in this thesis, as the appropriate solution to harmonic problems. The operational principle, power circuit configuration, dimensioning, and control strategy of the active filter will be the focus of this chapter.

II.2 Principle of parallel active filtering

The shunt active power filter mitigates current harmonics by injecting compensating currents of equal magnitude but opposite phase into the grid. In this case, the shunt active power filter functions as a current source, injecting harmonic components generated by the load but shifted in phase by 180° [3]. This principle is applicable to any type of load deemed a harmonic source. Furthermore, with an appropriate control scheme, the active power filter can also improve the load power factor. Consequently, the power distribution system perceives both the non-linear load and the active power filter as an ideal resistor. The current compensation characteristics of the shunt active power filter are depicted in Figure I.1 [20].

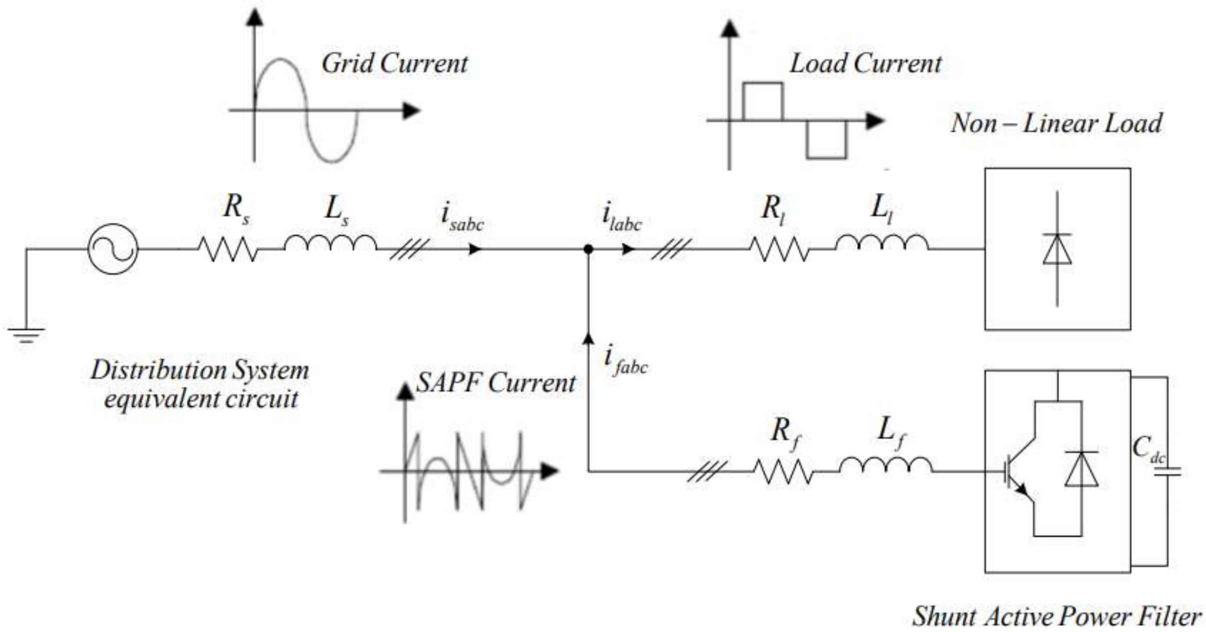

Figure II.1 Compensation characteristic of shunt active power filter [20].

II.2.1 Power part

The power section primarily consists of a static converter, which serves as the source of compensation current, comprising a voltage or current inverter based on controllable power switches with anti-parallel diodes for commutation and blocking, an output filter, and an energy storage circuit, either capacitive in the case of a voltage inverter or inductive in the case of a current inverter.

Figure II.2 shows a three-phase voltage structure inverter. The active filter is connected to the network via an inductive output filter L_f .

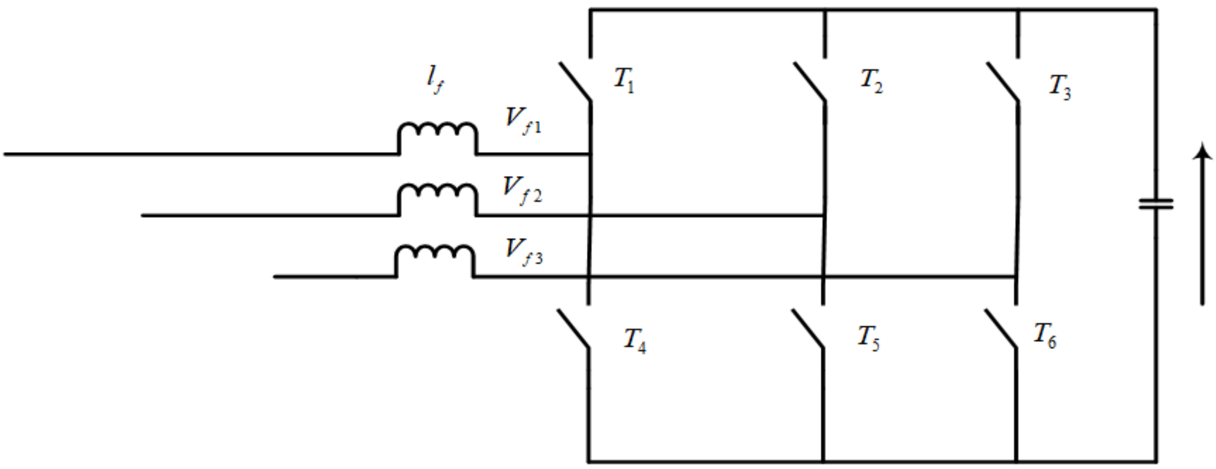

Figure II.2 Three-leg voltage inverter used in a voltage-structured active power filter (APF).

The switches are reversible in current. They include semiconductor components that are controlled in opening and closing. It can be MOSFET, IGBT or GTO. MOSFET are for low power and very high frequency switching, IGBT are for high power and high switching frequencies, GTO are for very high power with a limit related to the allowed switching frequencies. These switches are mounted in parallel with the power diodes to ensure conduction continuity in the voltage inverter, Figure II.3.

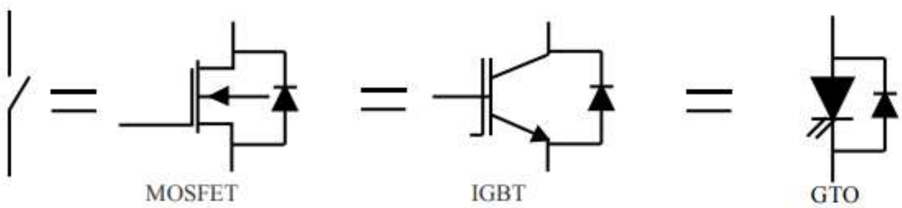

Figure II.3 Equivalent switches.

II.2.2 Command part

The control part consists mainly of the following elements:

♦ Identification of reference currents (which will be the subject of the next chapter)

♦ Tracking of reference currents

♦ DC bus voltage regulation

♦ Modulation

II.2.2.1 The pursuit of reference currents

The structure of a voltage filter operating in parallel does not allow simultaneous closing of semiconductors of the same branch under the punishment of short-circuiting the storage capacitor. Otherwise, the same timeout branch, aka dead time, needs to be inserted between one switch's blocking command and the other switch's bait command. In the case of instantaneous switching, this mode of operation will not be taken into account and therefore there is no risk of short-circuiting the capacitor.

The control of the two semiconductors of the same arm is done in a complementary way, that is to say, if the first is open the other is closed. With this principle, the opening and closing of the inverter switches in Figure II.2 depend on the state of the control signals (S_1, S_2, S_3), as shown below:

$$S_1 = \begin{cases} 1 \; T_1 \text{ closed } T_4 \text{ open} \\ 0 \; T_4 \text{ closed } T_1 \text{ open} \end{cases} \tag{II-1}$$

$$S_2 = \begin{cases} 1 \; T_2 \; \textit{closed} \; T_5 \text{ open} \\ 0 \; T_5 \; \textit{closed} \; T_2 \text{ open} \end{cases} \tag{II-2}$$

$$S_3 = \begin{cases} 1 \; T_3 \; \textit{closed} \; T_6 \text{ open} \\ 0 \; T_6 \; \textit{closed} \; T_3 \text{ open} \end{cases} \tag{II-3}$$

The voltages between phases, imposed by the inverter, are then defined by:

$$\begin{bmatrix} v_{f1} - v_{f2} \\ v_{f2} - v_{f3} \\ v_{f3} - v_{f1} \end{bmatrix} = \begin{bmatrix} S_1 - S_2 \\ S_2 - S_3 \\ S_3 - S_1 \end{bmatrix} V_{dc} \tag{II-4}$$

The output voltages of the inverter, denoted v_{f1}, v_{f2}, v_{f3} are referenced with respect to another network neutral and satisfy the following equations:

$$\begin{bmatrix} v_{f1} \\ v_{f2} \\ v_{f3} \end{bmatrix} = \begin{bmatrix} v_{s1} \\ v_{s2} \\ v_{s3} \end{bmatrix} + l_f \frac{d}{dt} \begin{bmatrix} i_{f1} \\ i_{f2} \\ i_{f3} \end{bmatrix} \qquad \text{(II-5)}$$

The network voltages being assumed to be balanced, and knowing that the sum of the currents injected by the inverter is zero, allows us to write:

$$\begin{cases} v_{s1} + v_{s2} + v_{s3} = 0 \\ i_{f1} + i_{f2} + i_{f3} = 0 \end{cases} \qquad \text{(II-6)}$$

We can deduce from equations (II-5) and (II-6) the following relation:

$$v_{f1} + v_{f2} + v_{f3} = 0 \qquad \text{(II-7)}$$

Equations (II-4) and (II-7) can be solved and we get:

$$\begin{bmatrix} v_{f1} \\ v_{f2} \\ v_{f3} \end{bmatrix} = \begin{bmatrix} 2S_1 & -S_2 & -S_3 \\ -S_1 & 2S_2 & -S_3 \\ -S_1 & -S_2 & 2S_3 \end{bmatrix} \frac{V_{dc}}{3} \qquad \text{(II-8)}$$

Thus, we can express eight possible cases of output voltage of the active filter V_f (referred to neutral n of the source), as shown in Table II.1. V_f represents the voltage vectors that the inverter must produce in order to generate the reference voltages, this is only possible if the vector formed by the latter remains inside the hexagon shown in Figure II.4 [21]. The parallel active filter is connected to the mains through an inductive filter (l_f) to provide controllability of the power filter current and also acts as a first order passive filter to suppress high frequency ripples produced by switching of the inverter. Neglecting the effects of the capacitor C of the output filter on the reference current I_{inj} (for the low frequency harmonics which are far from the switching frequency of the switches), we can write the following relation characterizing the current of the active filter I_{inj}:

$$L_f \frac{d}{dt} I_{inj} = V_f - V_s \qquad \text{(II-9)}$$

Table II.1 Inverter output voltages.

N°case	S_1	S_2	S_3	V_{f1}	V_{f2}	V_{f3}	V_f
0	0	0	0	0	0	0	0
1	1	0	0	$2v_{dc}/3$	$-v_{dc}/3$	$-v_{dc}/3$	$\sqrt{\frac{2}{3}}\ v_{dc}$
2	0	1	0	$-v_{dc}/3$	$2v_{dc}/3$	$-v_{dc}/3$	$\sqrt{\frac{2}{3}}\ v_{dc}\ e^{j\frac{2\pi}{3}}$
3	1	1	0	$v_{dc}/3$	$v_{dc}/3$	$-2v_{dc}/3$	$\sqrt{\frac{2}{3}}\ v_{dc}\ e^{j\frac{\pi}{3}}$
4	0	0	1	$-v_{dc}/3$	$-v_{dc}/3$	$2v_{dc}/3$	$\sqrt{\frac{2}{3}}\ v_{dc}\ e^{-j\frac{2\pi}{3}}$
5	1	0	1	$v_{dc}/3$	$-2v_{dc}/3$	$v_{dc}/3$	$\sqrt{\frac{2}{3}}\ v_{dc}\ e^{-j\frac{\pi}{3}}$
6	0	1	1	$-2v_{dc}/3$	$v_{dc}/3$	$v_{dc}/3$	$\sqrt{\frac{2}{3}}\ v_{dc}\ e^{-j\pi}$
7	1	1	1	0	0	0	0

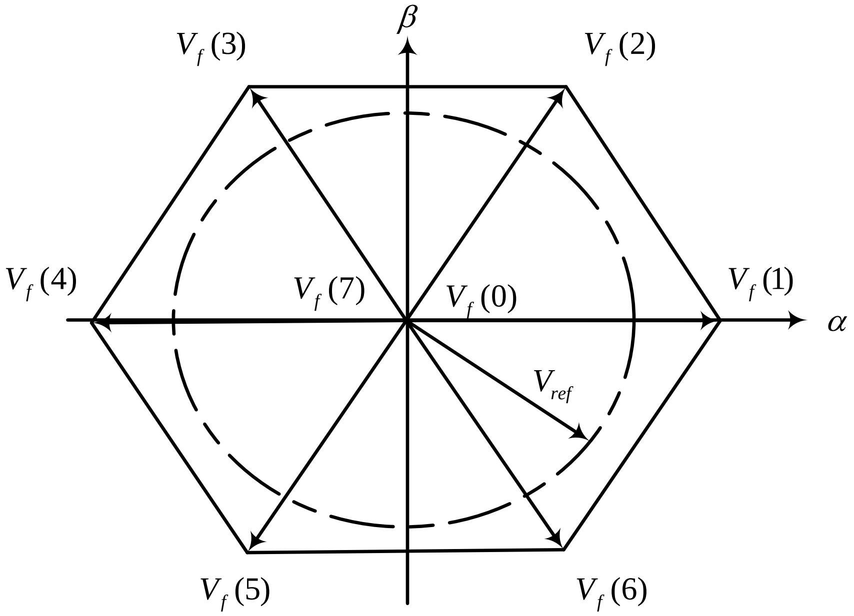

Figure II.4 Vector representation of the voltage vectors provided by the voltage inverter.

Consider ΔI_f the difference between the reference current and the measured current:

$$\Delta I_f = I_{ref} - I_{inj} \tag{II-10}$$

From equations (II-9) and (II-10), we obtain the following expression:

$$L_f \frac{d}{dt}\Delta I_f = (V_s + L_f \frac{d}{dt} I_{ref}) - V_f \quad \text{(II-11)}$$

The term in parentheses of relation (II-11) can be defined as the reference voltage $V_{f_{ref}}$, which gives us the following relation:

$$V_{f_{ref}} = V_s + L_f \frac{d}{dt} I_{ref} \quad \text{(II-12)}$$

The difference between $V_{f_{ref}}$ and V_f then creates an error on the current. According to equation (II-12), the reference voltage is summed by two terms at different frequencies. The first is the network voltage that can be directly measured V_s. The second value represents the voltage drop

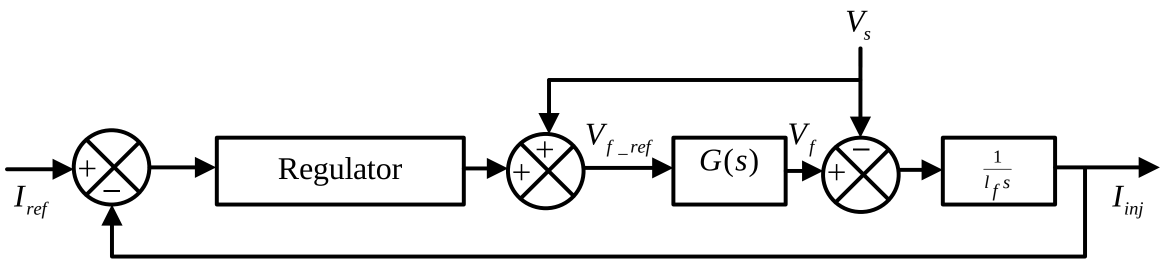

Figure II.5 Diagram of filter current regulation.

Across the terminals of the inductor l_f, when the second inductor is crossed by a current equal to the reference current. This term must be found by a current regulator, as shown in Figure II.5.

In this diagram, $G(s)$ represents the gain function of the inverter given by:

$$G(s) = K.\frac{1}{\tau.s} \quad \text{(II-13)}$$

$$K = \frac{V_{dc}}{2V_p} \quad \text{(II-14)}$$

With:

V_{dc}: The voltage on the DC side of the inverter.

V_p: The amplitude of the triangular carrier.

τ: The delay caused by the calculation of the disturbing currents.

The regulator must satisfy the general objectives of the regulation as well as the constraints related to the rejection of the disturbances.

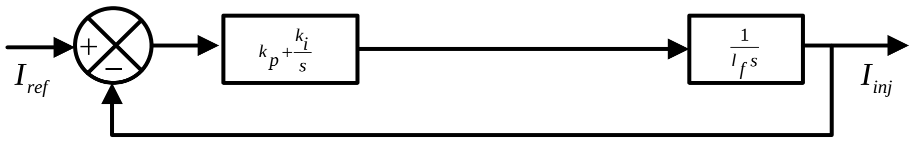

Figure II.6 Simplified diagram of filter current regulation.

Generally, the most used regulator is the proportional integral (PI) regulator. Indeed, it is one of the simplest to implement (Figure II.6) [22].

The PI proportional-integral regulator is composed of two gains and an integral, where its open-loop transfer function is given by:

$$H_{pi}(s) = k_p + \frac{k_i}{s} \tag{II-15}$$

Where k_p is the proportional gain and k_i is the integral gain.

The transfer function Figure II.6 can be rewritten as:

$$H_{pi}(s) = k_p \frac{1+\tau_{pi}s}{\tau_{pi}s} \tag{II-16}$$

Or:

$\tau_{pi} = \frac{k_p}{k_i}$ is the time constant of the regulator, and $f_0 = \frac{\omega_0}{2\pi} = \frac{k_i}{2\pi k_p}$ its cut off-frequency.

The PI-style regulator provides both fast dynamic response and steady-state static error rejection. The effect of this type of regulator is illustrated in its Bode diagram in Figure II.7. As shown in this figure, this regulator has a high gain in the frequency range $\left[0, \omega_0/2\pi\right]$, which means it manages to attenuate the harmonic components in its pass band. Outside this range, this gain is limited, the regulator cannot suppress or attenuate harmonic components.

II.2.2.2 DC bus voltage regulation

Maintaining voltage at the capacitor terminals is necessary to compensate for losses in the filter and to limit variation in dynamic mode. The reference voltage of the DC bus must satisfy the current controllability constraint, the following condition must be met [23].

$$\sqrt{\frac{2}{3}}V_{dc-ref} \geq V_{S_{\max}} + L_f\left(\frac{di_{ref}}{dt}\right)_{\max} \qquad \text{(II-17)}$$

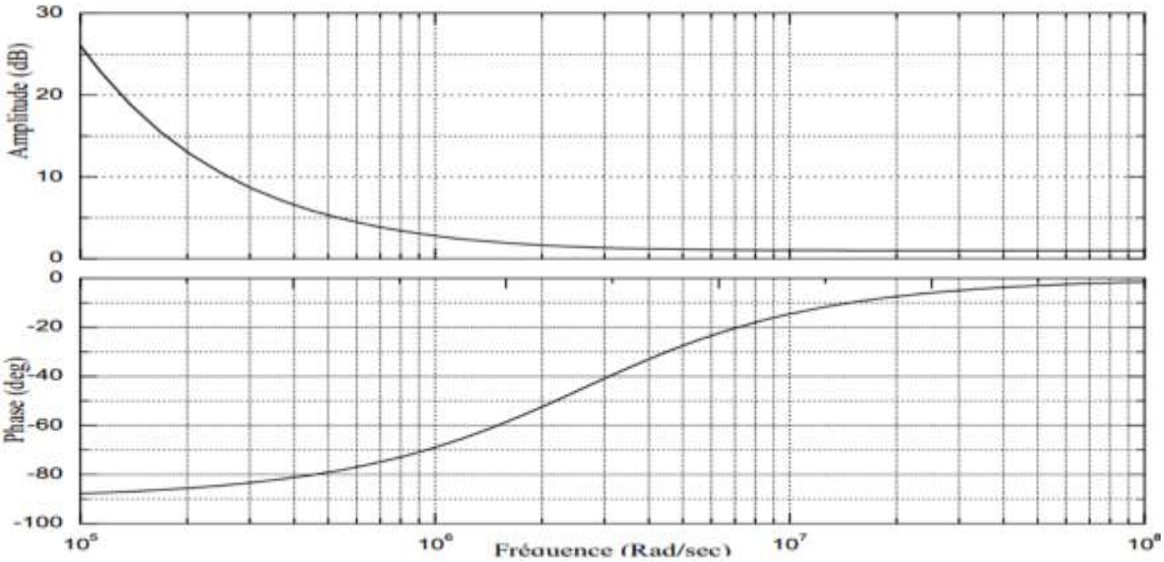

Figure II.7 Bode diagram of a PI regulator.

The average voltage v_{dc} across the capacitor must be maintained at a constant value. Losses in the output switch and filter are the main possible causes of this voltage. The adjustment of the DC voltage across the terminals of the storage capacitor must be done by adding the operating base currents to the reference currents. The output of the regulator $p(c)$ is internally appended with a sign of the interfering active power $\tilde{p}$ and produces the active base current, thereby correcting v_{dc} .

A first-order low-pass filter sufficient to filter out fluctuations, in the case of a rectifier, as a nonlinear load. The transfer function of the regulator is given by [21]:

$$FT(s) = \frac{k_c}{1+\tau_c s} \qquad \text{(II-18)}$$

With:

- k_c : regulator gain
- τ_c : time constant

The Bode diagram of this regulator is shown in Figure II.8 :

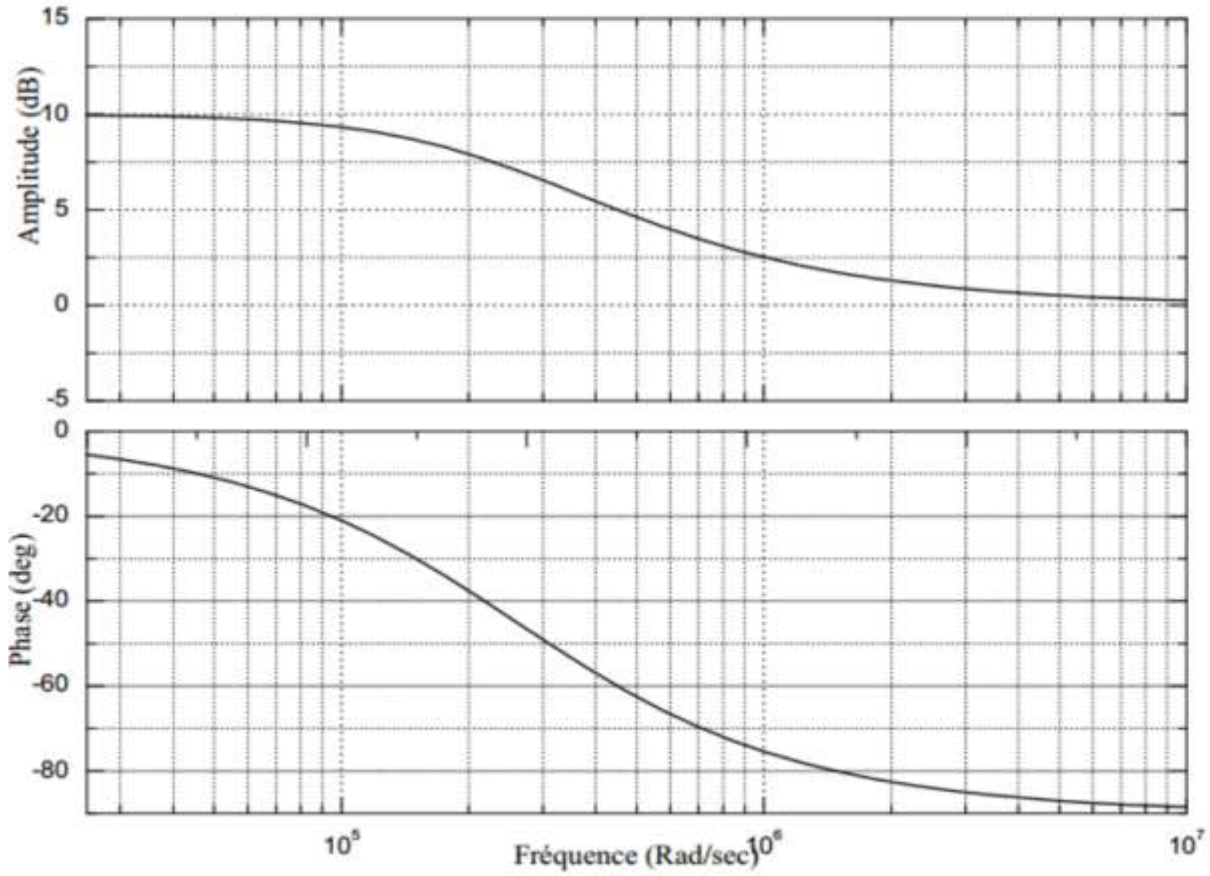

Figure II.8 Bode diagram of a low pass regulator

To describe the relationship between the active power absorbed by the capacitor and the voltage across it, the energy stored in the output filter and the switching losses are ignored. We then have:

$$P(c) = \frac{d}{dt}\left(\frac{1}{2} c v_{dc}^2\right) \tag{II-19}$$

The linearization of equation (II-19) in the vicinity of the reference voltage v_{dc}^* gives us the following expression

$$P(c) = c v_{dc}^* \left(\frac{d}{dt} v_{dc}\right) \tag{II-20}$$

The closed loop transfer function is of the form:

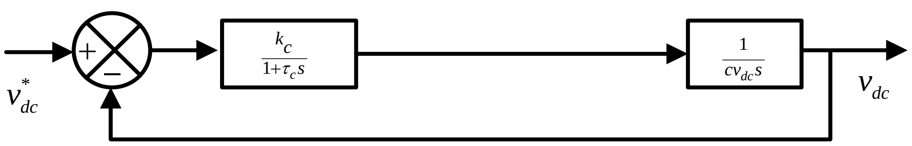

Figure II.9 DC voltage regulation loop

$$F(s) = \frac{\omega_c^2}{s^2 + 2\xi\omega_c + \omega_c^2} \tag{II-21}$$

With:

$$\omega_c = \sqrt{\frac{k_c}{cv_{dc}^* \tau_c}}, \ \xi = \frac{1}{2}\sqrt{\frac{cv_{dc}^*}{k_c \tau_c}}$$

The regulation is stable for all the values of k_c, nevertheless the product $k_c\tau_c$ is chosen to have a satisfactory damping.

II.2.2.3 Control by the method of pulse width modulation

By reviewing literature [24], it is possible to trace the historical development of PWM inverter control techniques. To clarify the current situation, three distinct approaches need to be identified.

The first, the most used, because of its ease of implementation by analogous techniques, is based on natural sampling techniques [25][26]. More recently, a second switching strategy has been proposed [27], known as conventional PWM, which is considered to have some advantages when implemented digitally or microprocessor-based. The third switching approach is called optimal PWM, based on minimizing certain performance criteria[28][29].

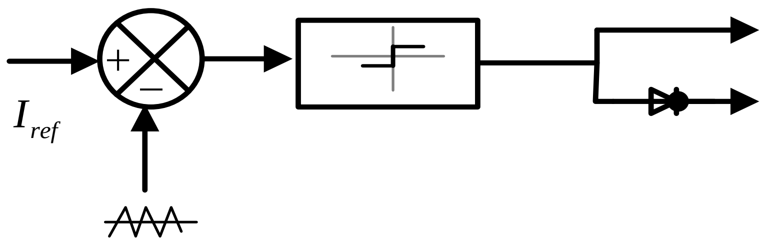

Figure II.10 Principle of current control by PWM.

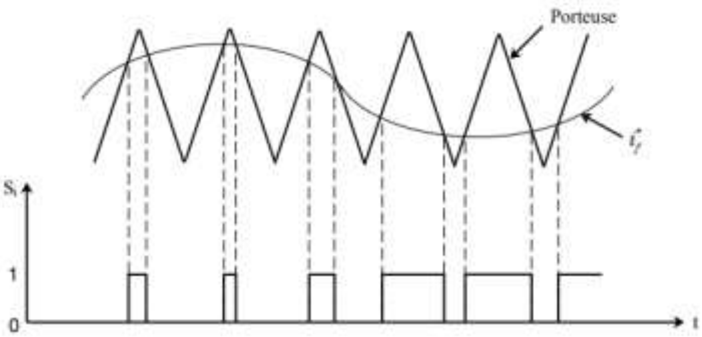

Figure II.11 Control of switches by PWM.

Most of the PWM voltage inverter type frequency converters use the first natural PWM control method, from Figure II.10, where it can be seen that the triangle signal (carrier) is compared directly fed with a sinusoidal modulated signal (reference signal) to determine the switching time. , and hence the received pulse duration, see Figure II.11. It is important to note that the logic state and the width of the switching bandwidth are determined by the instantaneous intersection between these two signals.

The resulting pulse duration is proportional to the amplitude of the reference signal at the time the switching occurs. This has two important consequences. The first is that the centers of the received pulses are unequal or evenly spaced. Second, it is not possible to determine the pulse width using analytical expressions [30]. Indeed, according to Figure II.12 can show that the pulse width can only be determined by a transcendental equation of the form [31]:

$$t_p = \frac{T}{2}\left\{1 + \frac{M}{2}\left(\sin\omega_m t_1 + \sin\omega_m t_2\right)\right\} \tag{II-22}$$

According to this transcendental formula that exists between switching pulses, it is not possible to use microprocessor hardware to directly calculate the widths of the modulated pulses. It is certainly possible to simulate the process in microprocessor software and use the logic principles of the microprocessor to determine the pulse width.

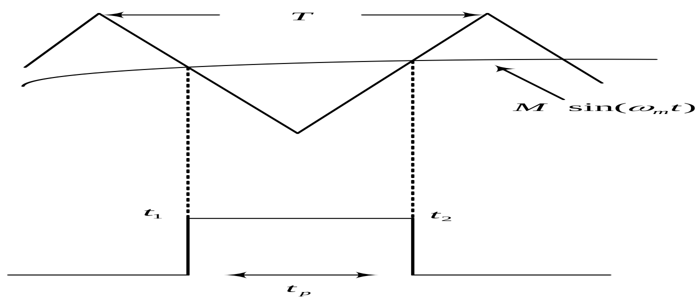

Figure II.12 natural PWM.

Where ω_m is the pulsation of the modulator.

II.2.2.4 Control by hysteresis method

The method is powerful and easy to use, in fact it guarantees full control of the current without the need for in-depth knowledge of the model of the controlled system. Furthermore, this technique is the most suitable solution for current-driven inverters. It is intended to keep the required current in a sample, known as the hysteresis band, around the desired reference current. The conversion commands are determined based on the error. When the current increases and the error exceeds a certain positive value, the state of the switching instructions changes and the current starts to decrease until the error reaches a certain negative value, then the switch instructions change will change Figure II.13 and Figure II.14 [2][32].

If simplicity of implementation is the main advantage of this control method, variable switching frequency is the main disadvantage of this method. This frequency variation mainly affects the operation of power electronics that cannot support high switching frequencies in high power applications.

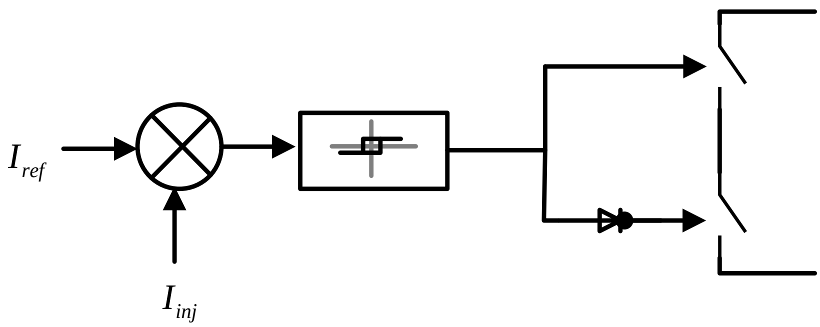

Figure II.13 Principle of current control by hysteresis

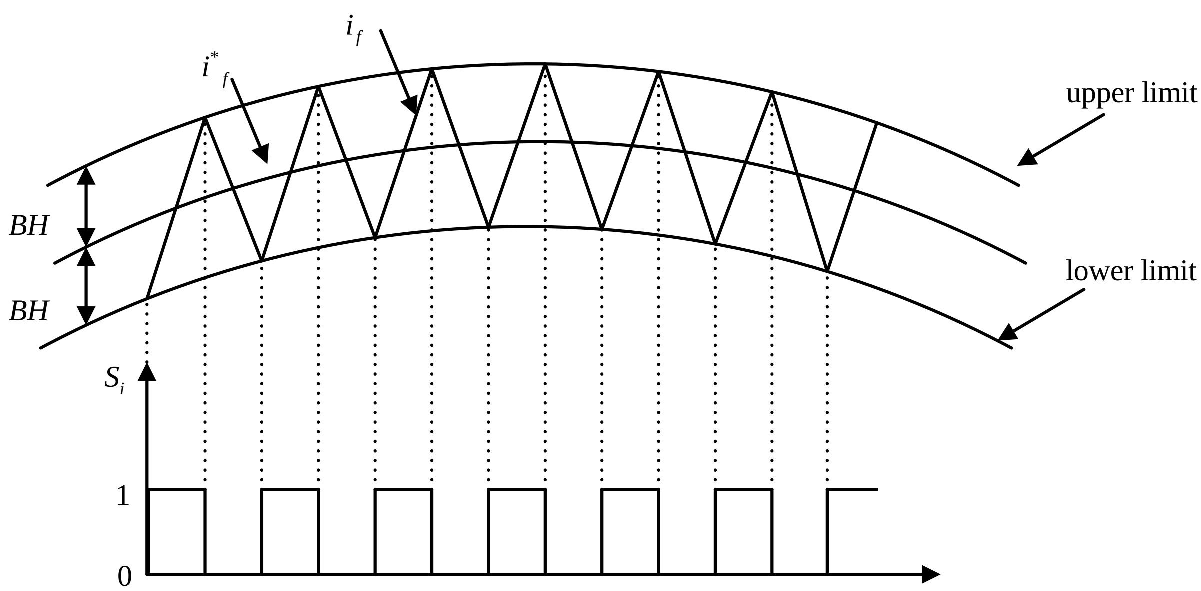

Figure II.14 Control of switches by hysteresis

In order to solve the problem of variable switching frequency, new hysteresis control strategies such as modulated hysteresis [33][34], variable band hysteresis [19][35], have been proposed.

II.3 Parallel active filter control strategies

Implementing a parallel active filter to compensate for harmonic currents requires generating initial reference currents, and then regulating these generated reference currents. For this purpose, the FAP control consists of two main blocks: the control part and the source part. The control section contains identification and adjustment of reference harmonic currents and a DC bus tuning loop. The power section contains an output filter that connects the FAP to the mains, a parallel active filter, and a capacitive storage element.

II.4 Simulation of the entire network, parallel active filter and non-linear load

Simulating the network, active filter, and non-linear load combination is an important step to study the parameters and operation of the active filter in harmonic current compensation. After the system description phase to be studied, a set of simulation results will be processed and discussed, highlighting the main currents associated with the active filter.

II.4.1 Description of the assembly, network, active filter and non-linear load

The considered system consists of a power supply network, a diode bridge rectifier representing the nonlinear load and an active filter with voltage structure,

Figure II.15.

II.4.1.1 Electrical Network Modeling

The electrical network is represented by a sinusoidal voltage source in series with an impedance, called a short circuit, from which the network is modeled by a balanced three-phase fem, by an inductance L_s and a resistance R_s Figure II.16

$$\begin{bmatrix} e_1 \\ e_2 \\ e_3 \end{bmatrix} = \sqrt{2}E \begin{bmatrix} \sin(\omega t) \\ \sin\left(\omega t - \frac{2\pi}{3}\right) \\ \sin\left(\omega t + \frac{2\pi}{3}\right) \end{bmatrix} \tag{II-23}$$

.

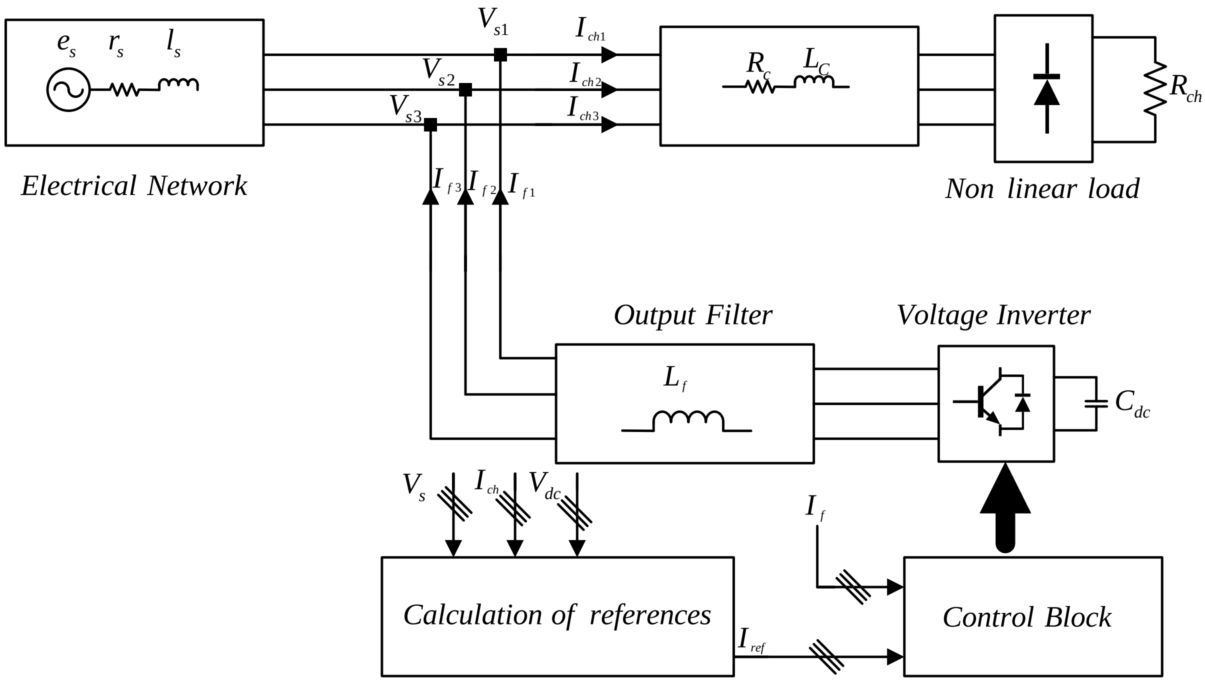

Figure II.15 Synoptic diagram of the network assembly, parallel active filter and non-linear load.

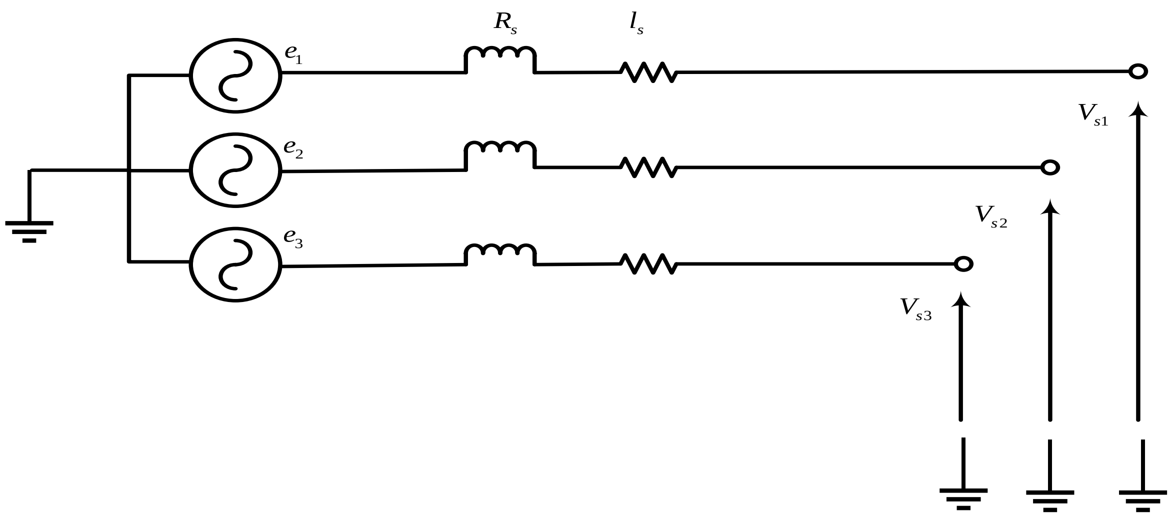

Figure II.16 Synoptic diagram of the electrical network.

$$Z_s = R_s + jL_s\omega \tag{II-24}$$

II.4.1.2 Modeling of the pollutant load

To understand the characteristics and applications of the parallel active filter, it is important to discuss the general characteristics of non-linear loads because the majority of high power VA industrial loads are provided by three-phase networks. Three wires and have their topology. Three-phase rectifier. These loads are sources of harmonic current or voltage that is why nonlinear loads are classified into two types: nonlinear loads with harmonic current sources and nonlinear loads with harmonic voltage sources.

Figure II.17.a shows a typical three-phase thyristor rectifier with an inductor and a resistor on the DC side. Due to the sufficient value of the DC side inductance, it produces almost constant current. The harmonic current content a the rectifier input (load current) depends mainly on the rectifier, with a typical THD value of 25-30%.Therefore, this type of load acts as a source of harmonic current.

However, as shown in Figure II.17.b, a diode rectifier with a capacitor on the DC side is an example of a nonlinear load of a harmonic voltage source. Although the harmonic current content at the input of the rectifier is affected by the impedance of the AC side and is highly distorted ($typically\ THD > 70\%$), these types of nonlinear loads act as a voltage source rather than a current source. Called non-linear harmonic voltage source loads.

Based on the above discussion, the equivalent circuit of each phase of a harmonic current source nonlinear load can be represented by an equivalent

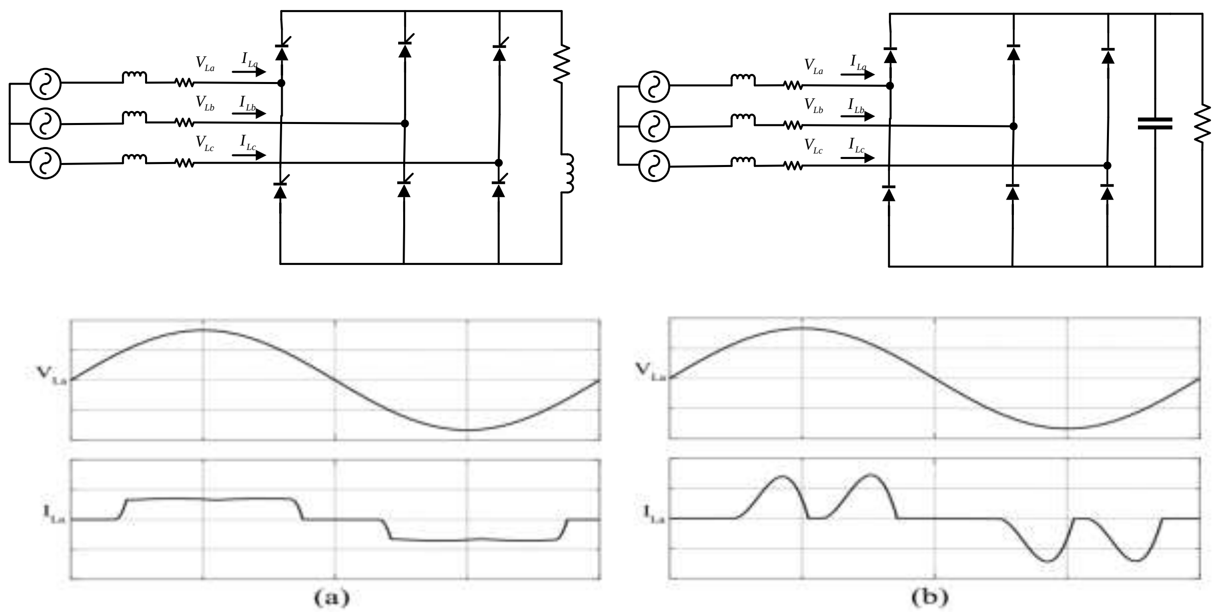

Figure II.17 Typical three-phase non-linear loads and their input signals: a- a thyristor rectifier delivering an RL load, b- a diode rectifier delivering an RC load.

Norton circuit as shown in Figure II.18.a. The equivalent circuit of each phase of a nonlinear load with harmonic voltage source is given by Thevenin's equivalent circuit, Figure II.18.b. A pure harmonic current source is a special case of the equivalent Norton scheme with $Z_l \to \infty$, and a pure harmonic voltage source is a special case of the equivalent Thevenin scheme with $Z_l \to \infty$ [36].

II.4.2 Equivalent diagram of the network assembly, parallel active filter and non-linear load

Figure II.19 shows the Norton equivalent diagram of a parallel active filter for a harmonic current source nonlinear load. The source current I_l and the parallel impedance Z_l represent the equivalent source current. This is the total current loaded by the load. A three-phase source is represented by a voltage source V_s and a network impedance Z_s

Since the purpose of the FAP is to compensate the harmonic currents of the loads to produce a sinusoidal source current, the FAP is implemented as a harmonic current generator, generating harmonic currents of equal and opposite magnitude. Opposite in magnitude. Phase with nonlinear loads, where the FAP in the figure is shown as an I_F current source. The filter current is determined by:

$$I_F = G(s) I_l \tag{II-25}$$

Where $G(s)$ is the FAP transfer function. By the analysis of the equivalent diagram, the current of the source I_s and the current of the load I_l are given by the equations (II-26) and (II-27) respectively.

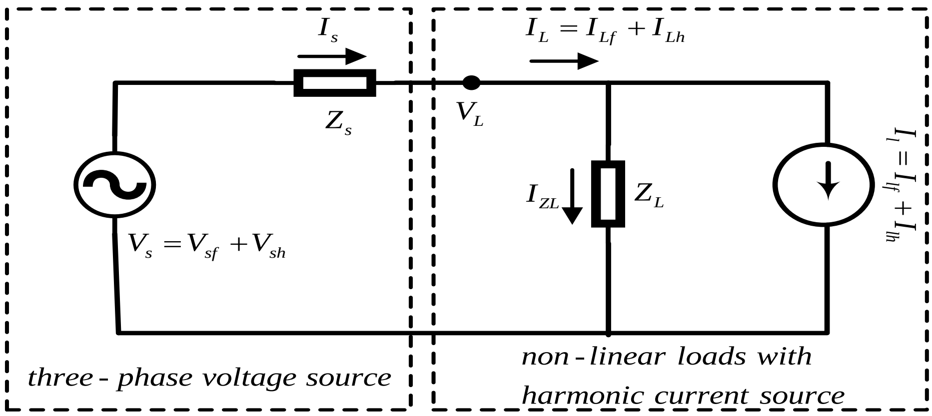

(a)

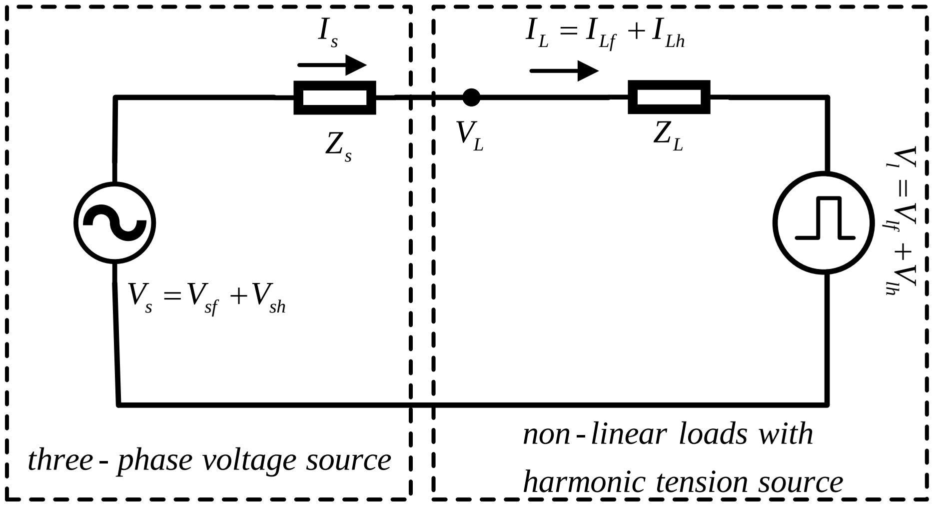

(b)

Figure II.18 Model of the equivalent diagram of a phase: a- nonlinear load with harmonic current source represented by the equivalent Norton diagram, b- nonlinear load with harmonic voltage source represented by the equivalent Thevenin diagram

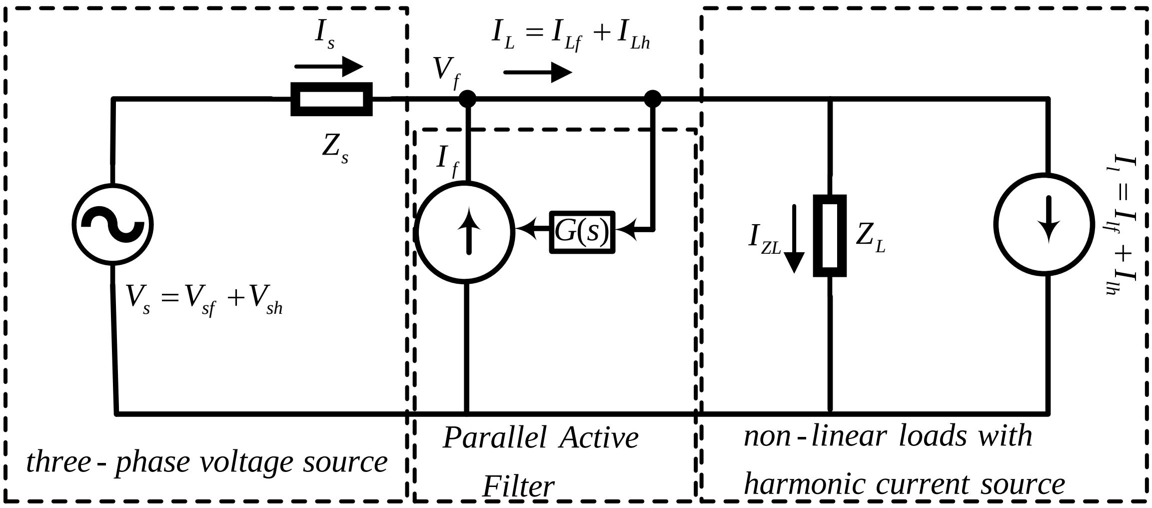

Figure II.19 Application of an active filter parallel to a nonlinear load with a harmonic current source

$$I_s = \frac{Z_l}{Z_s + \frac{Z_l}{1-G(s)}} I_l + \frac{1}{Z_s + \frac{Z_l}{1-G(s)}} V_s \tag{II-26}$$

$$I_l = \frac{\dfrac{Z_l}{1-G(s)}}{Z_s + \dfrac{Z_l}{1-G(s)}} I_l + \frac{1}{(1-G(s))\left(Z_s + \dfrac{Z_l}{1-G(s)} \right)} V_s \qquad \text{(II-27)}$$

In a perfect FAP, $G(s)$ the transfer function is equal to zero at the fundamental frequency $\left(|G(s)|_f = 0 \right)$, and approximately equal to unity at all other harmonic frequencies. Therefore, $G(s)$ is assumed to have a characteristic of a Notch filter at the fundamental frequency, so it satisfies the following condition:

$$\left| \frac{Z_l}{1-G(s)} \right|_h >> |Z_s|_h \qquad \text{(II-28)}$$

We deduce from equations (II-25)(II-26)(II-27) the following relations:

$$I_F \approx I_{lh} \qquad \text{(II-29)}$$

$$I_{sh} \approx (1-G(s))I_{lh} + \frac{1-G(s)}{Z_l} V_{sh} \approx 0 \qquad \text{(II-30)}$$

$$I_{Lh} \approx I_{lh} + \frac{1}{Z_l} V_{sh} \qquad \text{(II-31)}$$

The previous equations show that the performance of the FAP depends on the system parameters Z_L and Z_s, and the transfer function of the FAP $G(s)$.

II.4.3 Characteristics of the pollution load

The non-linear load consists of a three-phase rectifier bridge that feeds on the load $RL\ (R_d, L_d)$ with an additional inductance L_c at the input of the rectifier to limit the di/dt gradient. The total inductance $L_{tot} = L_s + L_c$ against sudden changes in current, the current of a nonlinear load, can be expressed by the following relationship:

$$i_d(t) = I_{d_{moy}} + \sum (a_n \cos(n\omega t) + b_n \sin(n\omega t)) \tag{II-32}$$

With: $I_{d_{moy}}$ is the average current of the nonlinear load, it is given by:

$$I_{d_{moy}} = \frac{1}{2\pi} \int_0^{2\pi} i_d(t) d(\omega t) \tag{II-33}$$

a_n *and* b_n: are the coefficients of the Fourier series.

The coefficients a_1 and b_1 of the fundamental component can be calculated as follows:

$$a_1 = \frac{2}{2\pi} \int_0^{2\pi} i_d(t) \cos(\omega t)\ d(\omega t) = \frac{1}{\pi} \left[\int_{\pi/6}^{5\pi/6} I_d \cos(\omega t)\ d(\omega t) - \int_{7\pi/6}^{11\pi/6} I_d \cos(\omega t)\ d(\omega t) \right] = 0 \tag{II-34}$$

$$b_1 = \frac{2}{2\pi} \int_0^{2\pi} i_d(t) \sin(\omega t)\ d(\omega t) = \frac{1}{\pi} \left[\int_{\pi/6}^{5\pi/6} I_d \sin(\omega t)\ d(\omega t) - \int_{7\pi/6}^{11\pi/6} I_d \sin(\omega t)\ d(\omega t) \right] = \frac{2\sqrt{3}}{\pi} I_d \tag{II-35}$$

The effective value I_1 of the fundamental current of the load is given by:

$$I_1 = \frac{\sqrt{a_1^2 + b_1^2}}{\sqrt{2}} = \frac{2\sqrt{3}}{\pi\sqrt{2}} I_d \tag{II-36}$$

The effective value of the charging current is given by:

$$I_{eff} = \sqrt{\frac{2}{2\pi} \int_{\pi/6}^{5\pi/6} i_d^2 d(\omega t)} = \sqrt{\frac{2}{3} I_d^2} = \sqrt{\frac{2}{3}} I_d \tag{II-37}$$

The rectifier is connected under a voltage of $230V / 400V$, the dimensioning of the rectifier is carried out for a firing angle equal to 0°

The output voltage of a thyristor rectifier is:

$$U_d = \frac{3V\sqrt{6}}{\pi} \cos(\alpha) \tag{II-38}$$

$$R_d = \frac{U_{d\max}^2}{P_{\max}} \tag{II-39}$$

The choice of inductance L_d is made according to the choice of $\tau_d = \frac{L_d}{R_d}$, such as the pulsation index $p = 6$, therefore $T_d = 3.3ms$.

To obtain a sufficiently smooth current at the output, it is necessary that $\frac{\tau_d}{T_d} \geq 1$, so, we calculate L_d for $T_{d\min} = \tau_{d\min} = 3.3ms$.

II.4.4 Active filter sizing

The effective value of the charging current is:

$$I_{eff} = \sqrt{\frac{2}{3}} I_d \tag{II-40}$$

In this case, the effective value of the sum of the harmonic currents $\left(I_{eff}\right)_{harm}$ is defined by:

$$\left(I_{eff}\right)_{harm} = \sqrt{I_{eff}^2 - I_1^2} \tag{II-41}$$

With: I_1 RMS value of the fundamental component of the current on the AC side.

We will therefore have:

$$\left(I_{eff}\right)_{harm} = \sqrt{\left(\frac{2}{3} - \frac{6}{\pi^2}\right) I_d^2} = 0.242.I_d \tag{II-42}$$

As the purpose of the filter is to remove all harmonics, its nominal power will be equal to:

$$\left(S_{nom}\right)_{filtr} = \sqrt{3} U_n \left(I_{eff}\right)_{filtr} \tag{II-43}$$

$$\left(S_{nom}\right)_{filtr} = \sqrt{3} U_n \left(0.242.I_d\right)_{harm} \tag{II-44}$$

The nominal power of the non-linear load is:

$$\frac{\left(S_n\right)_{filtr}}{\left(S_n\right)_{ch}} = \frac{\sqrt{3}.U_n.(0.242.I_d)}{\sqrt{3}.U_n.\frac{\sqrt{6}}{\pi}.I_d} = 0.31 \tag{II-45}$$

II.4.5 Simulation results

For the simulation of the network, non-linear load and active filter assembly, the non-linear load considered is an uncontrolled three-phase rectifier bridge where the semiconductors are considered perfect.

Table II.2 Parameters of system.

Parameters	**symbol**	**Value**
System voltages (line to line) Vrms	V_S	380
Frequency	f	50
Filter (series SAPF)	L_s, R_s	$0.25\Omega, 0.42mH$
Filter (shunt SAPF)	L_f, R_f	$0.5\Omega, 3mH$
Capacitance	C	$1000\mu F$
Proportional gain	K_p	20
Integral gain	K_i	200
Sample time	t	$1e^{-4}$
Non-linear load	R	60

Harmonic currents and balanced sinusoidal voltages: In this section, the supply network voltages are considered ideal, meaning that source voltages are balanced and free of harmonics, and the load is balanced. Figure II.20 depicts, from top to bottom, the waveforms of source voltages and currents of the nonlinear load.

II.4.5.1 Harmonic currents and balanced sinusoidal voltages

In this part the voltages of the supply network are considered ideal, this means that the source voltages are balanced and do not contain harmonics and the load is balanced. Figure II.20 shows from top to bottom the waveforms of source voltages and currents of the nonlinear load.

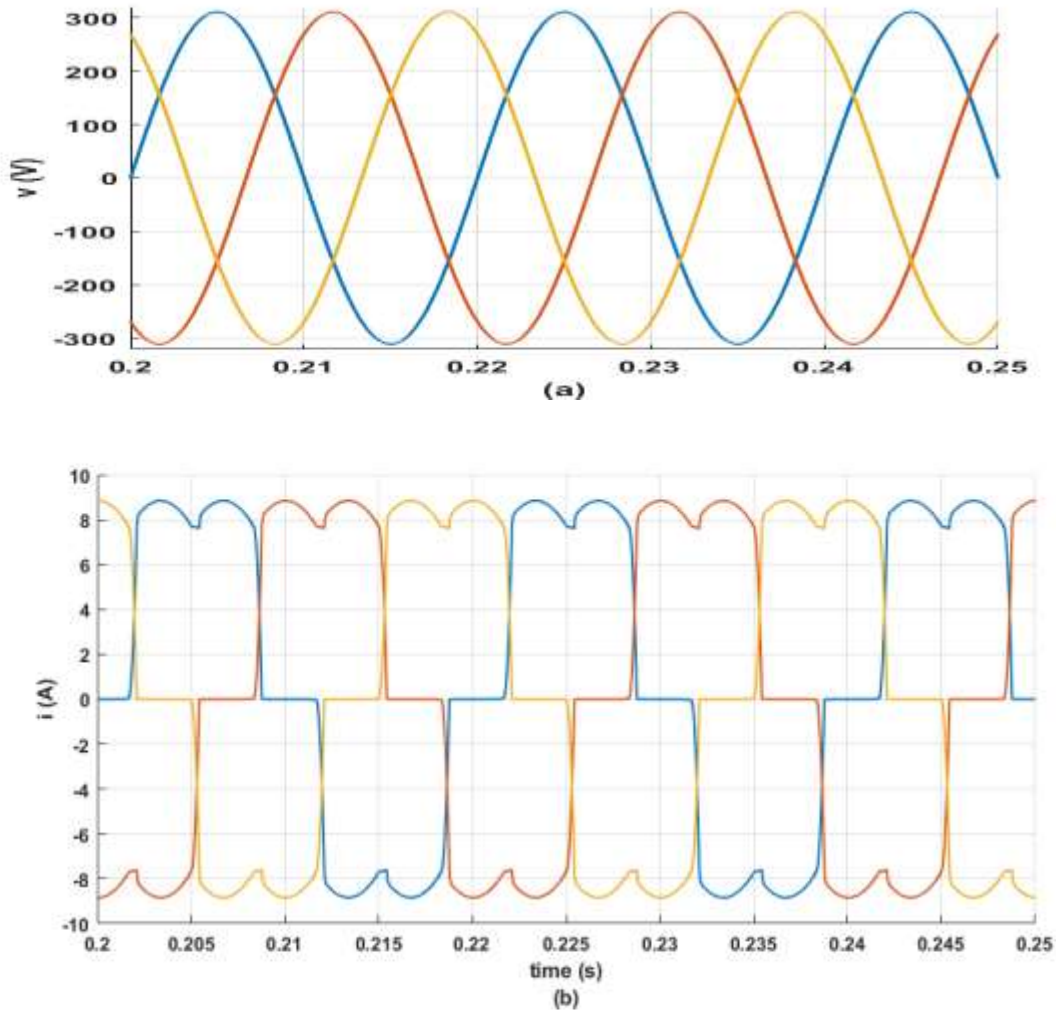

Figure II.20 Waveforms - balanced conditions – from top to bottom: (a) the voltages of the electrical network, (b) the source current before filtering.

Figure II.21 presents, from top to bottom, the reference current generated by the instantaneous power algorithm and the current of the active filter. Figure II.22 gives the filtered current of the first phase, and the voltage v_{dc} of the DC bus. We see that the voltage v_{dc} is almost constant and oscillates around its reference.

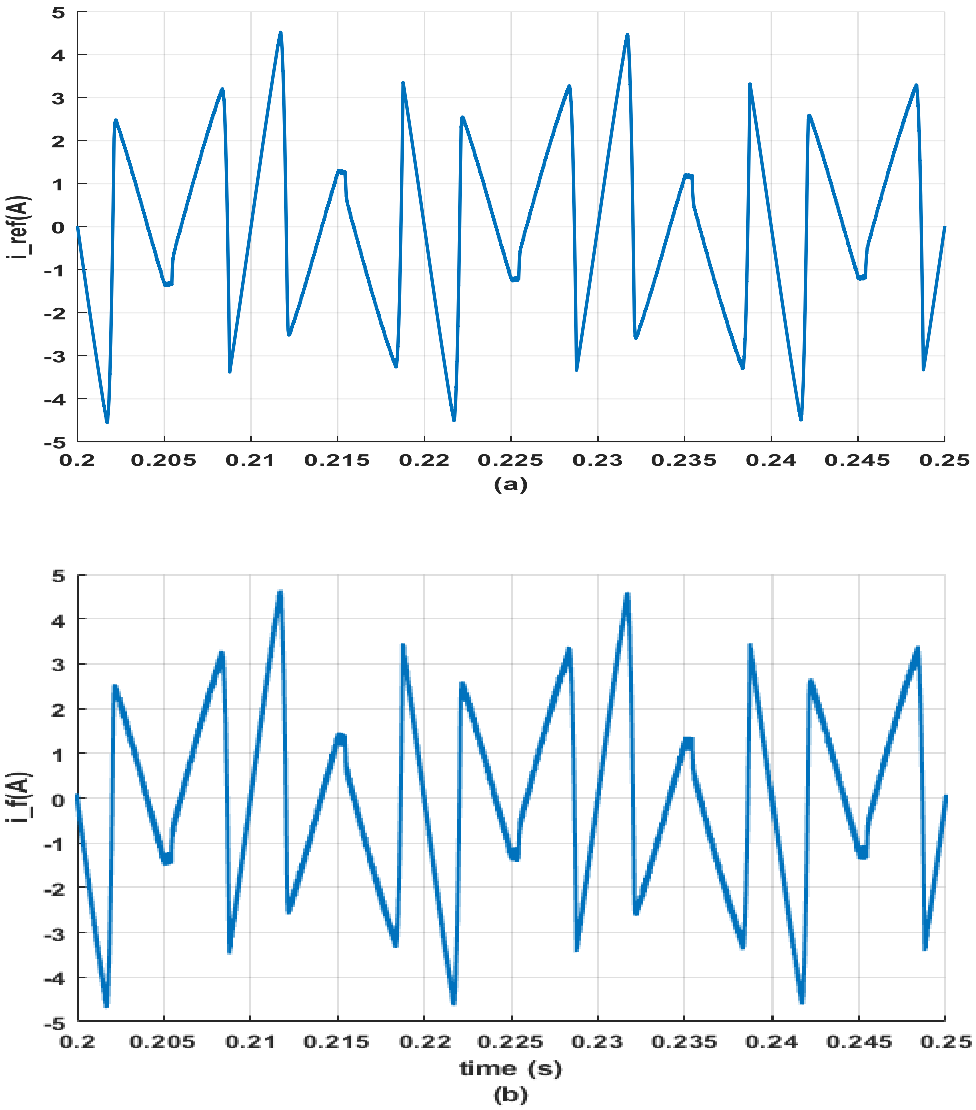

Figure II.21 Waveforms - balanced conditions - from top to bottom: (a) the reference current and (b) the current injected by the active filter.

The spectral analysis of the currents of the nonlinear load and the filtered current is presented in the Figure II.23. According to this figure, we note that by the application of the active parallel filter an improvement in the shape of the current was obtained, as it is indicated in the Figure II.22. The disturbed current is cleaned up to a satisfactory level, this is confirmed by the harmonic spectrum which goes from a THD of $28.29\ \%$ to a THD of $1.33\ \%$ considering the first 25 most significant harmonics (5, 7, 11, 13, 17, 19, 23 and 25).

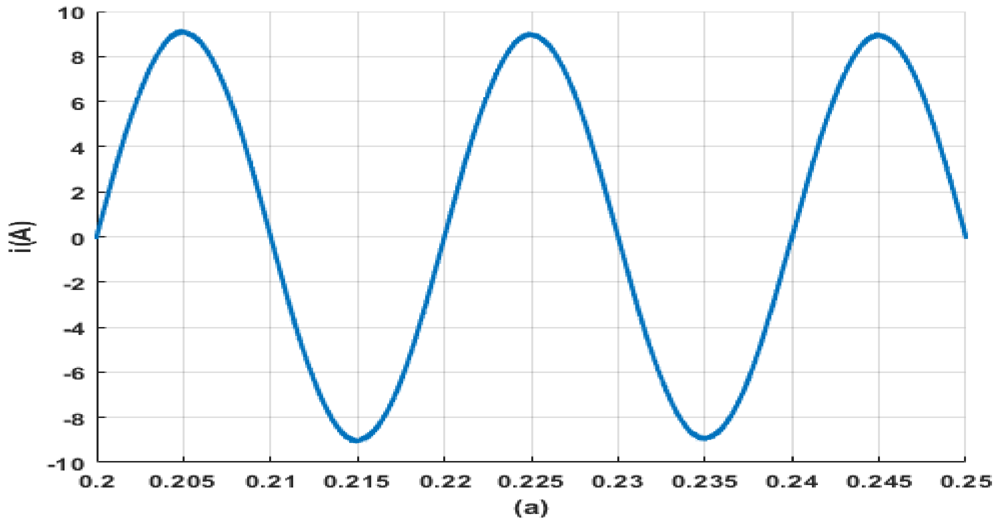

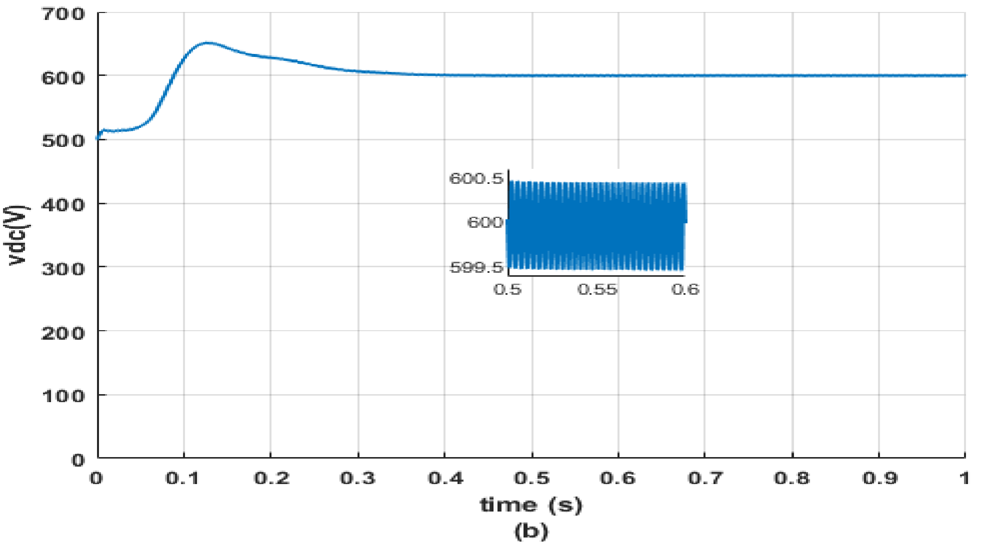

Figure II.22 Waveforms - balanced condition - from top to bottom: (a) the source current after filtering and (b) DC bus voltage.

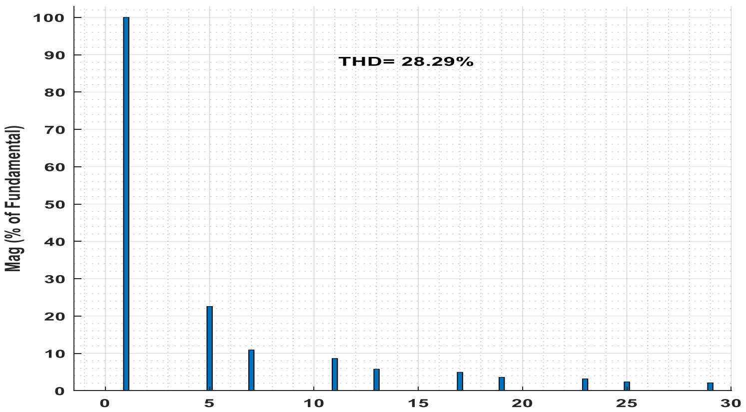

(a)

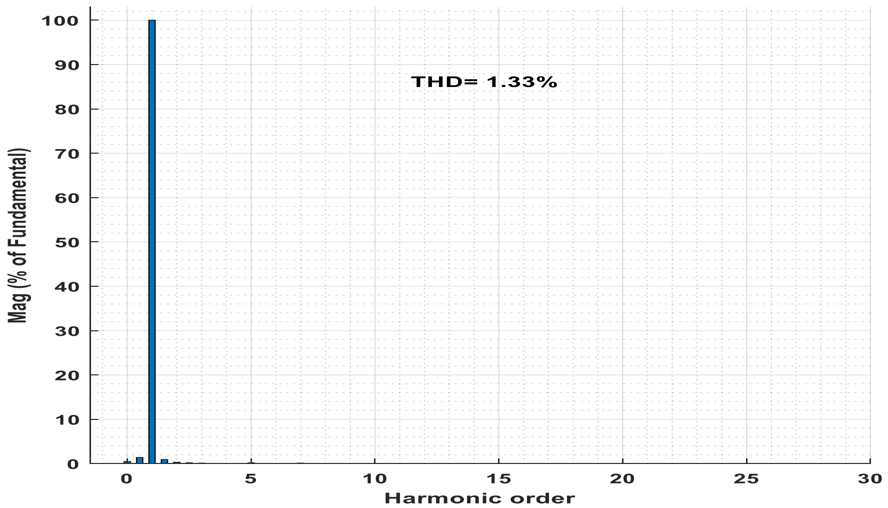

(b)

Figure II.23 Shapes of the current spectra - balanced condition - from top to bottom: (a) current spectrum of the non-linear load and (b) spectrum of the filtered current.

II.4.6 Harmonic currents and unbalanced voltages

In this paragraph we consider a voltage imbalance to examine the performance of the parallel active filter under these conditions, the Figure II.24 shows the simulation results obtained when the voltages of the source are unbalanced as well as the currents of the non-linear load. Figure II.25 exposes, from top to bottom, the reference current generated and the current injected by the active filter i_f^* obtained in the case of an imbalance at the level of the supply voltages.

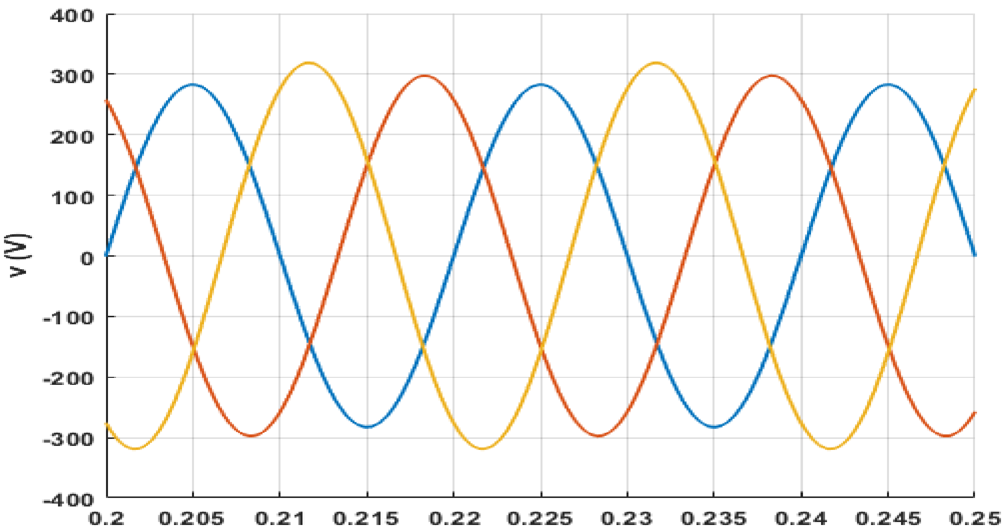

(a)

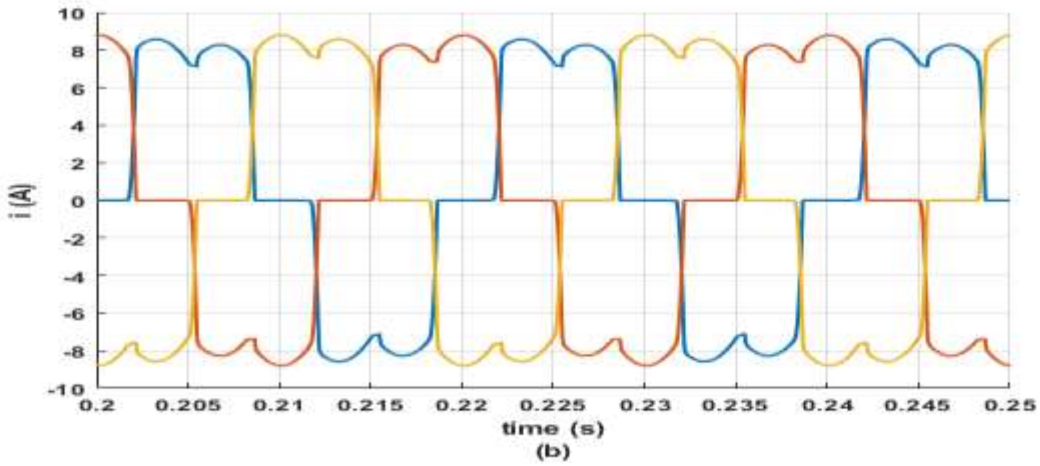

Figure II.24 Waveforms - unbalanced conditions – from top to bottom: (a) the voltages of the electrical network, (b) the source current before filtering.

Figure II.26 gives the shape of the source current after filtering, and the voltage v_{dc} across the capacitor. It can be seen that the performance of the active filter is affected by the imbalance of the electrical network, and on the other hand, the amplitude of the oscillation of the voltage v_{dc} has increased compared to the balanced case. This is mainly explained by the inadequacy of the use of the control algorithm without taking into consideration the effect of unbalance of the voltages of the source.

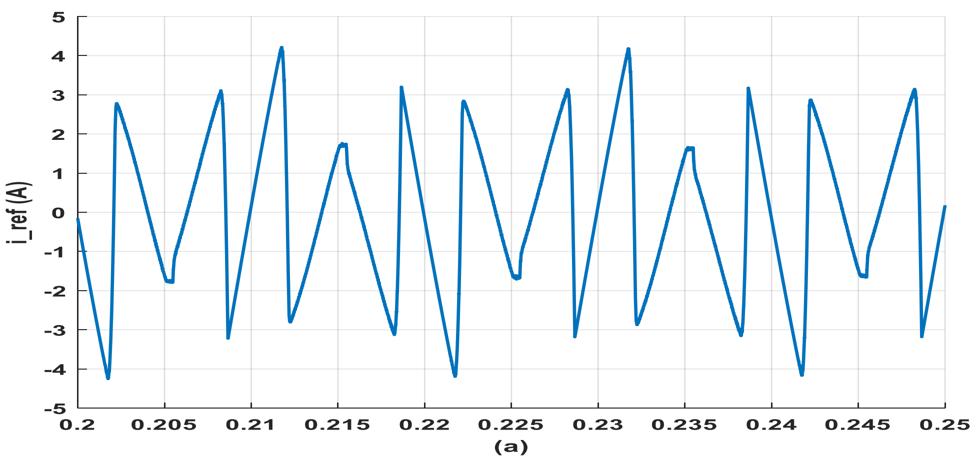

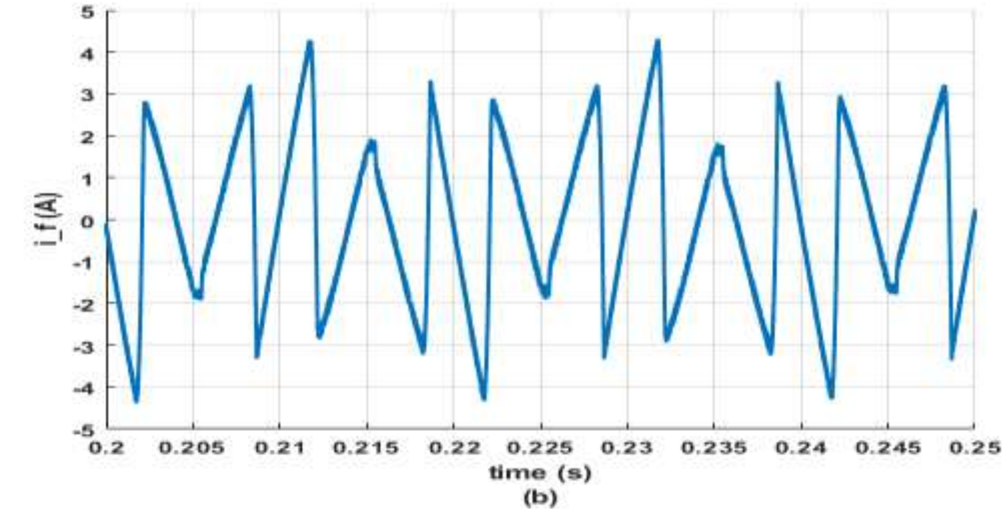

Figure II.25 Waveforms - unbalanced conditions - from top to bottom: (a) the reference current and (b) the current injected by the active filter.

In the case of an imbalance, the spectral analysis of the currents of the nonlinear load and the current compensated by the active filter are shown in the Figure II.27.

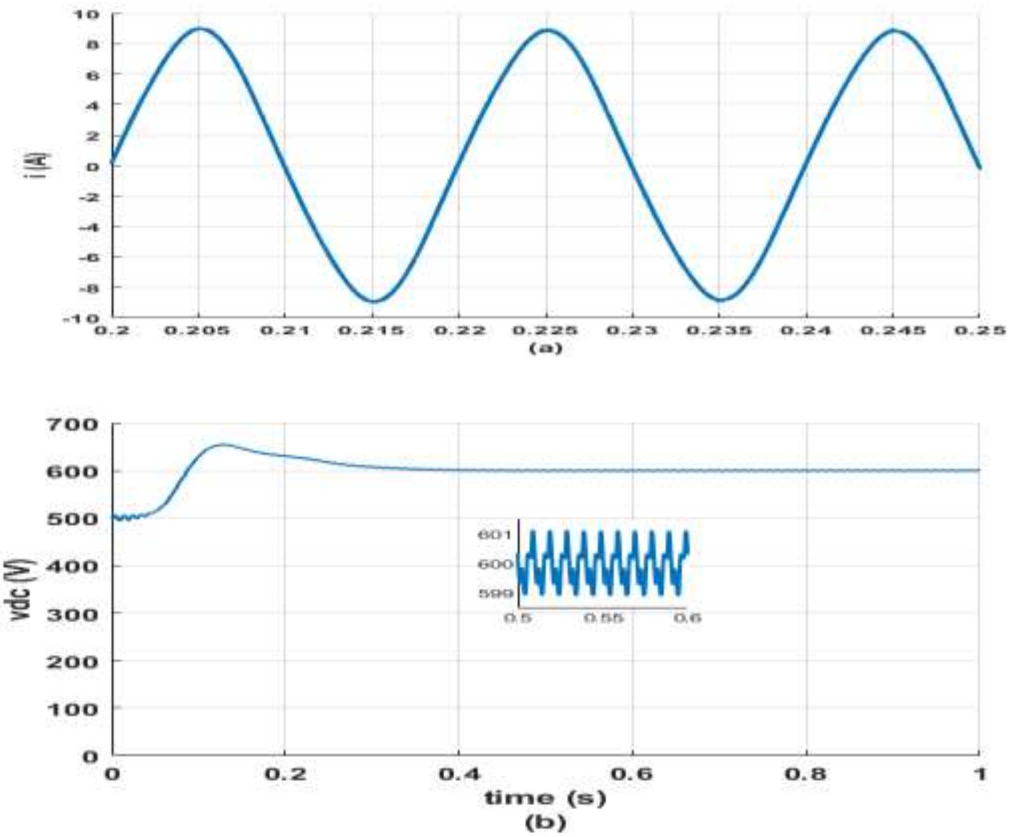

Figure II.26 Waveforms - unbalanced conditions - from top to bottom: (a) the source current after filtering and (b) DC bus voltage.

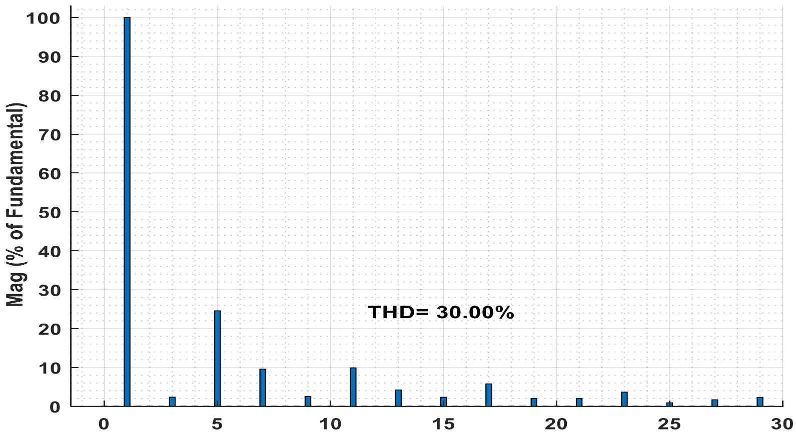

(a)

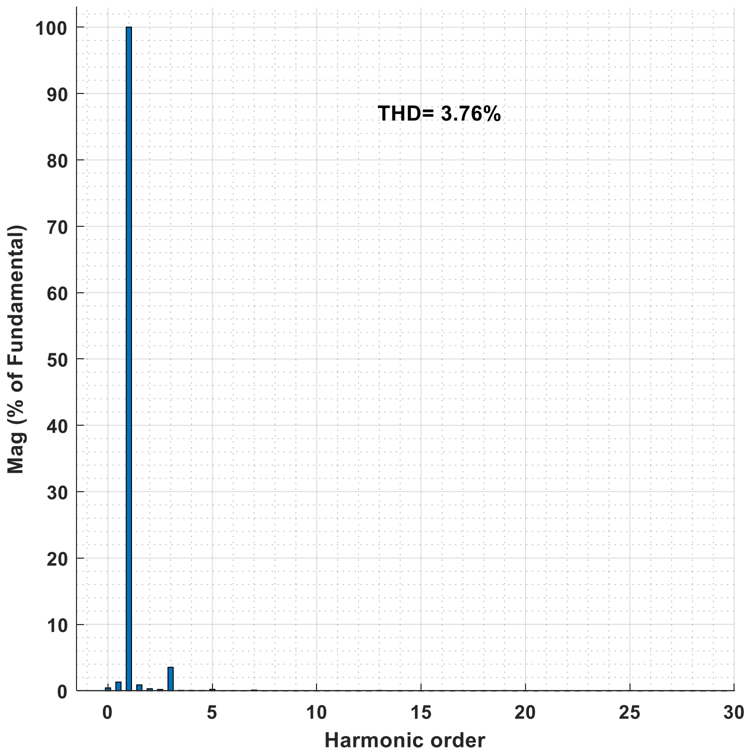

(b)

Figure II.27 Shapes of the current spectra - unbalanced conditions – from top to bottom: (a) current spectrum of the non-linear load and (b) spectrum of the filtered current.

It can be noted that the rate of odd harmonics is partially increased compared to the previous case of Figure II.23.

Indeed, in this figure the THD of the current of the nonlinear load is $30\ \%$ and the THD of the filtered current is $3.76\ \%$, therefore other measures to be taken in the case of presence in addition to pollution of the voltages of the source.

II.4.7 Harmonic currents and voltages balanced with load variation

In this paragraph, the behaviour of the parallel active filter in the case of a variation of the load is considered. Figure II.28 presents from top to bottom the supply voltages and the currents of the nonlinear load, where a variation of the load is introduced at time $t = 0.8s$. Figure II.29 shows reference currents and active filter current, and Figure II.30 shows filtered current and voltage v_{dc}. We notice that the behaviour of the filter in this case is similar to that of the first balanced case, but its behaviour differs at the level of the DC bus voltage at the instant of the variation of the load, where the DC bus regulator brings back the voltage to his reference.

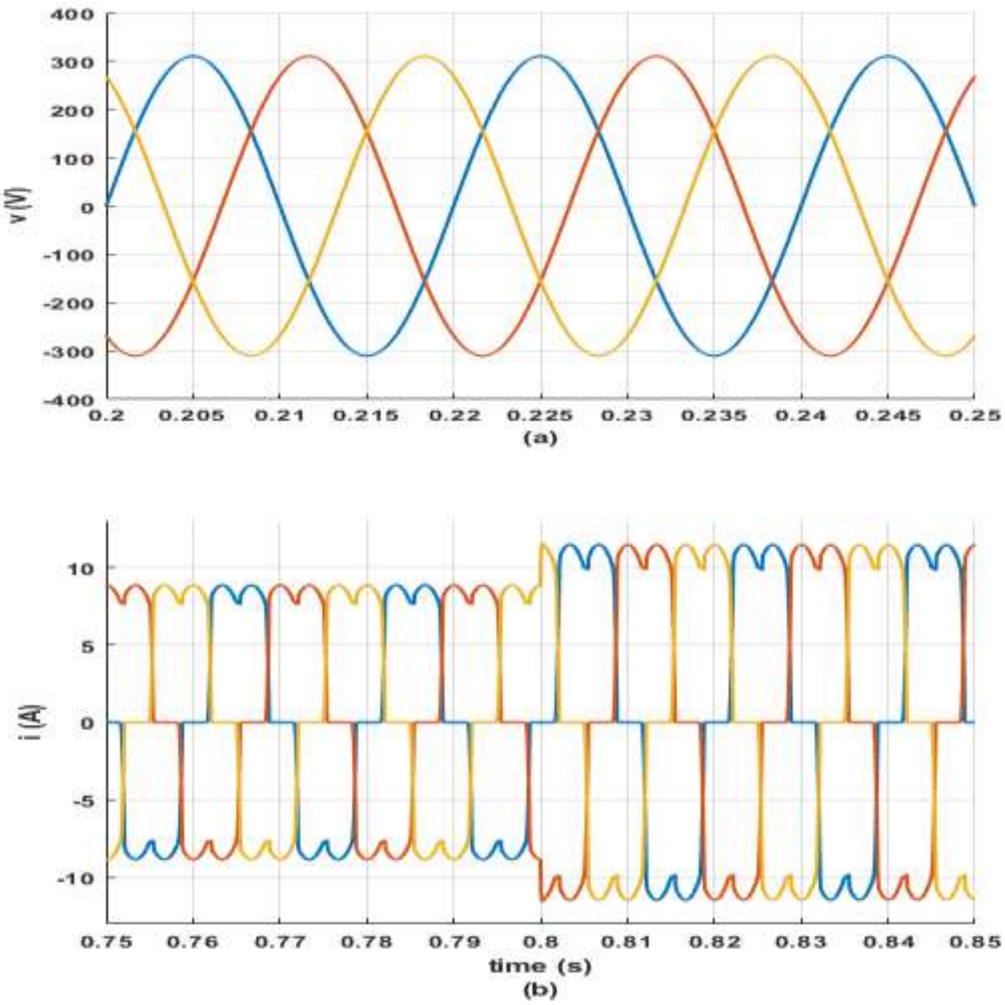

Figure II.28 Waveforms - case of a load variation - from top to bottom: (a) the voltages of the electrical network, (b) the source current before filtering.

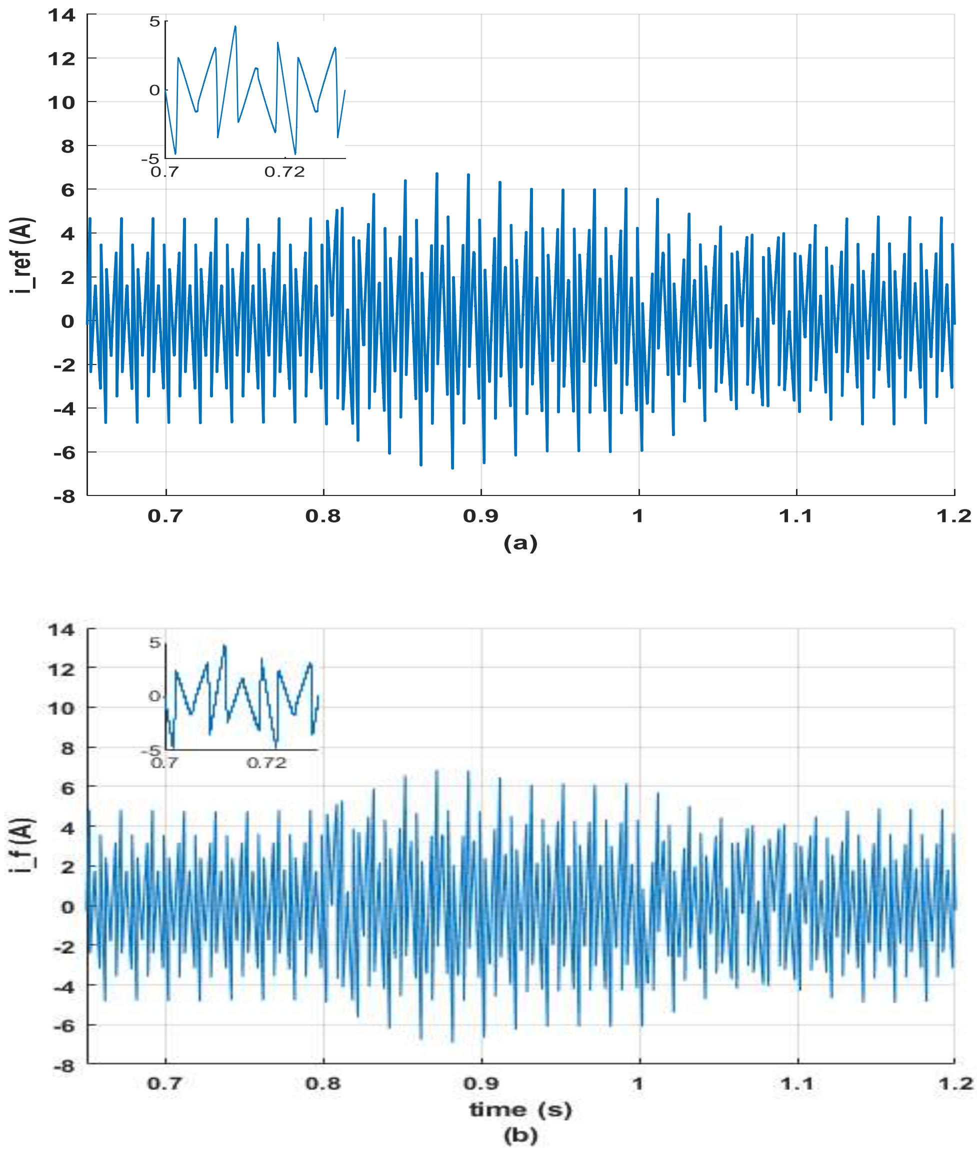

Figure II.29 Waveforms - case of a load variation - from top to bottom: (a) the reference current and (b) the current injected by the active filter.

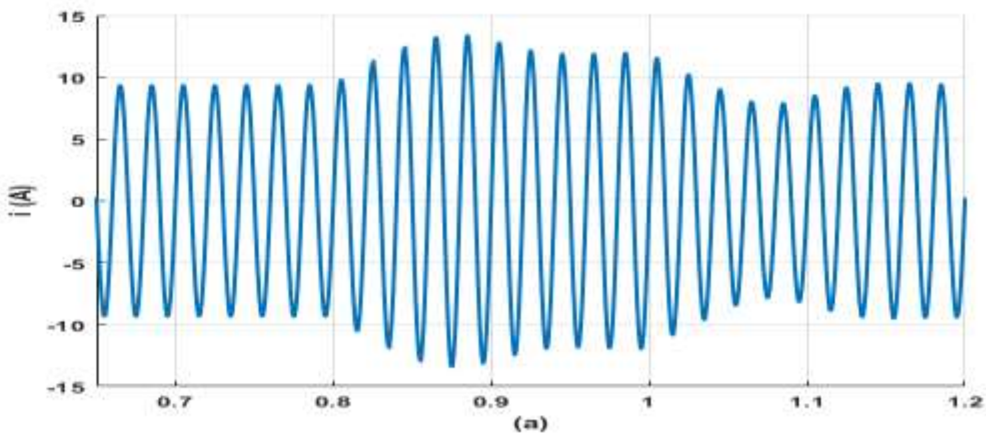

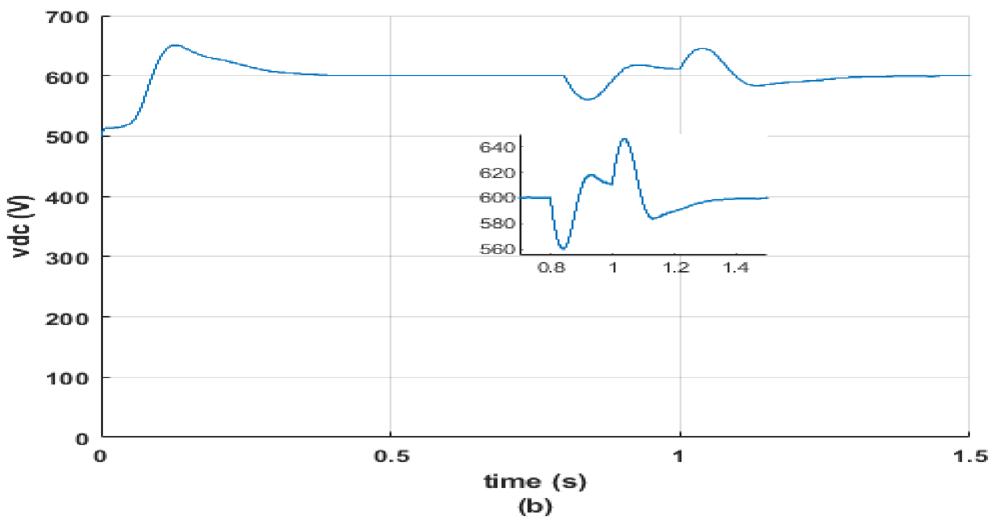

Figure II.30 Waveforms - case of a load variation - from top to bottom: (a) the source current after filtering and (b) DC bus voltage.

II.5 Influence of parameters

II.5.1 Variation of the decoupling inductance

For a constant voltage v_{dc} and a given width of the hysteresis band, the variation of the THD as a function of LF is shown in Figure II.31. It is obvious that the increase of this inductance goes to the detriment of the filtering quality.

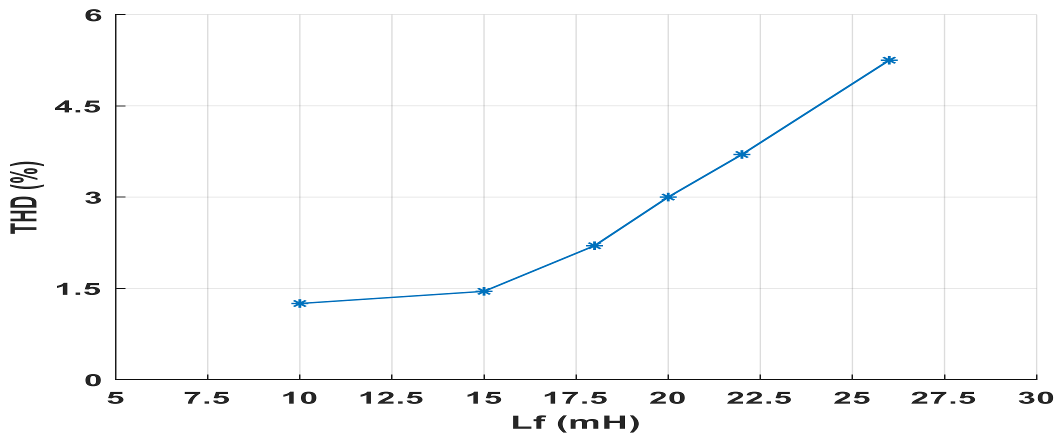

Figure II.31 Variation of the THD % according to the decoupling inductance.

II.5.2 DC bus voltage variation

For a constant decoupling inductance and a given hysteresis bandwidth, the variation curve of the THD of the filtered currents is described in Figure II.32. It can be noted that the effective reduction of the THD goes in the direction of the increase of v_{dc} . On the other hand, the reverse voltage of the power components poses a barrier to the maximum allowed value.

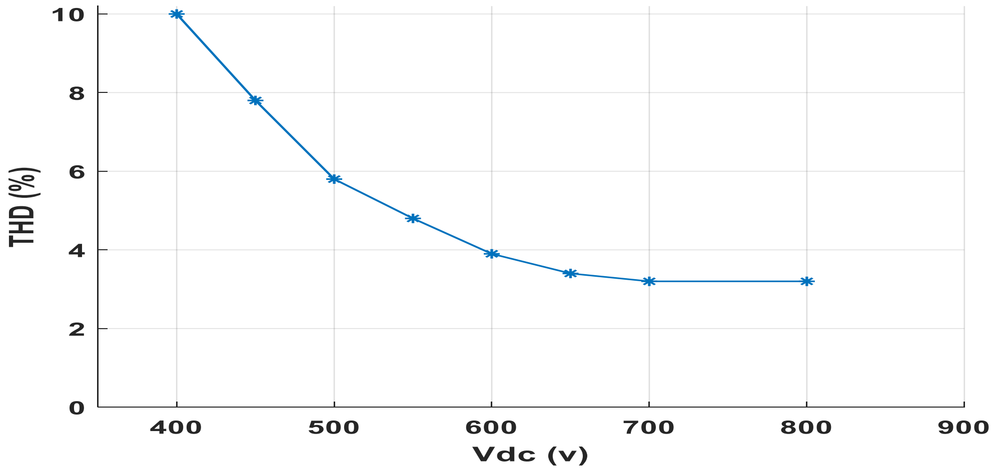

Figure II.32 Variation of THD % as a function of DC voltage.

II.5.3 Hysteresis Bandwidth Variation

Figure II.33 shows the influence of the hysteresis bandwidth on the THD of the currents in the source after filtering. It is obvious that the quality of the filtering goes in the direction of reducing the width of the hysteresis band, while signalling the frequency limit imposed by the power components.

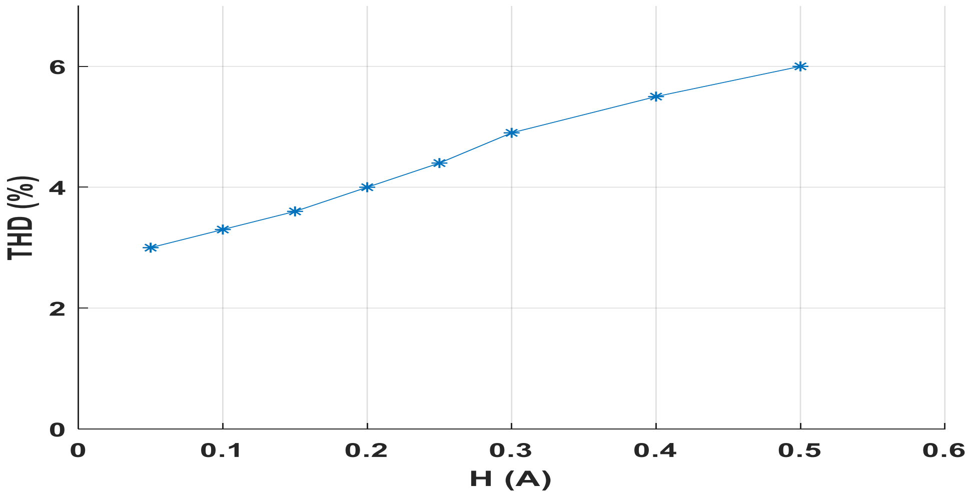

Figure II.33 Variation of the THD % according to the width of the band.

II.6 Conclusion

In this chapter, we have presented the structure of parallel active filters as well as their various constituent elements. The configuration of the power circuit, the size of the output filter parameters to reduce the ripple of the filter current is mainly due to the cut-off frequency of the power switch, the control strategy and the operating principle of the filter system.

An example of simulation was presented to demonstrate the advantages and operating principle of the APF, where the performance of the active filter is influenced by external conditions of the power grid, various sizing parameters, and control.

Chapter III :

Strategies of detecting harmonic currents

III.1 Introduction

The purpose of active power filters is to act directly and flexibly to compensate for harmonics or to reduce their impact on the power supply network. To be able to achieve this goal, the procedure for determining reference harmonic quantities must respond in real time and with accuracy to project good filter quality. Algorithms for determining the harmonic current or voltage reference are grouped in the literature into two domains, the frequency domain or the time domain [37].

III.1.1 Identification in the frequency domain

The Discrete Fourier Transform (DFT), Fast Fourier Transform (FFT), Recursive Discrete Fourier Transform (RDFT) and Kalman Filter are commonly used methods in the frequency domain. However, the large number of computation iterations and the slow response times compared to the time required for real-time filtering applications make them obsolete and draw attention to time-domain algorithms.

III.1.2 Time domain identification

Time-domain harmonic detection methods provide minimal computational speed and time compared to frequency-domain methods. Many methods have been published in the scientific literature [38], such as instantaneous power theory [39][40], synchronous reference theory [41], band pass filter-based theory, algorithm based on multivariable filter. And sliding mode-based methods [6][42]. The objective of this chapter is to present and compare the most well-known methods that satisfy the trade-off between response times and filter quality of harmonic references.

III.2 Trigonometric method (TRI-single-phase method)

The TRI-single-phase trigonometric method is based on the generation of two trigonometric functions $\cos(2.\pi.f.t)$ and $\sin(2.\pi.f.t)$ where (f) is the pre-recognized frequency of the power grid voltage [43][44]. These two functions are related to the load current (I_{L1}, I_{L2}, I_{L3}) for the extraction of the fundamental components of these currents. The method is based on the estimation of the active component I_{Lfa} and responsive I_{Lfr} of the current of each fundamental phase allows identifying the current on each phase, which allows us to regenerate the latter. Thus, to find the harmonic current generated by the load, a simple subtraction suffices.

Consider the load current (I_L) absorbed by the nonlinear load via the first phase:

$$I_L(\theta_s) = \sum_1^{\infty} I_L \sin(h\theta_s - \varphi_s) = \sum_1^{\infty} I_{L1} \sin(\theta_s - \varphi_1) + \sum_2^{\infty} I_L \sin(h\theta_s - \varphi_h) \quad \text{(III-1)}$$

With: $\theta_s = \omega t$

The fundamental component of the voltage at the connection point of the active filter to the first phase is expressed by:

$$v_{sa}(\theta_s) = v_s\sqrt{2}\sin(\theta_s) \qquad \text{(III-2)}$$

By multiplying the equation (III-1) by $\sin(\theta_s)$ *and* $\cos(\theta_s)$ we get the expressions (III-3) and (III-4) respectively:

$$I_{L1}(\theta_s)\sin(\theta_s) = \frac{I_{L1}}{2}\cos(\varphi_1) - \frac{I_{L1}}{2}\cos(2\theta_s - \varphi_1) + \sin(\theta_s)\sum_{h=2}^{\infty} I_L \sin(h\theta_s - \varphi_h) \qquad \text{(III-3)}$$

$$I_{L1}(\theta_s)\cos(\theta_s) = \frac{I_{L1}}{2}\sin(\varphi_1) + \frac{I_{L1}}{2}\cos(2\theta_s - \varphi_1) + \cos(\theta_s)\sum_{h=2}^{\infty} I_L \sin(h\theta_s - \varphi_h) \qquad \text{(III-4)}$$

The relations (III-3) and (III-4) show that only the continuous components are proportional, respectively, to the amplitude of the active fundamental current and to the amplitude of the reactive current and that the first alternating components have an equal frequency twice the network frequency. Therefore, these AC components will be filtered using a low-pass filter whose cut-off frequency is relatively low in order to prevent the low-frequency ripple from propagating to the output. However, it is unavailable to respect a good compromise between the efficient filtering of the parasitic frequencies and a fast dynamics of the extraction algorithm.

After filtering, we get:

$$\left[I_{L1}(\theta_s)\sin(\theta_s)\right]_{filtre} = \frac{I_{L1}}{2}\cos(\varphi_1) \qquad \text{(III-5)}$$

$$\left[I_{L1}(\theta_s)\cos(\theta_s)\right]_{filtre} = \frac{I_{L1}}{2}s\,in(\varphi_1) \qquad \text{(III-6)}$$

We can then reconstitute the fundamental current. Thus, by multiplying (III-5) and (III-6) respectively by $2\sin(\theta_s)$ *and* $2\cos(\theta_s)$, we deduce the following fundamental current equation:

$$I_{Lf} = I_{L1}(\theta_S)\sin(\theta_s) - I_{L1}\sin(\varphi_1) - \cos(\theta_s) = I_{Lfa} + I_{Lfr} = I_{L1}\sin(\theta_s - \varphi_1) \qquad \text{(III-7)}$$

III.2.1 Identification algorithm

The figure below illustrates the algorithm for extracting the fundamental current according to the tri-phase method.

$$I_{L1} = I_L - I_{L1f} \quad \text{(III-8)}$$

I_L : Current of the disturbed load

I_{L1f} : fundamental component of the disturbed current

I_{L1} : harmonic component of the disturbed current

This method is applicable to single-phase and three-phase systems and does not require mains voltage.

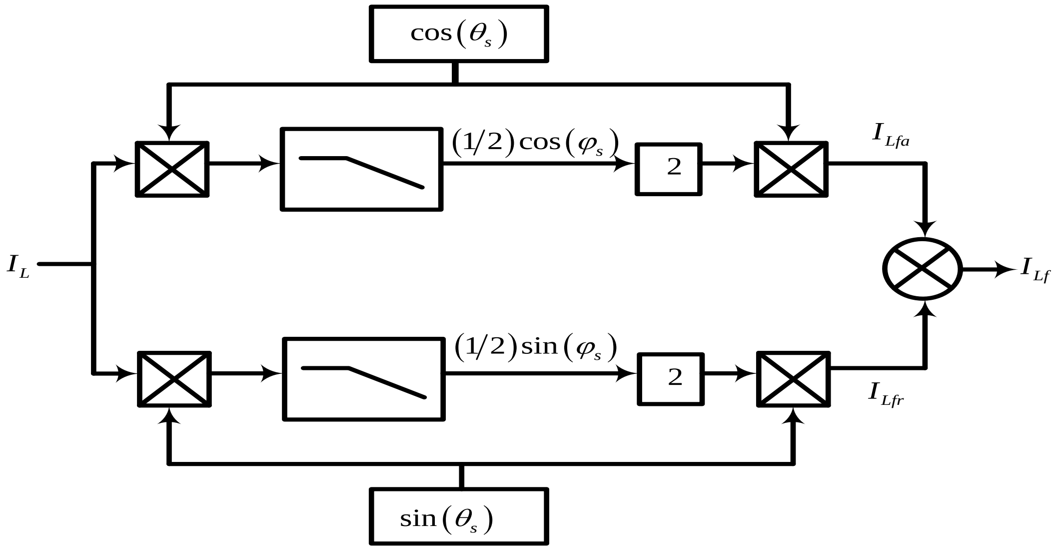

Figure III.1 Fundamental extraction algorithm by TRI-single-phase method

III.3 Instantaneous active and reactive power method (IARP)

III.3.1 Identification of harmonics by the instantaneous active and reactive power method

The instantaneous active and reactive power method (frequently called pq method) was introduced by HIROFUMI Akagi [45]. Its principle is based on the transition from three-phase systems consisting of phase-to-neutral voltages and line currents, to a two-phase system (αβ reference) using the Concordia transformation, in order to calculate the instantaneous powers. Then, the use either of a low pass filter, or of a high pass filter in order to eliminate the DC component of the active power in order to keep only the harmonic component of the signal knowing that the fundamental component is transformed into a DC component and the harmonic components into AC components.

The Concordia transformation, defined by equation (III-9), allows the voltages and currents to be expressed by the following relation

$$[c_{32}] = \sqrt{\frac{2}{3}} \begin{bmatrix} \frac{1}{\sqrt{2}} & \frac{1}{\sqrt{2}} & \frac{1}{\sqrt{2}} \\ 1 & -\frac{1}{2} & -\frac{1}{2} \\ 0 & \frac{\sqrt{3}}{2} & -\frac{\sqrt{3}}{2} \end{bmatrix} \quad \text{(III-9)}$$

$$\begin{bmatrix} v_0 \\ v_{s\alpha} \\ v_{s\beta} \end{bmatrix} = [c_{32}] \begin{bmatrix} v_{sa} \\ v_{sb} \\ v_{sc} \end{bmatrix} \quad \text{(III-10)}$$

$$\begin{bmatrix} i_0 \\ i_{s\alpha} \\ i_{s\beta} \end{bmatrix} = [c_{32}] \begin{bmatrix} i_{sa} \\ i_{sb} \\ i_{sc} \end{bmatrix} \quad \text{(III-11)}$$

With:

v_α, v_β *and* I_α, I_β The orthogonal components in the reference α, β respectively, of the voltages of the electrical network v_s and of the currents absorbed by the non-linear loads I_L .

And, the $(v_0$ *and* $i_0)$ components with index (0) represent the zero-sequence components of the three-phase system

The instantaneous active power $P(t)$ is defined by the following relationship:

$$P(t) = v_{s1} I_{L1} + v_{s2} I_{L2} + v_{s3} I_{L3} \quad \text{(III-12)}$$

This expression can be written in the stationary frame by:

$$\begin{cases} P(t) = v_{s\alpha} I_{L\alpha} + v_{s\beta} I_{L\beta} \\ P_0(t) = v_{s0} I_{L0} \end{cases} \quad \text{(III-13)}$$

With $P(t)$ the instantaneous active power, $P_0(t)$ the instantaneous zero-sequence power. The advantage of the transformation in the stationary frame is the separation of the homo polar sequences from the three-phase current or voltage system. In the same way, the instantaneous reactive power can be written in the following form:

$$q(t) = -\frac{1}{\sqrt{3}}\left[\left(v_{s1} - v_{s2}\right) I_{L3} + \left(v_{s2} - v_{s3}\right) I_{L1} + \left(v_{s3} - v_{s1}\right) I_{L2}\right] = \left(v_{s\alpha} I_{L\beta} - v_{s\beta} I_{L\alpha}\right) \qquad \text{(III-14)}$$

Power q has a broader meaning than usual reactive power. Indeed, unlike reactive power, which only considers the fundamental frequency, reactive power takes into account all the harmonic components of current and voltage. This is why it is given another name (reactive power) with the reactive volt-ampere unit.

From the relations (III-13) and (III-14) we can establish the following matrix relation:

$$\begin{bmatrix} p \\ q \end{bmatrix} = \begin{bmatrix} v_{s\alpha} & v_{s\beta} \\ -v_{s\beta} & v_{s\alpha} \end{bmatrix} \begin{bmatrix} i_{l\alpha} \\ i_{l\beta} \end{bmatrix} \qquad \text{(III-15)}$$

In the general case, each of the powers p and q has a continuous part and an alternating part, which allows us to write the expression below:

$$\begin{cases} p = \bar{p} + \tilde{p} \\ q = \bar{q} + \tilde{q} \end{cases} \qquad \text{(III-16)}$$

With:

$\bar{P}$: DC power of the active fundamental component of current and voltage;

$\bar{q}$: The continuous power of the reactive fundamental component of current and voltage;

$\tilde{P}$ *and* $\tilde{q}$: The alternating powers corresponding to the sum of the disturbing components of the current and the voltage;

The continued powers can be separated by a second-order low-pass filter. However, the alternating components are obtained directly by a simple subtraction of the continued components just obtained from the active and reactive powers, as shown in Figure III.2.

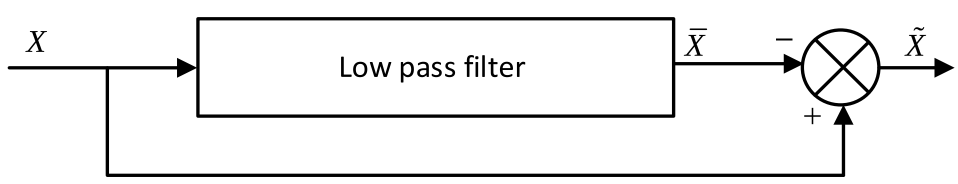

Figure III.2 Diagram representing the principle of power separation

III.3.2 Calculation of harmonic currents

By reversing the relation (III-15), we can recalculate the currents in the stationary frame as shown in the following equation [46]:

$$\begin{bmatrix} I_{L\alpha} \\ I_{L\beta} \end{bmatrix} = \frac{1}{v_{s\alpha}^2 + v_{s\beta}^2} \begin{bmatrix} v_{s\alpha} & -v_{s\beta} \\ v_{s\beta} & v_{s\alpha} \end{bmatrix} \begin{bmatrix} P_L \\ q_L \end{bmatrix} \tag{III-17}$$

From equations (III-16) and (III-17), the current in the stationary frame is broken down into three components: activates, reactivates the harmonics. As shown by the following relationship:

$$\begin{bmatrix} I_{L\alpha} \\ I_{L\beta} \end{bmatrix} = \underbrace{\frac{1}{\Delta} \begin{bmatrix} v_{s\alpha} & -v_{s\beta} \\ v_{s\beta} & v_{s\alpha} \end{bmatrix} \begin{bmatrix} \bar{P}_L \\ 0 \end{bmatrix}}_{\text{active current}} + \underbrace{\frac{1}{\Delta} \begin{bmatrix} v_{s\alpha} & -v_{s\beta} \\ v_{s\beta} & v_{s\alpha} \end{bmatrix} \begin{bmatrix} 0 \\ \bar{q} \end{bmatrix}}_{\text{reactive current}} + \underbrace{\frac{1}{\Delta} \begin{bmatrix} v_{s\alpha} & -v_{s\beta} \\ v_{s\beta} & v_{s\alpha} \end{bmatrix} \begin{bmatrix} \tilde{P}_L \\ \tilde{q}_L \end{bmatrix}}_{\text{Current harmonics}} \tag{III-18}$$

With $\Delta = \dfrac{1}{v_{s\alpha}^2 + v_{s\beta}^2}$ assumed to be constant if we consider the assumption that network voltages are sinusoidal and balanced. The expression (III-18) shows that the identification of the various components of the current in the stationary frame amounts to separating continuous terms from the instantaneous active and reactive powers. The harmonic currents (identified currents) are the references of the I_f^* filter and are calculated from the inverse Concordia transformation defined by:

$$\begin{bmatrix} I_{fa}^* \\ I_{fb}^* \\ I_{fc}^* \end{bmatrix} = \sqrt{\frac{2}{3}} \begin{bmatrix} 1 & 0 \\ -\frac{1}{2} & \frac{\sqrt{3}}{2} \\ -\frac{1}{2} & -\frac{\sqrt{3}}{2} \end{bmatrix} \begin{bmatrix} I_{L\alpha} \\ I_{L\beta} \end{bmatrix} \tag{III-19}$$

Where $I_{L\alpha}$ and $I_{L\beta}$ are the harmonic currents calculated from relation (III-18).

Figure III.3 shows the block diagram for the calculation of the reference currents corresponding to the PQ theory.

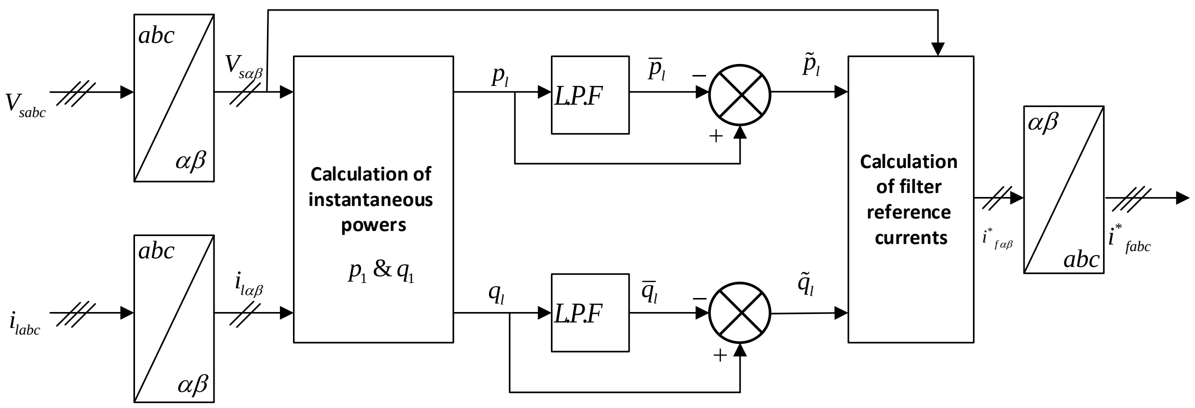

Figure III.3 Schematic diagram of the instantaneous power method.

The active and reactive powers method uses low-pass filters to separate the active and reactive power components and requires a system for extracting direct voltage from the electrical network.

- It is not applicable for single-phase systems.
- Mains voltage must be healthy (sinusoidal and balanced).

III.4 Synchronous Repository Method (SR)

In the synchronous reference method [41], the three-phase currents of the load are expressed in the dq system. If θ is the transformation angle, the transformation is defined by:

$$\begin{bmatrix} I_{Ld} \\ I_{Lq} \\ I_{L0} \end{bmatrix} = \sqrt{\frac{2}{3}} \begin{bmatrix} \cos(\theta) & \cos\left(\theta - \frac{2\pi}{3}\right) & \cos\left(\theta + \frac{2\pi}{3}\right) \\ -\sin(\theta) & -\sin\left(\theta - \frac{2\pi}{3}\right) & -\sin\left(\theta + \frac{2\pi}{3}\right) \\ \frac{1}{\sqrt{2}} & \frac{1}{\sqrt{2}} & \frac{1}{\sqrt{2}} \end{bmatrix} \begin{bmatrix} I_{La} \\ I_{Lb} \\ I_{Lc} \end{bmatrix} \quad \text{(III-20)}$$

The synchronous frame method uses in each phase a phase-locked loop, PLL (Phase Locked Loop), to detect the angular position θ of the synchronous frame dq. The latter is synchronized with the three-phase voltages and rotates at a constant speed.

By exploiting the $\cos(\theta)$ *and* $\sin(\theta)$ signals drawn from the "fundamental" grid voltage, we obtain the expression for the currents in the d-q system rotating at the pulsation of the fundamental component of the grid voltage:

$$\begin{bmatrix} I_{Ld} \\ I_{Lq} \end{bmatrix} = \begin{bmatrix} \sin(\hat{\theta}) & -\cos(\hat{\theta}) \\ \cos(\hat{\theta}) & \sin(\hat{\theta}) \end{bmatrix} \begin{bmatrix} I_{\alpha} \\ I_{\beta} \end{bmatrix} = \begin{bmatrix} I_{dc} \\ I_{qc} \end{bmatrix} + \begin{bmatrix} I_{dh} \\ I_{qh} \end{bmatrix} \quad \text{(III-21)}$$

Either

$$\begin{bmatrix} I_{Ld} \\ I_{Lq} \end{bmatrix} = \begin{bmatrix} \sin(\hat{\theta}) & \cos(\hat{\theta}) \\ -\cos(\hat{\theta}) & \sin(\hat{\theta}) \end{bmatrix} \begin{bmatrix} I_{dc} \\ I_{qc} \end{bmatrix} + \begin{bmatrix} \sin(\hat{\theta}) & \cos(\hat{\theta}) \\ -\cos(\hat{\theta}) & \sin(\hat{\theta}) \end{bmatrix} \begin{bmatrix} I_{dh} \\ I_{qh} \end{bmatrix} \quad \text{(III-22)}$$

Where, I_{dc} and I_{qc} are continuous components, I_{dh} and I_{qh} are pulsating components, (harmonic). The separation of I_{dc} and I_{qc} from the components I_{dh} and I_{qh} is done by means of a low-pass filter.

The harmonic components in the α-β reference are calculated by the following expression:

$$\begin{bmatrix} I_{\alpha h} \\ I_{\beta h} \end{bmatrix} \begin{bmatrix} \sin(\hat{\theta}) & -\cos(\hat{\theta}) \\ \cos(\hat{\theta}) & \sin(\hat{\theta}) \end{bmatrix}^{-1} \begin{bmatrix} I_{dh} \\ I_{qh} \end{bmatrix} = \begin{bmatrix} \sin(\hat{\theta}) & \cos(\hat{\theta}) \\ -\cos(\hat{\theta}) & \sin(\hat{\theta}) \end{bmatrix} \begin{bmatrix} I_{dh} \\ I_{qh} \end{bmatrix} \tag{III-23}$$

Concordia's inverse transformation makes it possible to trace harmonic currents (balanced or unbalanced):

$$\begin{bmatrix} I_{Lah} \\ I_{Lbh} \\ I_{Lch} \end{bmatrix} = \sqrt{\frac{2}{3}} \begin{bmatrix} 1 & 0 \\ -\frac{1}{2} & \frac{\sqrt{3}}{2} \\ -\frac{1}{2} & -\frac{\sqrt{3}}{2} \end{bmatrix} \begin{bmatrix} I_{\alpha h} \\ I_{\beta h} \end{bmatrix} \tag{III-24}$$

The algorithm for identifying harmonic currents using the synchronous reference method is shown schematically in Figure III.4.

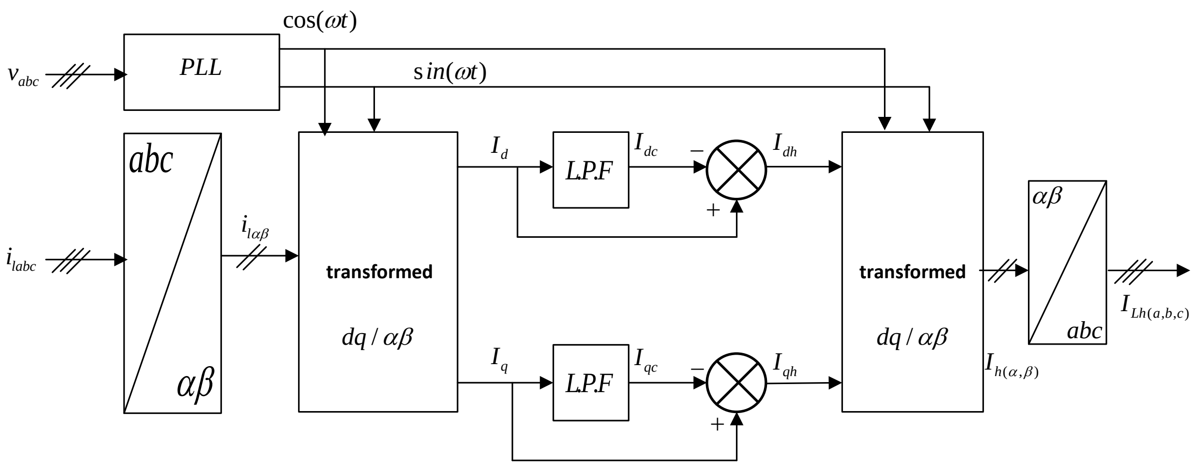

Figure III.4 Principle of identification of harmonics by the SRF method.

III.5 Simulation results

In this part, the identification methods considered are applied in the case of balanced nonlinear loads. Simulation results based on Matlab Simulink software are presented and discussed.

III.5.1 Balanced non-linear three-phase load

The phase voltages of the electrical network as well as the phase currents of the balanced non-linear three-phase load are presented in the Figure III.5. It can be seen that despite the voltages being sinusoidal, the load currents are distorted and therefore the presence of harmonics.

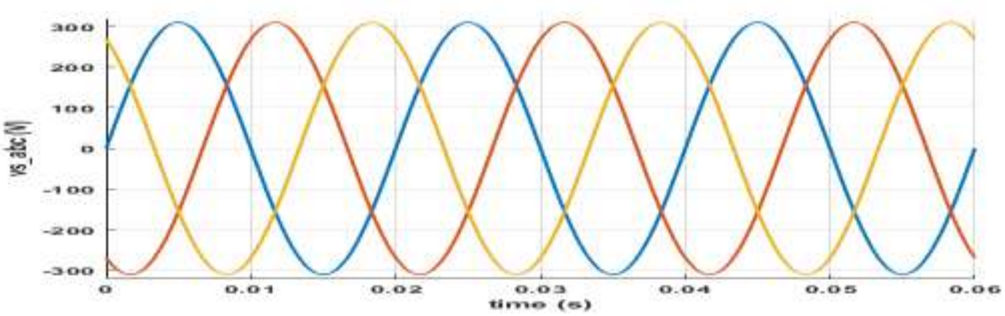

(a)

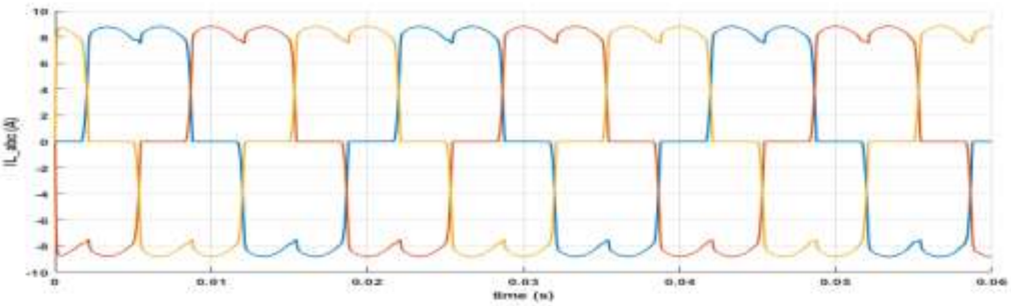

(b)

Figure III.5 Balanced non-linear load voltage and current.

III.5.2 Trigonometric method (TRI-single-phase method)

The three-phase harmonic currents identified present the same waveform with a phase shift of 120° with respect to each other, Figure III.6. The fundamental three-phase currents identified in Figure III.6-a are almost sinusoidal of the same amplitude with a phase shift of 120° with respect to each other. The harmonic currents identified in phases a, b, c of the load are presented in Figure III.6-b, c and d

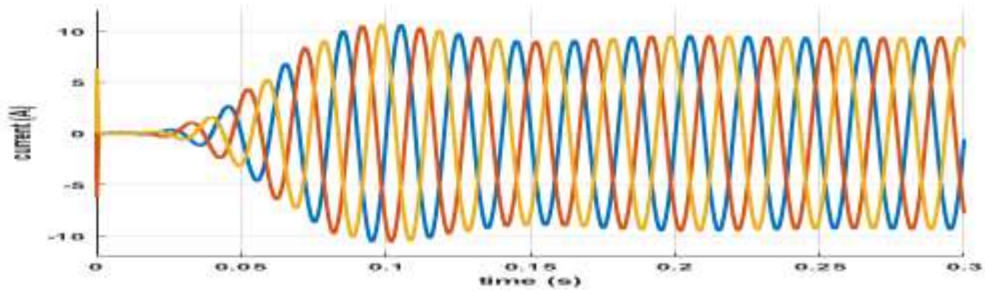

(a)

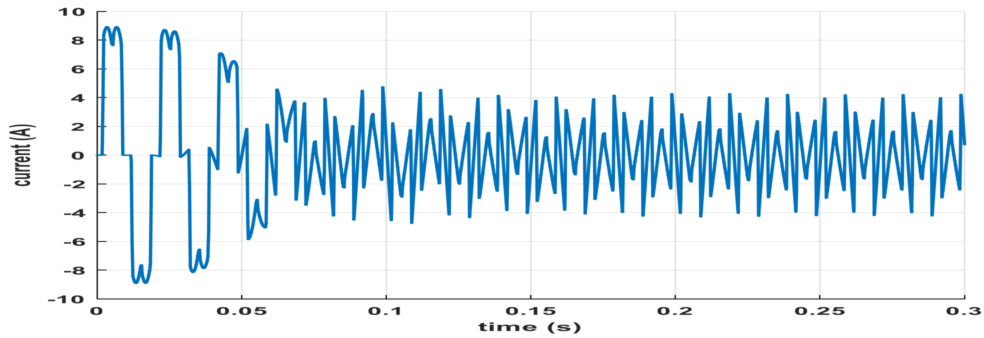

(b)

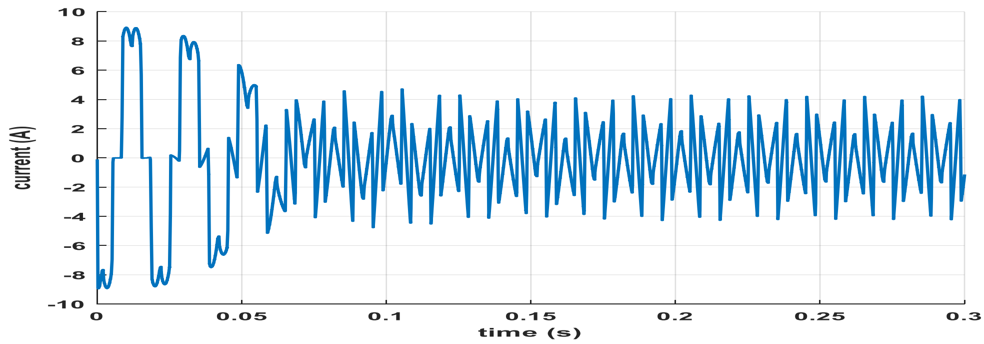

(c)

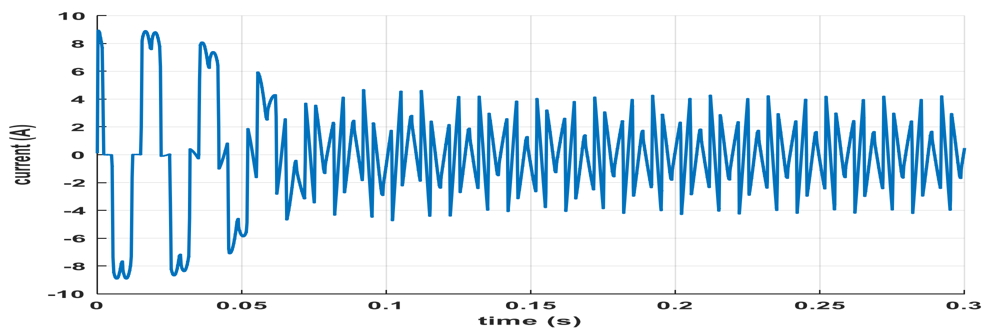

(d)

Figure III.6 Harmonic currents and fundamental components identified by the trigonometric method.

III.5.3 Instantaneous active and reactive power method (IARP)

Figure III.7 presents the phase voltages as well as the currents of the balanced three-phase non-linear load in the reference (α, β) and the active power with its average value and the reactive power. The voltages V_α *and* V_β are sinusoidal and two-phase (they are 90° out of phase). The currents i_α *and* i_β are polluted and diphasic. The active power p is pulsating around its average value p_m. The reactive power is pulsating around zero (its average value is zero) because the three-phase diode rectifier PD3 does not consume reactive energy (for each phase, the network voltage and the polluted load current are in phase).

The three-phase harmonic currents identified present the same waveform with a phase shift of 120° with respect to each other, Figure III.8. They are similar to the currents identified by the previous method.

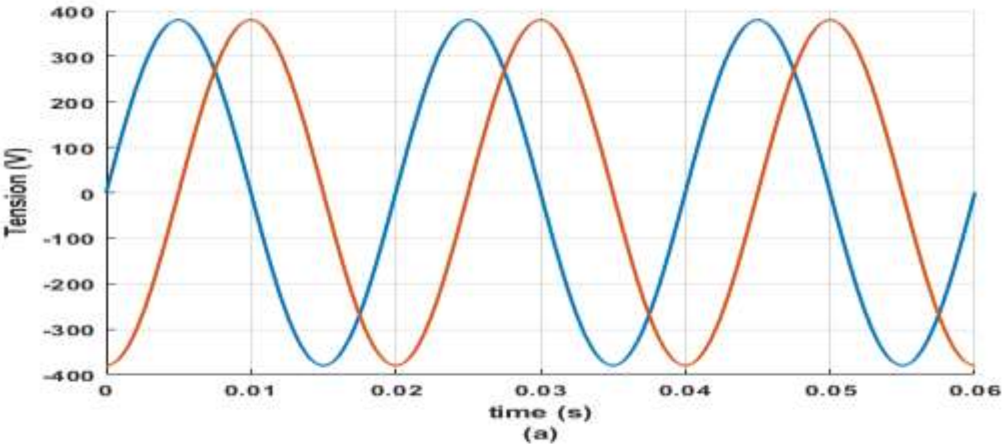

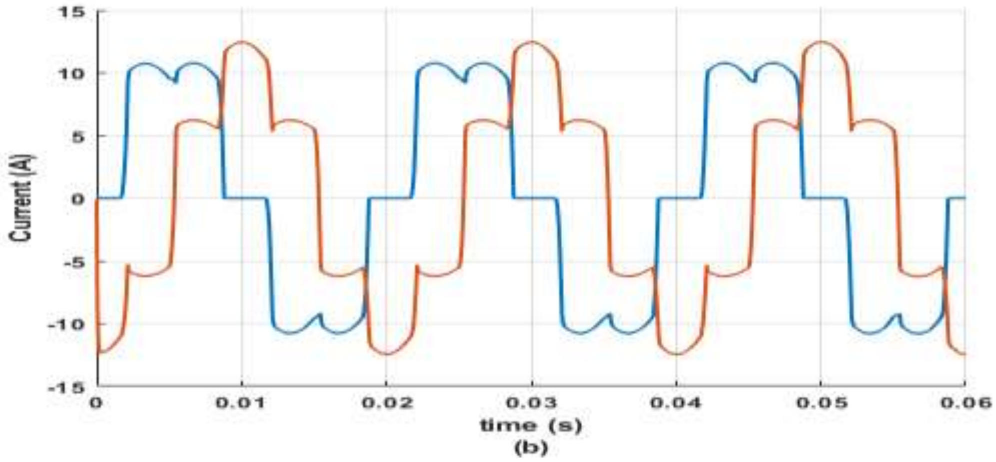

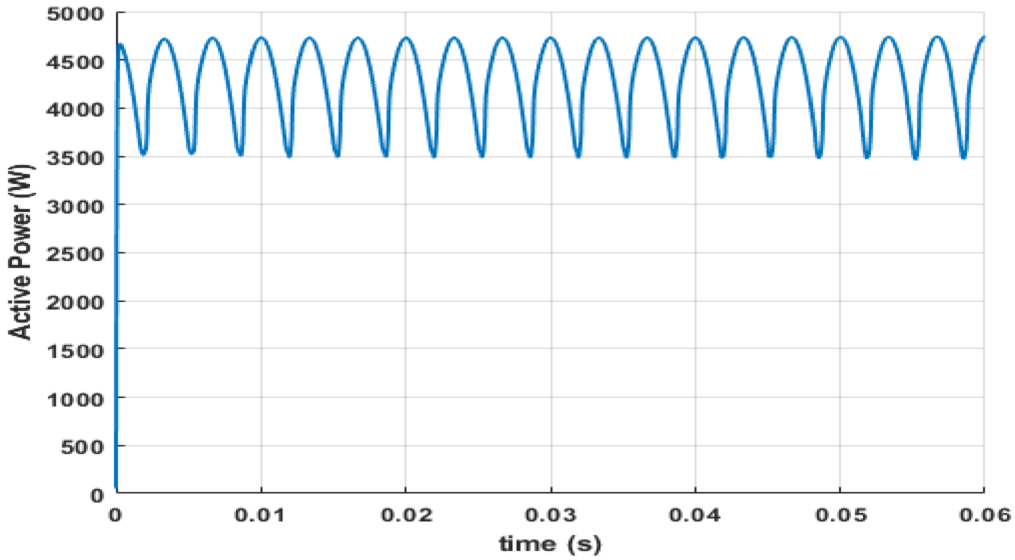

(c)

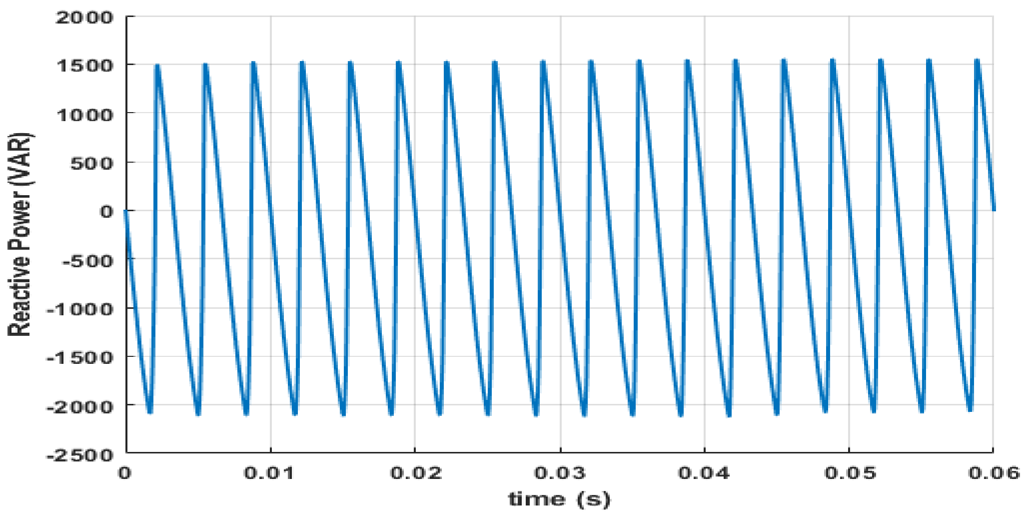

(d)

Figure III.7 (a) Phase voltages of the electrical network and (b) three-phase load current in the Concordia benchmark, (c) active power (W) and its average value and (d) reactive power (VAR).

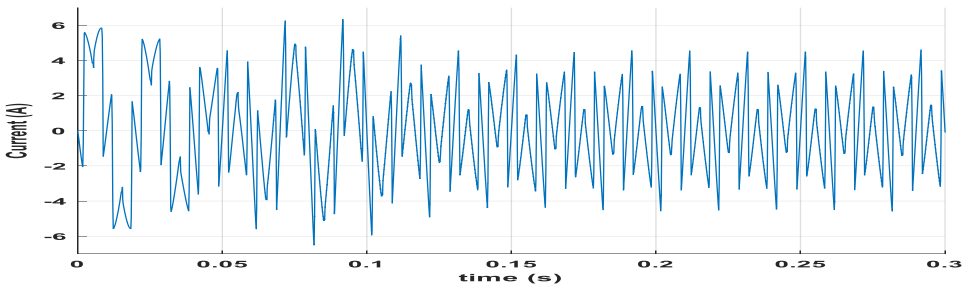

(a)

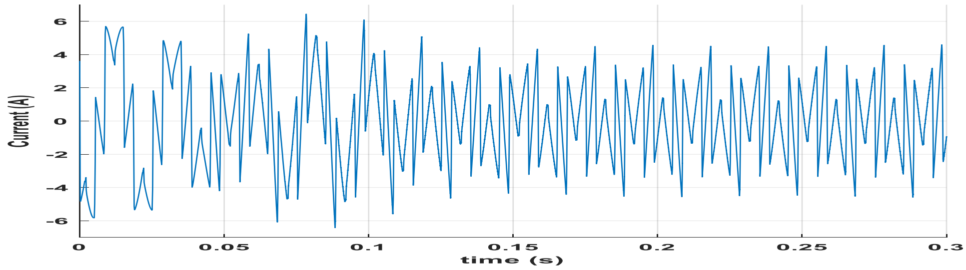

(b)

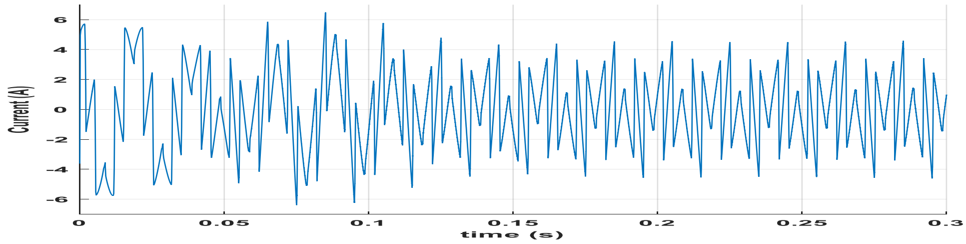

(c)

Figure III.8 Three-phase harmonic currents identified by the instantaneous active and reactive power method.

III.5.4 Synchronous Repository Method (SR)

In Figure III.9 are presented the load currents in the reference dp their average values and harmonic components in the reference dp the current i_d is a pulsating current oscillating around its average value i_{dm}. Similarly, the current i_q is a pulsating current oscillating around its mean value i_{qm}.

The three-phase harmonic currents identified present the same waveform with a phase shift of $120°$ with respect to each other, Figure III.10. They are similar to the currents identified by the two previous methods.

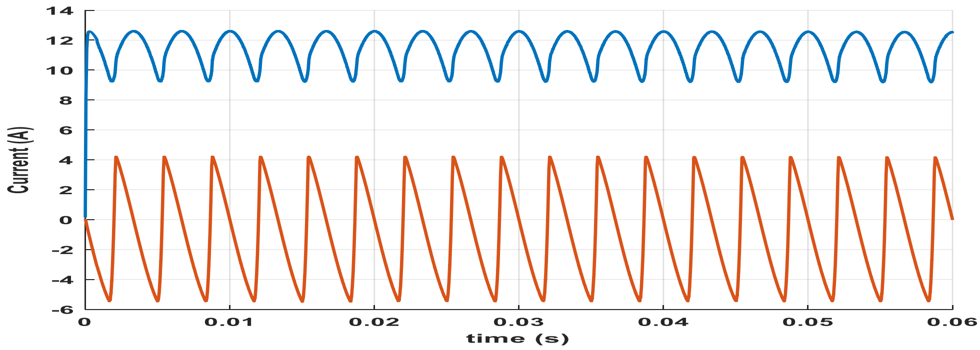

(a)

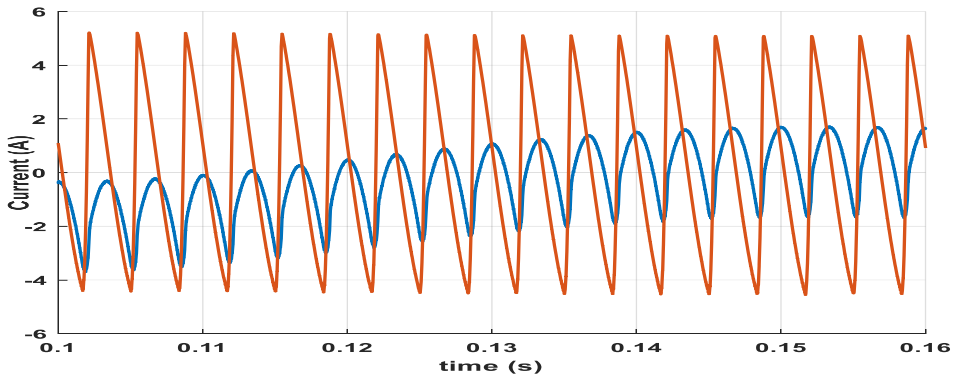

(b)

Figure III.9 Load currents in the Ref (DQ).

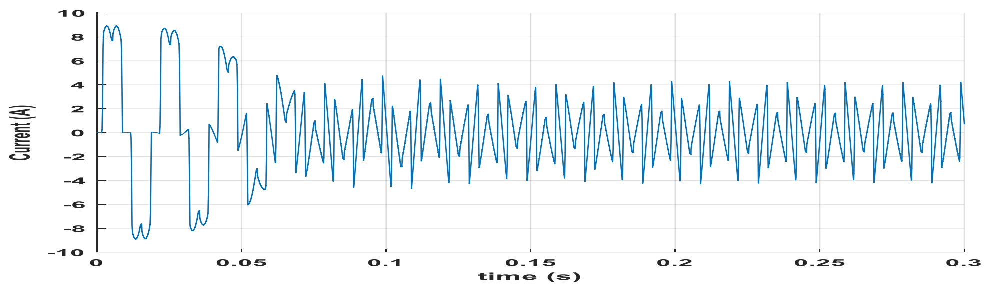

(a)

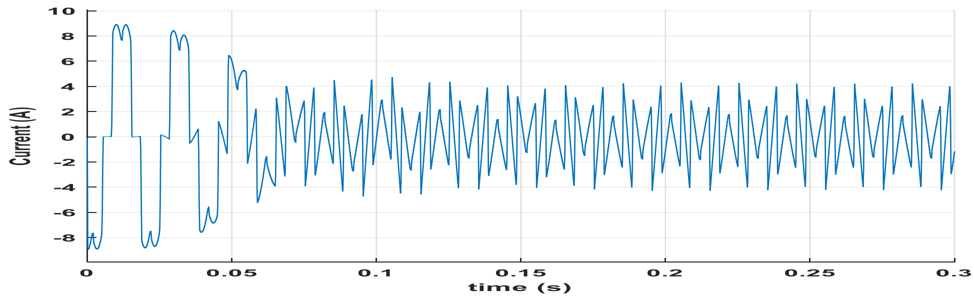

(b)

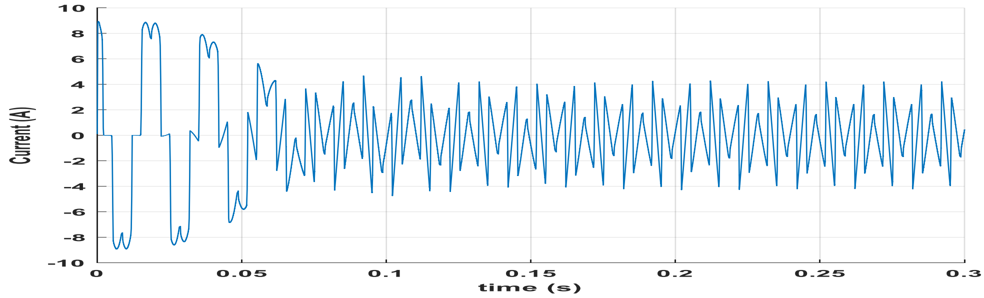

(c)

Figure III.10 Three-phase harmonic currents identified by the synchronous reference method.

III.6 Comparison of methods

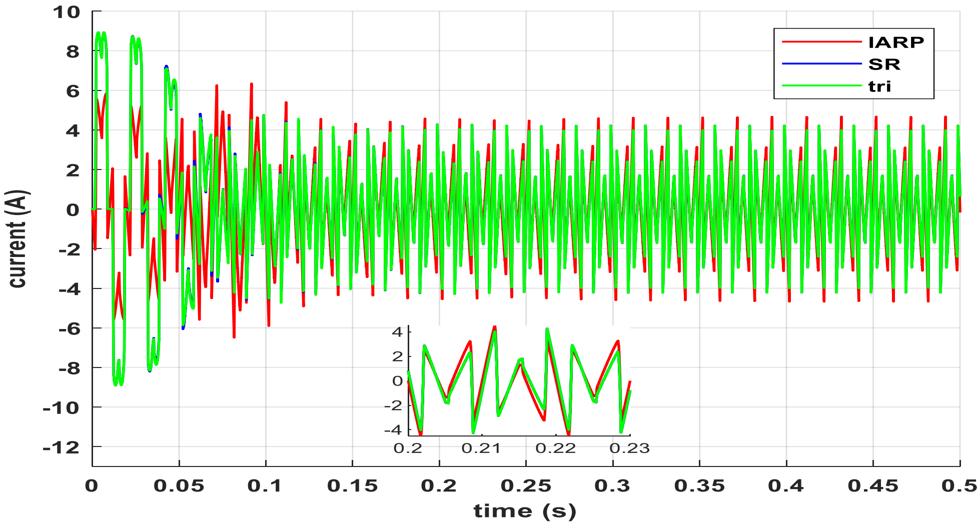

Figure III.11 Comparison of Method Outcomes.

Figure III.11 presents a zoom between the instants $0.2-0.23$sec of the superimposition of the three methods. So, we notice that the results are close.

The simulation of the methods considered for the identification of balanced three-phase harmonic currents made it possible to define the ability of each method to identify the harmonic current and the unbalance current.

III.7 Conclusion

The effectiveness of harmonic identification is crucial for the optimal performance of compensation systems based on active filters. Even the most efficient control system cannot adequately correct distortions if the parasitic harmonics are inaccurately identified. Three different identification methods for extracting harmonic currents from those absorbed by nonlinear loads have been analyzed and compared. The analysis indicates that these methods exhibit nearly identical performance in terms of their ability to identify harmonic currents. This suggests that while the choice of method may not significantly impact overall performance, precise harmonic identification remains essential for achieving effective compensation.

Chapter IV :

Control of Z-source inverter

IV.1 INTRODUCTION

The use of inverters in industry has become a very wide field, especially multi-level inverters because they give a noticeable improvement in the spectral quality of the signal curve generated compared to conventional inverters therefore, it has attracted great interest from researchers, Especially on the part of developing control strategy, as industrial equipment increasingly uses variable speed motors, these inverters are especially widely used to control alternative current and the unbroken supply of energy. Inverters are being fed by a direct voltage source DC, or Z-source or PV+ rectifier DC-DC where we find that the Z-source inverters is one of the most apparent structures in the field of power electronics, as it has a wide range of applications. for example, it is used in special power supplies and variable speed engines of hybrid electric vehicles and many more [47].

The Z-source converter (ZSC) represents a novel approach in power conversion, boasting distinctive attributes capable of addressing the constraints associated with both Voltage Source Inverters (VSI) and Current Source Inverters (CSI) [48]. Illustrated in Figure IV.1 the ZSC is depicted as a 3-phase DC/AC converter (inverter). While the primary application of the Z-source topology is DC/AC conversion, it also finds utility in AC/DC and AC/AC power conversions [49][50]. The X-shaped impedance, constituting the Z-source network, comprises two split inductors and two capacitors, serving to establish coupling between the DC source and the inverter bridge.

The Z-source inverter (ZSI) possesses a distinctive buck-boost capability, allowing for an output voltage range theoretically spanning from zero to infinity, regardless of the input voltage. This capability is achieved through the utilization of a switching state known as the "shoot-through" state, which is not permissible in conventional Voltage Source Inverters (VSI) [51]. The shoot-through state occurs when both upper and lower switches of a phase leg are simultaneously turned on. In contrast to the conventional VSI switching pattern, which comprises eight permissible switching states, the ZSI introduces a unique configuration. Six of these states, termed the "active" states, enable the load to experience the input voltage, while the remaining two states, referred to as the "zero" states, involve either all upper or all lower switches being activated, resulting in the load experiencing zero voltage.

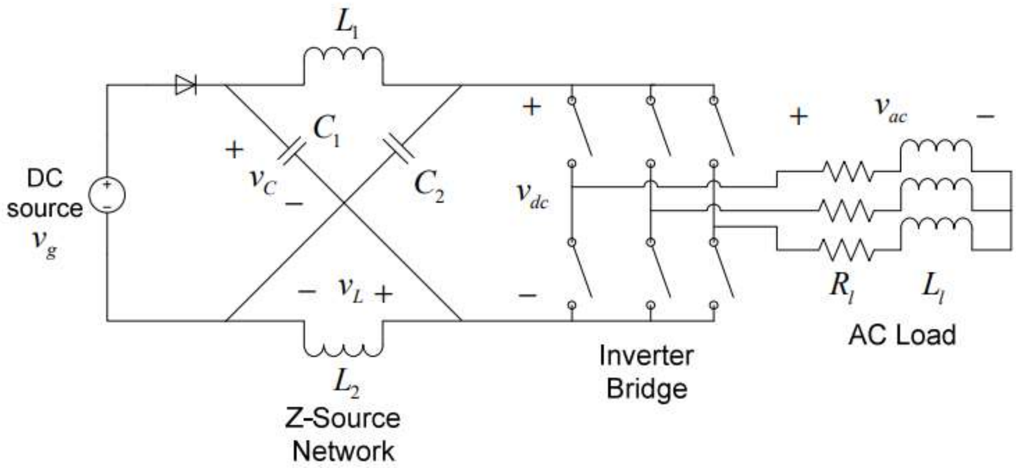

Figure IV.1 ZSC implemented as a three-phase inverter (ZSI).

Figure IV.2-a displays the carrier-based Pulse Width Modulation (PWM) switching pattern utilized in a Voltage Source Inverter (VSI). In this method, the reference signals for the three-phase voltages are compared to a triangular carrier signal. If a reference signal exceeds the carrier signal, the upper switch in the corresponding phase leg is activated while the lower switch in the same phase leg is deactivated, and vice versa. All eight permissible switching states of a VSI, including the two zero states, can be identified from Figure IV.2-a. The first zero state occurs when the carrier wave surpasses all reference signals, leading to the activation of all upper leg switches and deactivation of all lower leg switches. Conversely, the second zero state arises when the carrier wave falls below all reference signals

The incorporation of the shoot-through state into the carrier-based switching pattern of the VSI depicted in Figure IV.2-a can be seamlessly achieved without compromising the generation of the carrier-based PWM signal. Figure IV.2-b demonstrates the integration of the shoot-through state by evenly distributing its duration within the zero states. Observation of Figure IV.2-b reveals that the active states remain consistent for both the VSI and the ZSI in terms of carrier-based PWMs. Consequently, this ensures uniformity in the modulation index (M), defined as the ratio of the total active states to the entire period, across both switching patterns

The ZSI offers an additional benefit over the VSI when it comes to the practical implementation of the carrier-based PWM switching pattern. In conventional systems, "dead times" are typically inserted during transitions between switching states for protection purposes, which can result in output waveform distortion. However, due to the unique impedance network employed by the ZSI, these dead times become unnecessary.

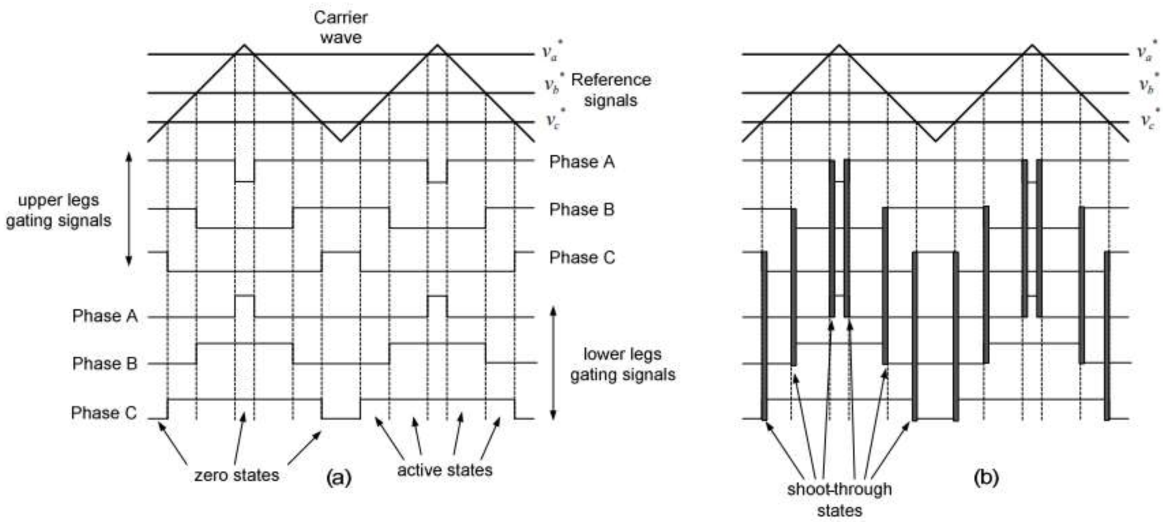

Figure IV.2 (a) Carrier based PWM for VSI (b) Modified carrier based PWM for ZSI.

IV.2 Modulation of the Z-Source Inverter

Figure III.2 demonstrated that the shoot-through states of. the Z-source converter (ZSC) can be integrated into the PWM switching pattern of a Voltage Source Inverter (VSI) [48]. Additionally, it was noted that maintaining consistency with the VSI PWM switching pattern is essential to prevent output waveform distortion. In [51], various sequences of possible switching states and their corresponding implementations of carrier-based PWM switching for Z-source inverters with different numbers of output phases are elaborated. This section will provide a summary of the proper introduction of shoot-through states into the modulation of an H-bridge (single phase) Z-source inverter, based on the discussions presented in [51]. This section will provide a summary of the proper procedure for introducing the shoot-through states effectively into the modulation of an H-bridge (single-phase) Z-source inverter, as detailed in [51].

Examining the H-bridge Z-source inverter depicted in Figure IV.3, and referring to the provided Table IV.1 for its switching states, it's evident that the active and null states, where the two switches of a phase-leg operate complementarily, are shared between both conventional VSI and the H-bridge Z-source inverter. Nevertheless, the remaining three shoot-through states, where either one phase-leg (H1 and H2) or two phase-legs (H3) are short-circuited, are exclusive to the H-bridge Z-source inverter, as indicated in [51].

Based on the discourse in the preceding section and the data in Table IV.1, it becomes evident that when the Z-source inverter enters a shoot-through state, the currents in the Z-source inductor are enhanced, while the output voltage of the inverter remains at 0V, akin to a null state where the AC load is short-circuited. Consequently, for a constant frequency, incorporating shoot-through states within the null intervals while keeping the active state intervals constant will not disrupt the normalized volt-second average per switching cycle. This characteristic enables the utilization of all existing volt-second PWM methods for controlling a Z-source inverter, requiring only minor adjustments to integrate the shoot-through states, as discussed in [51].

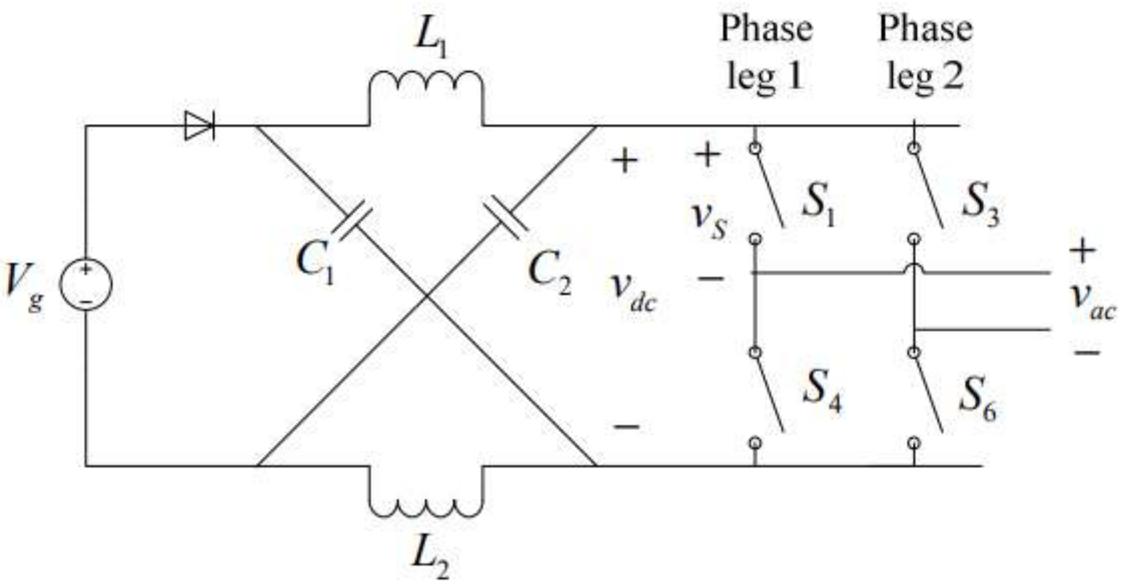

Figure IV.3 H-bridge (single phase) Z-source inverter.

Figure IV.4 illustrates a plausible PWM switching setup for both a conventional single-phase VSI and a single-phase Z-source inverter. In conventional VSI modulation, two state transitions take place per switching cycle (e.g., null {00} → active {10} → null {11}), with the active state positioned centrally within the switching period to reduce the harmonic distortion generated [52].

Table IV.1 Switching States of the H-bridge Z-source inverter ($\bar{S}_x$ is the complement of S_x).

State (*output voltage*)	S_1	S_3	S_4	S_6
Active $\{10\}$ (non-zero)	1	0	0	1
Active $\{01\}$ (non-zero)	0	1	1	0
Null $\{00\}$ (zero)	0	1	0	1
Null $\{11\}$ (zero)	1	0	1	0
$Shoot-through\ H1\ (zero)$	1	1	S_3	$\bar{S}_3$
$Shoot-through\ H2\ (zero)$	S_1	$\bar{S}_1$	1	1
$Shoot-through\ H3\ (zero)$	1	1	1	1

For Z-source inverter modulation, extra shoot-through states are thoughtfully integrated into the null intervals while maintaining a constant and centrally positioned active interval within the switching period, thus preserving all the harmonic advantages associated with central active state placement. Ideally, these shoot-through states should have identical time intervals to minimize the size of the Z-source network inductors [48]. Additionally, they should be incorporated immediately adjacent to the instants of state transitions of a conventional VSI to ensure a single device switching per state transition. Consequently, for a single-phase Z-source inverter with two state transitions per switching cycle, two equal-interval shoot-through states (0.5To) can be inserted. Their inclusion is depicted in Figure IV.4 [51].

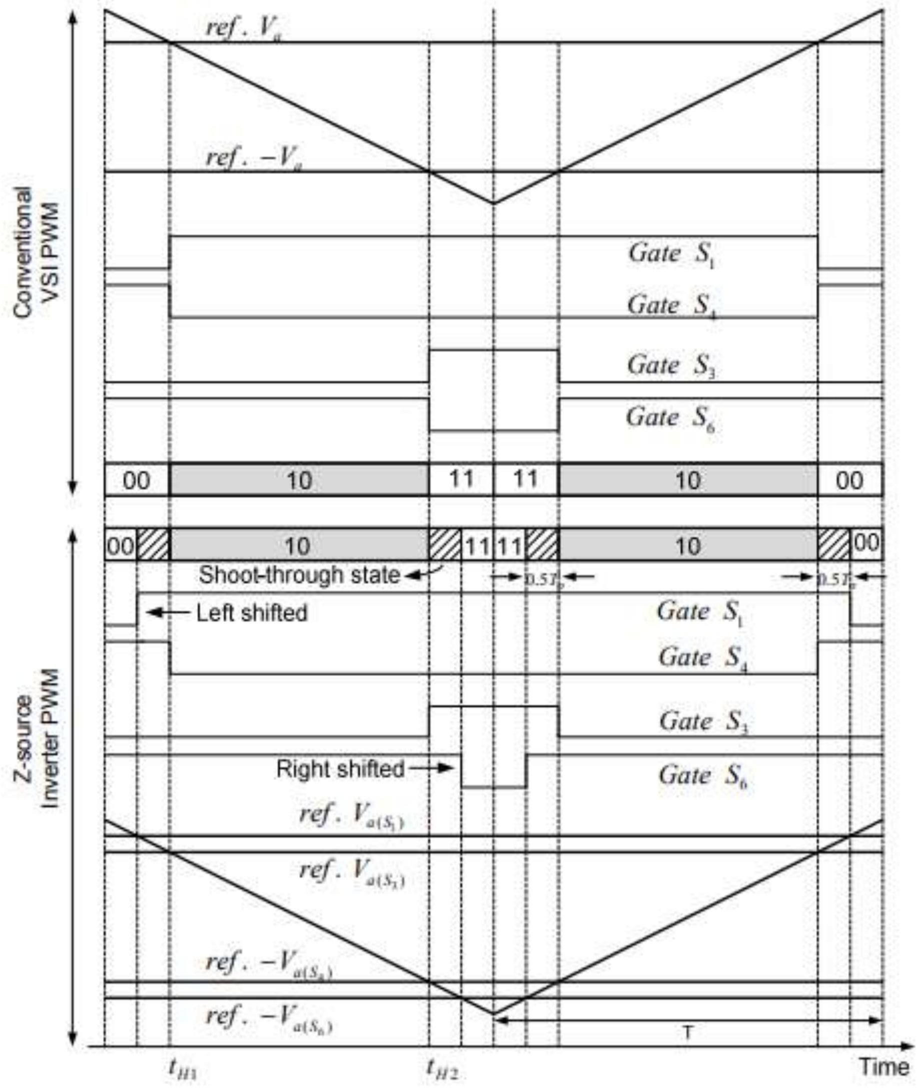

Figure IV.4 Modulation of H-bridge Z-source inverter.

To establish the desired state sequence depicted in Figure IV.4 through carrier-based implementation, it is necessary to formulate modulating reference signals tailored for carrier-based Z-source inverter modulation, based on the reference/carrier comparison diagrams provided in Figure IV.4. In a typical Voltage Source Inverter (VSI) configuration, the reference signals employed are as follows: $V_a = M \cos(\omega t)$ for modulating phase-leg $\{S_1, S_4\}$, and − Va for phase-leg $\{S_3, S_6\}$ .Typically, the initial state transition during the descending slope of the carrier wave occurs when the maximum value of the two signals $V_{\max} = \max(V_a, -V_a)$ The crossing of the descending slope of the carrier waveform occurs at time t_{H1} .

To incorporate a shoot-through state next to this transition $t_{H1} - 0.5T_0$ *to* t_{H1}, the upper switches (odd-numbered) and lower switches (even-numbered) of the relevant phase-leg should thus be controlled through modulation.

$$\begin{aligned} &V_{\max(SX)} = V_{\max} + T_0/T \\ &V_{\max(SY)} = V_{\max} \\ &\{X,Y\} = \{1,4\}\ or\ \{3,6\} \end{aligned} \tag{IV-1}$$

Where $V_{\max(SX)}$ causes the upper switch to turn ON at $t_{H1} - 0.5T_0$ *and* $V_{\max(SY)}$ causes the lower switch to turn OFF at t_{H1}. Obviously, these switching actions insert the desired shoot-through state H1, as illustrated in the lower half of Figure IV.4.

Continuing with a similar analysis, the second shoot-through state, H2, can be introduced from t_{H2} *to* $t_{H1} + 0.5T_0$ by employing the subsequent adjusted reference signals to control the remaining two switches

$$\begin{aligned} &V_{\min(SX)} = V_{\min} + T_0/T \\ &V_{\min(SY)} = V_{\min} \\ &\{X,Y\} = \{1,4\}\ or\ \{3,6\} \end{aligned} \tag{IV-2}$$

Where $V_{\min} = \min(V_a, -V_a)$ represents the minimum of V_a and $-V_a$. Without any alterations, the same derived equations (IV-1) and (IV-2) can likewise guarantee the accurate integration of shoot-through states when the carrier edge rises.

In a three-phase-leg Voltage Source Inverter (VSI), both continuous switching methods (such as centered Space Vector Modulation or SVM) and discontinuous switching methods (like 60-degree-discontinuous Pulse Width Modulation or PWM) are feasible. Each method possesses distinct null positioning at the onset and conclusion of a switching cycle, along with characteristic harmonic profiles. Analogous to how Pulse Width Modulation strategies are derived for an H-bridge Z-source inverter, it's feasible to derive various PWM techniques for a three-phase-leg Z-source inverter [51].

IV.3 Principle of operation

The general operation of a ZS converter can be illustrated by considering the AC part of the circuit as an equivalent DC load [51].

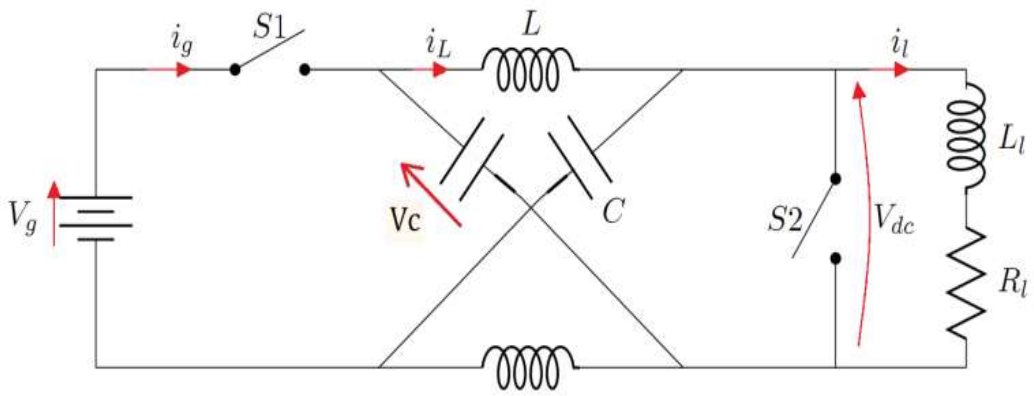

Figure IV.5 Simplified diagram of a ZS inverter.

To simplify the study, we content ourselves with an equivalent diagram (Figure IV.5), we have two main states (shoot-through, active state), in the shoot-through state the ZS circuit is short-circuited, in the active state, the ZS impedance network sees the load through the inverter. We make the following assumptions: $L_1 = L_2 = L$ and $C_1 = C_2 = C$ we will therefore have a symmetrical circuit from which: $v_{C_1} = v_{C_2} = v_C$ and $i_{L_1} = i_{L_2} = i_L$

With

V_g, v_C, v_L *and* v_{dc} : represent the DC source and voltages, capacitor, inductor and ZSC output respectively.

i_l, i_g, i_L, i_C : are respectively the load and source currents and the currents passing through the inductance and the capacitor.

There are four states to present, they depend on the configurations of switches S_1 and S_2.

IV.3.1 State 1: Shoot-through

When the switch S_1 is open and S_2 is closed, the impedance network ZS is short-circuited, so the load voltage is zero: there is no energy transfer. The duration of the shoot-through state is equal to T_0, and the switching period is equal to T. Figure IV.6

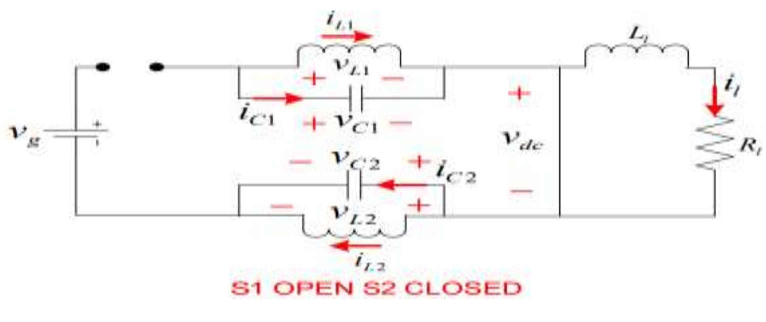

Figure IV.6 Shoot-through state of simplified ZSC.

We note that $v_C = v_L$, it follows:

$$\begin{cases} \dfrac{dv_C}{dt} = -\dfrac{i_L}{C} \\ \dfrac{di_L}{dt} = -\dfrac{v_C}{L} \\ v_{dc} = 0 \\ i_g = 0 \end{cases} \qquad \text{(IV-3)}$$

IV.3.2 State 2: Active State

If the converter is in the active state, the switch S_2 is open and S_1 is closed, the duration of this state is $(T - T_0)$: there is a transfer of energy. (Figure IV.7)

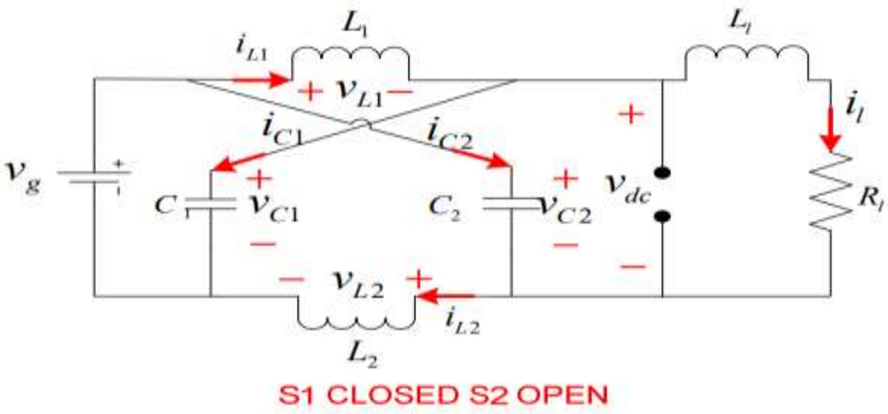

Figure IV.7 Active state of simplified ZSC.

$v_L = v_g - v_C$ *and* $i_g = i_L + i_C = i_L + C\dfrac{dv_C}{dt}$, it follows:

$$\begin{cases} \dfrac{dv_C}{dt} = -\dfrac{i_g - i_L}{C} \\ \dfrac{di_L}{dt} = -\dfrac{v_g - v_C}{L} \\ v_{dc} = v_C - v_L = 2v_C - v_g \\ i_g = i_L + i_C \end{cases} \qquad \text{(IV-4)}$$

IV.3.3 State 3: Zero State

when $S_1 = 0$ and $S_2 = 0$, we have: $i_L = -i_C = i_l$

$$\begin{cases} \dfrac{dv_C}{dt} = -\dfrac{i_L}{C} \\ \dfrac{di_L}{dt} = -\dfrac{v_c - v_{dc}}{L} \\ v_{dc} = v_C - v_L \\ i_g = 0 \end{cases} \tag{IV-5}$$

IV.3.4 State 4

when $S_1 = 1$ and $S_2 = 1$, we have:

$$\begin{cases} \dfrac{dv_C}{dt} = -\dfrac{i_g - i_L}{C} \\ \dfrac{di_L}{dt} = -\dfrac{v_g - v_C}{L} \\ v_{dc} = 0 \\ i_g = i_L + i_C \end{cases} \tag{IV-6}$$

To summarize all the states, we will have the following equations:

$$\begin{cases} \dfrac{dv_C}{dt} = -\dfrac{S_1 i_g - i_L}{C} \\ \dfrac{di_L}{dt} = -S_1 \dfrac{v_g - v_C}{L} + \overline{S}_1 \left[S_2 \dfrac{v_C}{L} + \overline{S}_2 \dfrac{v_C - v_{dc}}{L} \right] \\ v_{dc} = \overline{S}_2 \left(v_C - v_L \right) \\ i_g = S_1 \left(i_L + i_C \right) \end{cases} \tag{IV-7}$$

Where $\overline{S}_1 = 1 - S_1$ et $\overline{S}_2 = 1 - S_2$

IV.3.5 Boost factor

In the steady state, we know that the average value of the voltage during a switching period at the level of the inductor is zero, therefore:

$$\begin{cases} V_L = \dfrac{1}{T}\left[\int_0^{T_0} v_C dt + \int_{T_0}^{T}\left(v_g - v_C\right)dt\right] = 0 \\ V_C = \dfrac{1-\dfrac{T_0}{T}}{1-2\dfrac{T_0}{T}} V_g \end{cases} \tag{IV-8}$$

We pose $D = \dfrac{T_0}{T}$, D is the duty cycle, we get:

$$V_C = \frac{1-D}{1-2D} V_g \tag{IV-9}$$

On the other hand, the maximum voltage of the DC bus in a state of equilibrium is written:

$$V_{dcn} = 2V_C - V_g \tag{IV-10}$$

We therefore obtain the relationship between the input voltage and the maximum voltage of the DC bus:

$$V_{dcn} = \frac{1}{1-2D} V_g = BV_g \tag{IV-11}$$

Where B $= \dfrac{1}{1-2D}$ is the boost factor.

In Equation (IV-11), B is termed the boosting factor determined by D, and V_{dcn} represents the steady-state peak value of the DC-link voltage. This equation provides the voltage conversion ratio of the ZSC. With D ranging from zero to 0.5, B can assume any value from one to infinity. The output peak phase voltage (Vac) of the ZSI illustrated in Figure IV.3 can be mathematically represented as:

$$\begin{cases} V_{ac} = M\dfrac{V_{dcn}}{2} \\ M\left(The\ modulation\ rate\right) = \dfrac{V_{ref}\left(The\ magnitude\ of\ the\ reference\ voltage\right)}{\left(n-1\right)V_p\left(The\ amplitude\ of\ the\ carrier\right)} \\ n:\ number\ of\ levels \end{cases} \tag{IV-12}$$

Where M is the modulation rate of the inverter. Using Eq. (IV-11), Eq. (IV-12) can be rewritten as,

$$V_{ac} = MB\frac{V_g}{2} \tag{IV-13}$$

Equation (IV-13) includes an additional multiplication factor of B compared to the VSI voltage conversion ratio, thereby endowing the Z-source inverter with boosting capability

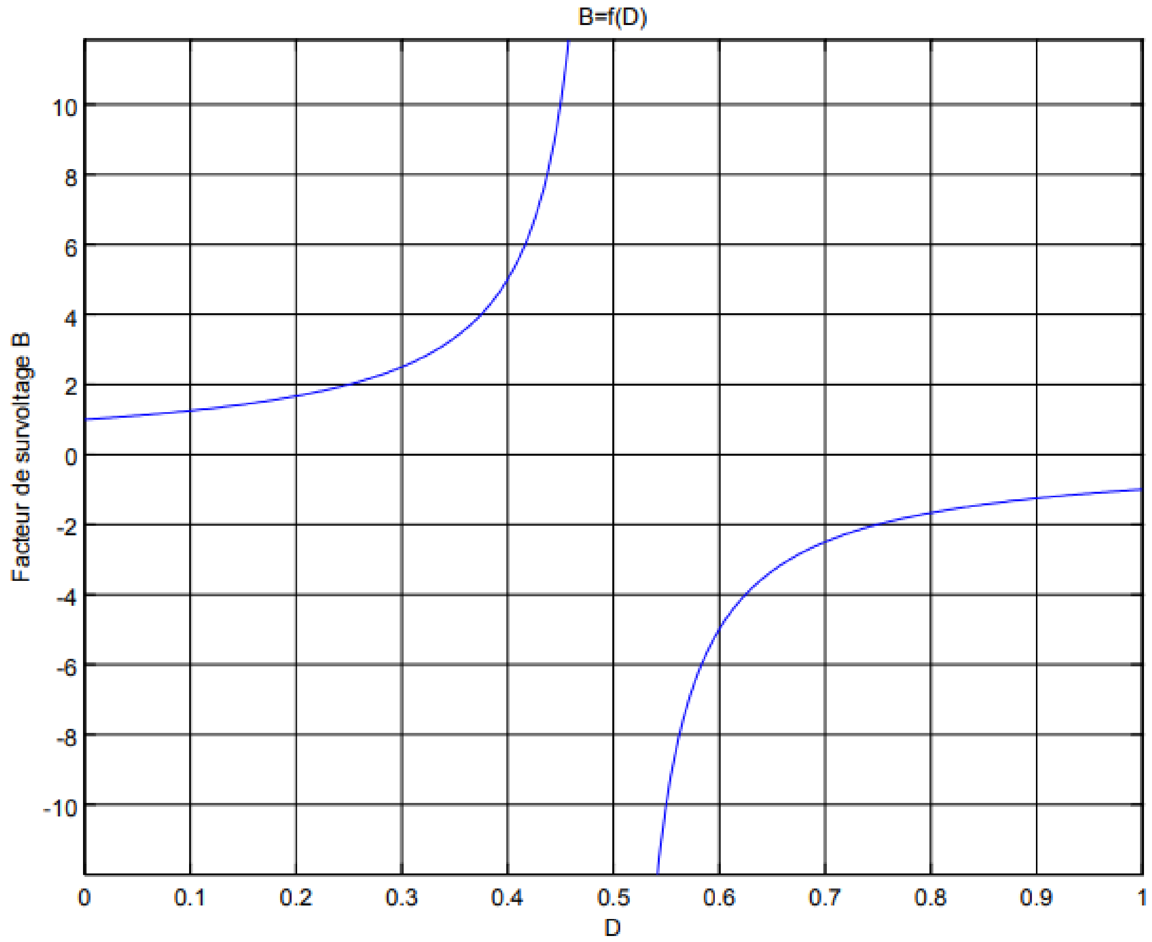

Figure IV.8 Variation of gain B as a function of the Shoot-Through duty cycle D.

Figure IV.8 represents the variation of gain B as a function of the Shoot-Through duty cycle D. If the duty cycle D is between 0 and 0.5, the output voltage can have values between 0 and infinity, so ZS has boosted the input voltage, if we add the ZS impedance network to a conventional inverter, we can boost the DC input voltage without using a boost chopper, hence the advantage of the ZS, it allows reducing the number of switches and the complexity of the control circuit.

IV.4 Boosting Methods

The preceding section highlighted the introduction of shoot-through states into a VSI PWM switching pattern. This section provides a concise overview of potential methods for enhancing the dc-link voltage (v_{dc}) in a 3-phase Z-source inverter, as outlined in [53] and [54].

In [48], a straightforward boosting technique was applied to regulate the shoot-through duty ratio. Figure 3.8 depicts the simple boosting approach, which utilizes a straight line (VP) equal to or exceeding the peak value of the three-phase references to introduce the shoot-through duty ratio in a conventional sinusoidal Pulse Width Modulation (PWM). In this setup, if the triangular carrier signal surpasses VP or falls below VN, the Z-source inverter enters a shoot-through state. The Z-source inverter preserves the six active states, remaining consistent with traditional carrier-based PWM control. In this straightforward boosting approach, the attainable shoot-through duty ratio diminishes as the modulation index (M) increases. The upper limit for the shoot-through duty ratio in the simple boosting method is capped at 1- M, gradually approaching zero when the modulation index reaches one. To generate an output voltage necessitating a high voltage gain, a lower modulation index must be employed. Nonetheless, employing small modulation indexes leads to heightened voltage stress on the devices [53].

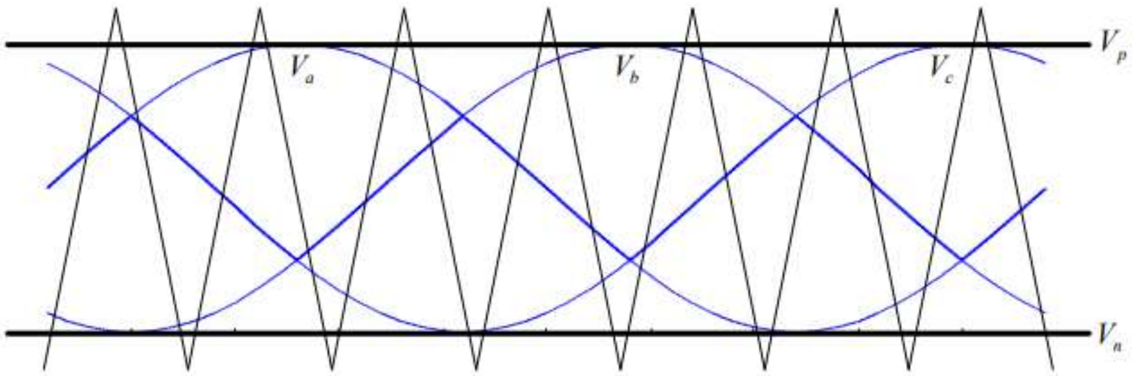

Figure IV.9 Simple boosting PWM generation waveforms of the ZSC

Based on Eq. (IV-13), the voltage gain of the Z-source inverter can be written as

$$G = \frac{V_{ac}}{V_g/2} = MB = \frac{M}{2M-1} \tag{IV-14}$$

As discussed in [48], the voltage stress (Vs) across the switches, as shown in Figure IV.3, is represented by BVG. The voltage stress under the simple boosting modulation method can be computed as follows:

$$V_s = BV_g = (2G-1)V_g \tag{IV-15}$$

Figure IV.10 illustrates the relationship between voltage stress across switches and voltage gain. Employing the simple boosting method results in notably high voltage stress across the switches. Consequently, this imposes limitations on achievable voltage gains due to the constraints imposed by device voltage ratings [53].

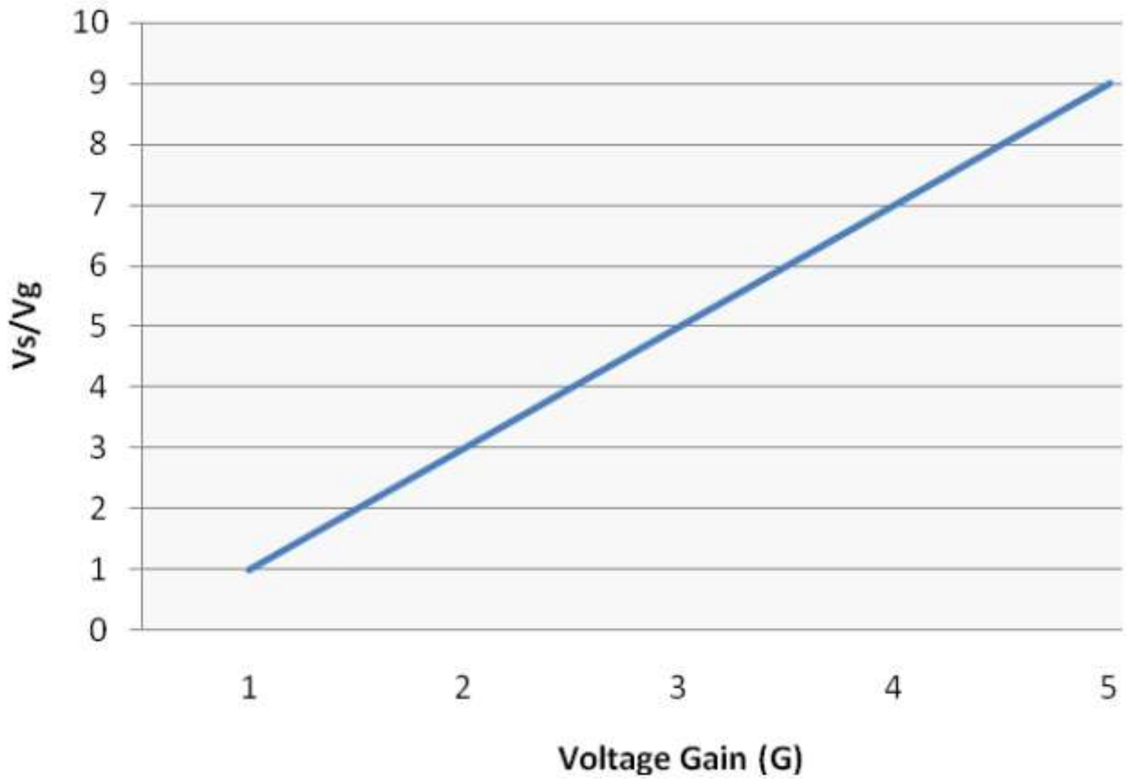

Figure IV.10 Switch voltage stress versus voltage gain in simple boosting method.

Figure IV.11 displays the maximum boosting strategy, elucidated in [53], serving as an alternative to the simple boosting method. This strategy closely resembles the traditional carrier-based PWM control approach. It preserves the six active states while converting all zero states into shoot-through states. Consequently, it achieves the maximum boosting factor (B) for any given modulation index without distorting the output waveform. In Figure IV.11, the circuit enters the shoot-through state when the triangular carrier wave exceeds the maximum curve of the references (Va, Vb, and Vc) or falls below the minimum of the references. The voltage stress for the maximum boosting method is derived in [53] as:

$$V_s = BV_g = \left(\frac{3\sqrt{3}G}{\pi} - 1\right)V_g \tag{IV-16}$$

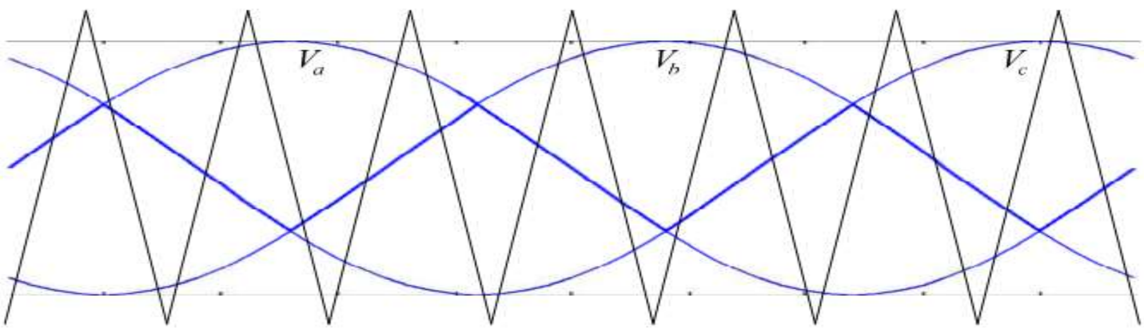

Figure IV.11 Maximum boosting PWM generation waveforms of the ZSC.

Figure IV.12 illustrates the relationship between voltage stress and voltage gain for the maximum boosting method. Contrasted with the simple control method depicted in Figure IV.10, the voltage stress in the maximum boosting method is significantly reduced. This indicates that the inverter can be operated to achieve a higher voltage gain without encountering excessive voltage stress.

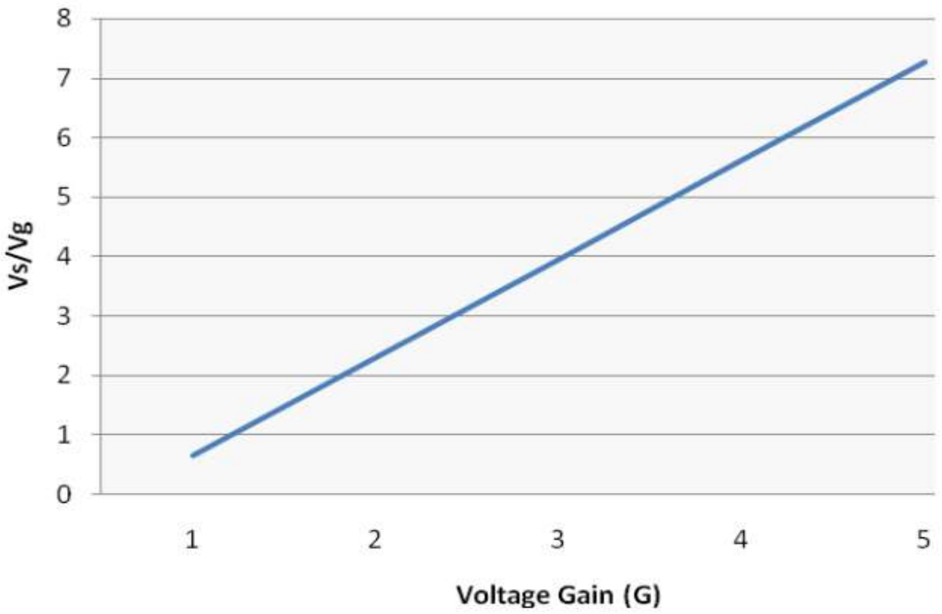

Figure IV.12 Switch voltage stress versus voltage gain in maximum boosting method.

The maximum boosting method can minimize voltage stress across the switches. Nonetheless, it is afflicted by the drawback of generating low-frequency ripples on the Z-source network, as demonstrated in[54]. An alternative boosting method has been proposed to attain the highest feasible voltage boost or gain while ensuring a consistent boost as perceived from the Z-source network. Furthermore, this method eliminates any low-frequency ripples linked with the output frequency, as elucidated in [54].

Figure IV.13 illustrates the schematic diagram of the constant boosting method proposed in [54]. This method aims to achieve the maximum voltage gain while maintaining a constant shoot-through duty ratio. It comprises five modulation curves: three reference signals (Va, Vb, and Vc) and two shoot-through envelope signals (VP and VN). When the carrier triangle wave exceeds the upper shoot-through envelope (VP) or falls below the lower shoot-through envelope (VN), the inverter enters a shoot-through zero state. In the interim, the inverter switches in a manner consistent with traditional carrier-based PWM control.

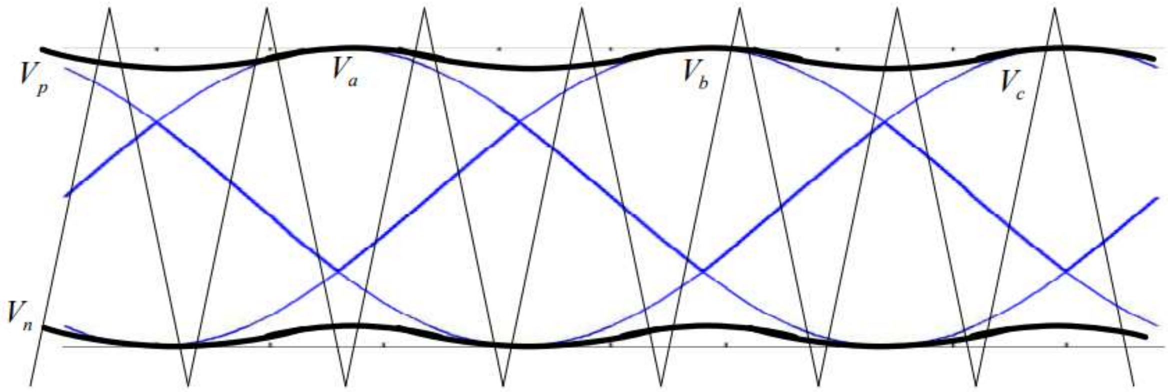

Figure IV.13 Constant boosting PWM generation waveforms of the ZSC.

During the first half-period, [0, π/3], as depicted in Figure IV.13, the upper and lower envelope curves can be defined by equations (IV-17) and (IV-18), respectively.

$$V_{P1} = \sqrt{3}M + \sin\left(\theta - \frac{2\pi}{3}\right)M \qquad for\ 0 < \theta < \frac{\pi}{3} \tag{IV-17}$$

$$V_{N1} = \sin\left(\theta - \frac{2\pi}{3}\right)M \qquad for\ 0 < \theta < \frac{\pi}{3} \tag{IV-18}$$

During the second half-period, [π/3, 2π/3], the envelope curves are defined by equations (IV-19) and (IV-20) , respectively.

$$V_{P1} = \sin(\theta)M \qquad for\ \frac{\pi}{3} < \theta < \frac{2\pi}{3} \tag{IV-19}$$

$$V_{N1} = \sin(\theta)M - \sqrt{3}M \qquad for\ \frac{\pi}{3} < \theta < \frac{2\pi}{3} \tag{IV-20}$$

The voltage stress for the constant boosting method was derived in [54] as

$$V_s = BV_g = \left(\sqrt{3}G - 1\right)V_g \tag{IV-21}$$

As depicted in Figure IV.14, the constant boosting method exhibits significantly lower voltage stress across the devices compared to the simple boosting method, albeit slightly higher than the maximum boosting method. The optimal voltage-stress ratio is one. The constant boosting method is particularly advantageous for applications necessitating a voltage gain of two to three. Additionally, this method demands minimal inductance and capacitance since the inductor current and capacitor voltage do not contain any low-frequency ripples associated with the output voltage. Consequently, this reduces the cost, volume, and weight of the Z-source network [54].

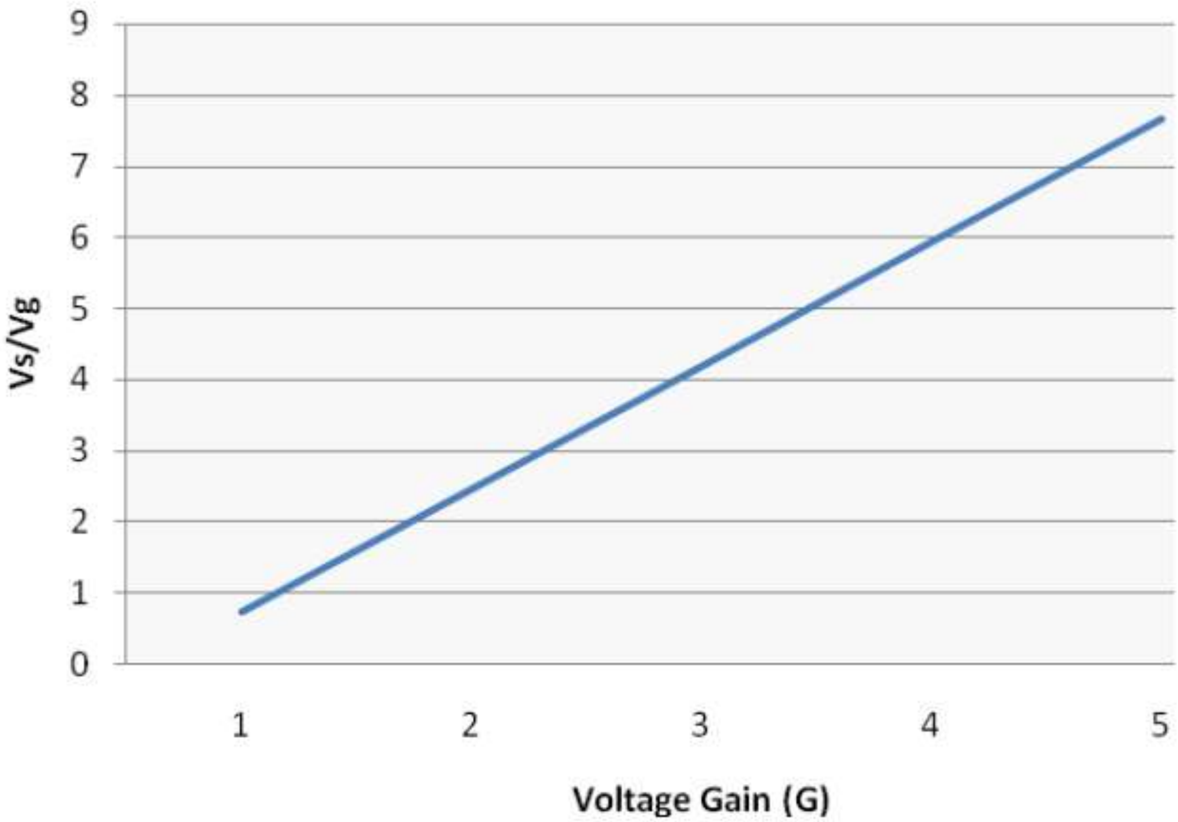

Figure IV.14 Switch voltage stress versus voltage gain in constant boosting method.

IV.5 Summary

This chapter provides a comprehensive review of the literature on Z-source converters (ZSC). It begins with a concise introduction discussing the fundamental properties of ZSC. Subsequently, the chapter delves into deriving steady-state relationships and determining the voltage conversion ratio based on the simplified ZSC circuit. Following this, a summarized overview of a modified modulation technique from the literature is presented. This technique involves distributing shoot-through states within the VSI PWM modulation pattern while maintaining consistent active states. Additionally, the chapter discusses three distinct boosting methods for the DC-link voltage, highlighting various outcomes in terms of voltage stress and the maximum achievable boosting.

Chapter V :

Shunt Active Power Filter Control based on Z-Source Inverter Fed by PV System

V.1 Introduction

The widespread use of non-linear loads in industrial applications has caused undesirable effects related to the power quality [55][56]. This increase within the use of non-linear masses encompasses a vital impact on consumers, because the main issues in power quality consist of current, voltage and frequency distortions. However, the demand permanently power quality is increasing thanks to the expansion of use of sensitive devices that require smooth sine waveforms [57][58]. To get eliminate the harmonic currents and proper the ability issue tormented by these non-linear loads, many alternative studies were carried out. Traditionally, passive filters are wont to suppress current harmonics and to mitigate energy pollution within the network for an extended time. However, this kind of filter presents many shortcomings reminiscent of large size, significant weight, and sensitivity to dynamic parameters that cause resonance issues. The aforementioned issues were effectively mitigated by using an active filter that was recognized approximately in the 1970s [59][60]. Shunt Active Power Filter (SAPF) is a flexible solution for harmonic current mitigation and power factor correction. In addition, it has the perfect ability to adapt to different types of loads. The SAPF combination is based on a voltage/current source inverter interacting with a link capacitor connected in parallel with non-linear loads [61][62]. The electrical converter generates the harmonic elements necessary to suppress the harmonic currents drawn by non-linear loads; Therefore, it makes the main current sinusoidal and in phase with the supply voltage [63][64]. As a result of the rise in penetration of renewable energy supply, several enhancements are remodelled the classic shunt active filters by connecting a renewable energy source to the DC aspect of the filter to scale back energy consumption from the electrical grid. Therefore, filters became of nice importance [65][66]. The latter has many advantages, including harmonic current elimination, reactive power compensation and simultaneous active power injection, but it has many disadvantages, such as B. non-linear properties and completes dependence on environmental conditions. There is an urgent need for accurate monitoring of the maximum energy harvested from photovoltaic sources [67]. To solve this problem, many maximum power point tracking (MPPT) techniques are proposed in the literature, similar to the perturbation and observation (P&O) technique, which is based on the perturbation of the photovoltaic and also on the observation of the behaviour of the output power. Conductance technique that uses the slope of the PV to calculate the point of highest energy. And the approaches are supported by artificial intelligence [67][68]. Unlike ancient two-stage PV systems consisting of a voltage supply electrical converter and a DC-DC boost converter, ZSI has several benefits admire having fewer power switches ZSI will convert the DC voltage from a photovoltaic cell to the specified AC voltage. ZSI options offer high-quality power output, with single-stage buck and boost functions. ZSI has an extra state known as Shoot-through that is formed by at the same time in operation the higher and lower keys of an identical leg. attributable to this extra state, the electrical phenomenon periodic voltage will be simply controlled employing a single-phase configuration [69][53].

V.2 SAPF topology based on Z-Source inverter

The Z-source SAPF supported by the PV is presented as shown in Figure V.1. The three-phase grid connected to the PV-SAPF system supplies consumers with linear and non-linear loads. A 3-leg ZSI has linked parallel to the client load through the interfacing inductor. The photovoltaic power generation system includes the photovoltaic panel, a booster DC-DC converter and a battery bank. The PV power generation system supplies DC power to the Z-source grid, which is used to maintain the SAPF sustained DC link voltage. To maintain the SAPF DC link voltage, the Z-source inverter is used. Excess power generation from the PV power generation system can be routed through the DC-DC converter circuit to the energy storage unit and start providing the energy stored in the battery when a PV system is not powerful enough [47].

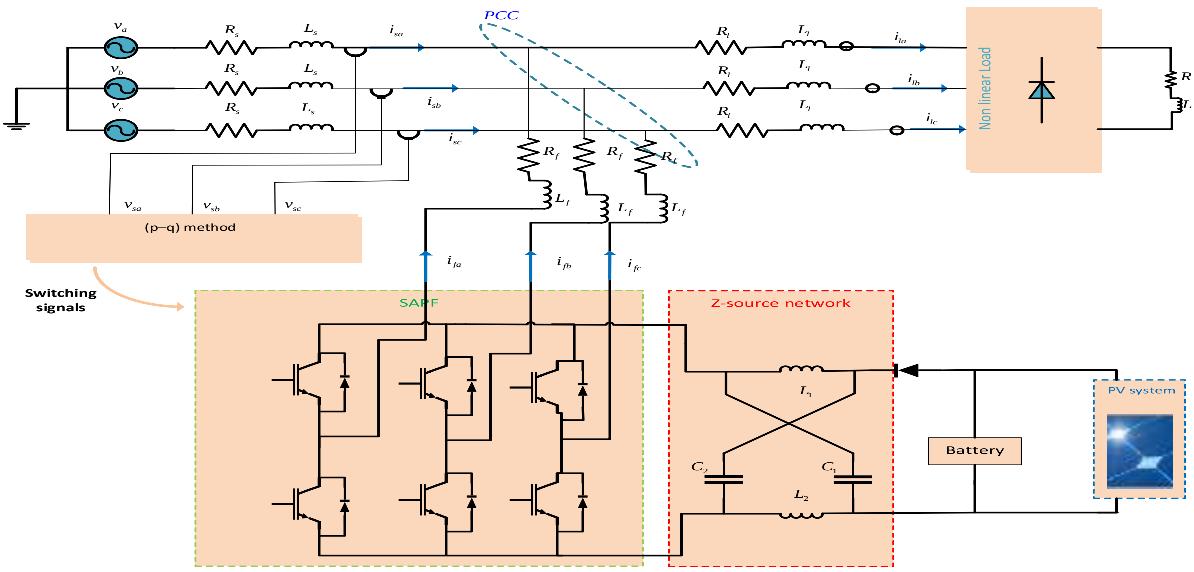

Figure V.1 General scheme of SAPF based on two-level ZSI.

V.2.1 PV power generating unit

The proposed SPV power generating unit includes an SPV panel, a low-step DC-DC boost converter, and a battery. The DC-DC boost converter contains a MPPT operate to attain the utmost power during the solar level reduction period. The output power generated by the PV power generating unit relies on the sunlight irradiation and the surrounding temperature, as indicated by the essential equations within the PV cell. Equivalent circuit of PV array and DC-DC converter with MPPT management electronic equipment is shown in Figure V.2. The PV cell has a current source; it is connected to a diode “ d ” in parallel. The present supply and diode configuration are linked to an interior resistance in series. The inner resistance of the current source and diode configuration is integrated within the series. The subsequent are the essential equations of the PV cell.

$$I_{ph} = I_d + I_{pv}$$
$$I_{pv} = I_{ph} - I_d \tag{V-1}$$

$$V_{pv} = \frac{AkT_c}{e} \ln\left(\frac{I_{ph} + I_d - I_c}{I_d}\right) - R_s I_c \tag{V-2}$$

Where I_{pv} is the PV cell output current in amps and I_d is the diode reverse saturation current. Photovoltaic cell voltage is displayed as:

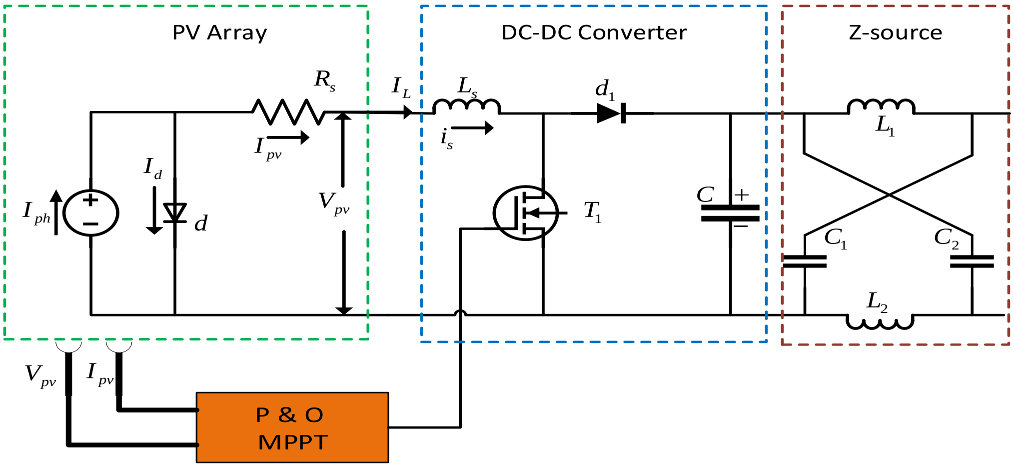

Figure V.2 Equivalent circuit of SPV array and DC-DC converter with MPPT control circuitry.

Where is the charge strength of the electrons $\left(1.602\times10^{-19}C\right)$, V_{pv} is the output voltage of the photovoltaic cells, A is curve fitting factor (0.001), I_{ph} is the current image in amps, k is Boltzmann constant $\left(1.38\times10^{-23}\, J/K\right)$, T_c is the operating temperature of the reference cell $\left(25^{\circ}C\right)$, I_c is the cell's output current in amps, R_s is the internal resistance of the cell (0.001 Ω).

The output voltage of the low-pass DC-DC boost converter (12V) is supplied to the Z-source inverter to boost the DC voltage level. The increased DC voltage maintains the DC link of the SAPF. The ZSI has two operational states, shoot through and non-shoot through. Both the top and bottom switches of one or more legs of the same phase are turned on during a shoot through. The equivalent ZSI circuit in shoot through state is presented in Figure V.3. Inductor voltage is equal to capacitor voltage VL = VC while T_{st} cycle.

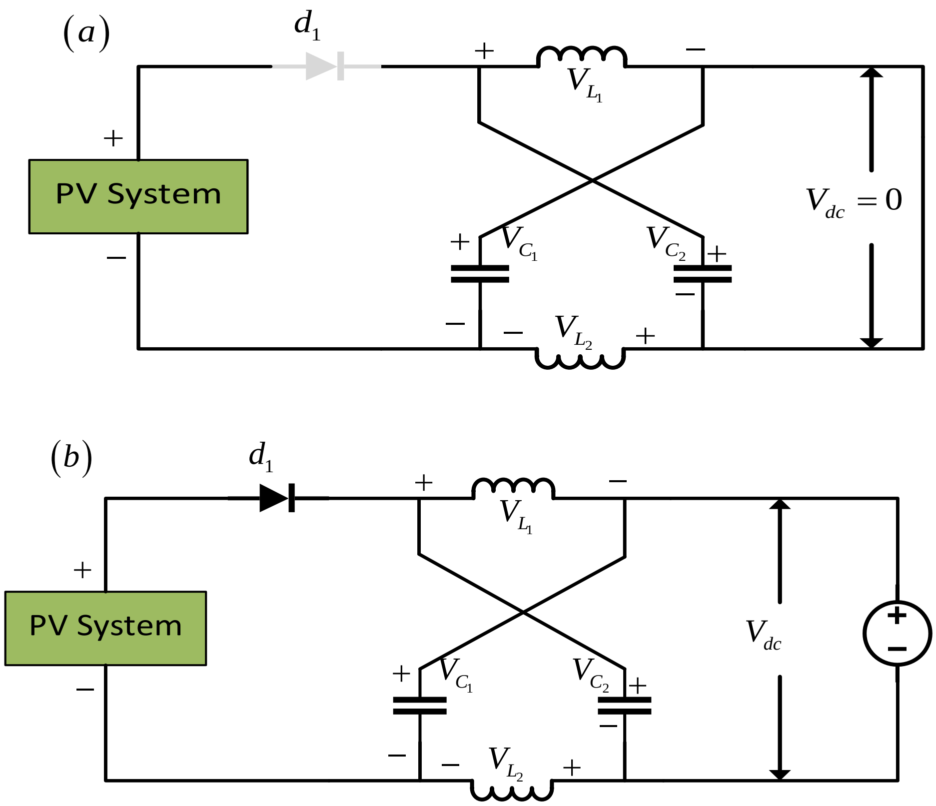

Figure V.3 Equivalent circuit of ZSI (a) Shoot through state (b) Non-shoot through.

The equivalent ZSI circuits in the state of NON-shoot through displays in Figure V.3-b, when DC voltage is applied via a three-phase inverter, in six switching states. The ZSI change pattern is shown in Figure V.4. No change in total zero-state time, each phase leg is switched on and off per duty cycle. The shoot through state time is assigned equally to each phase without changing the duration of the active state time. During the non-shoot through state, the inductance voltage V_L and also the input voltage V_i may be described as:

$$V_L = V_{dc} - V_c \tag{V-3}$$

The maximum DC-link voltage across the three-phase electrical converter bridge as:

$$V_i = \frac{1}{1-\frac{T_{st}}{T}} V_{dc} \tag{V-4}$$

$$V_i = BV_{dc} \tag{V-5}$$

$$B_i = \frac{1}{1 - \frac{T_{st}}{T}} \tag{V-6}$$

where, $B \geq 1$, B is the boost factor

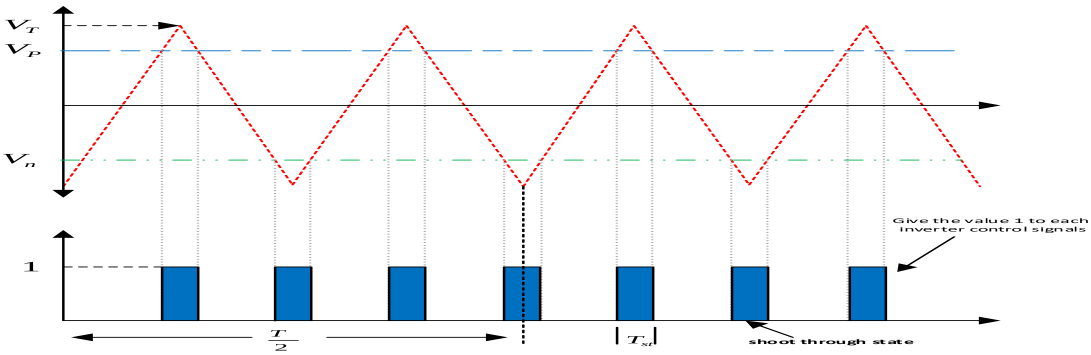

Figure V.4 Switching pattern for ZSI.

In this situation, the shoot-through time per switch cycle is maintained perpetually and therefore has a constant boost factor. Constant input voltage of the inverter is achieved by choosing the appropriate Shoot-through time per switching cycle. Three operation modes are used in the SAPF with proposed PV interface. The modes are (1) PV power generation mode (2) Battery backup mode (3) Continuous supply mode

V.2.2 PV power generation mode

The photovoltaic power generation mode is activated during the day or when solar radiation is much more accessible to generate enough energy. The PV Sustained SAPF acts as a harmonic and reactive power canceller, and excess power is stored in a battery. Figure V.5 shows the current flow chart for photovoltaic power generation mode.

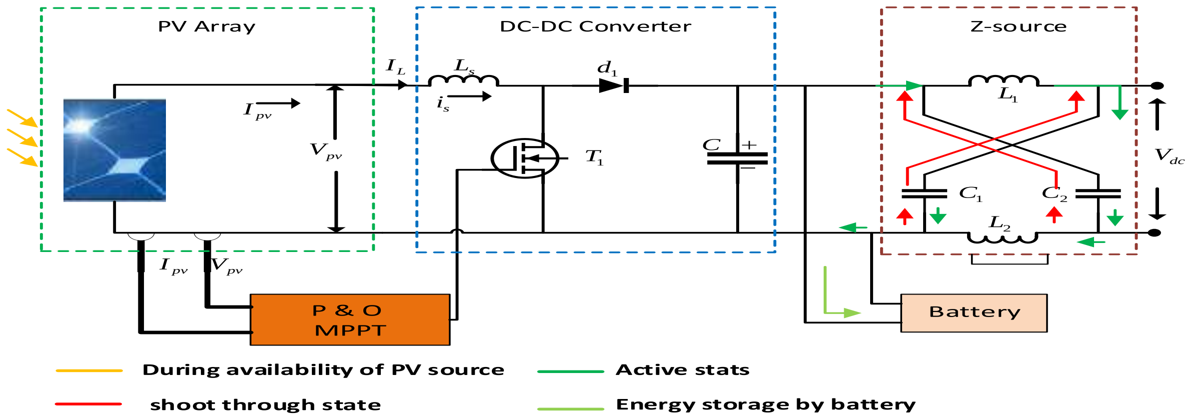

Figure V.5 Current flowchart for photovoltaic power generation mode.

V.2.3 Battery backup mode

Battery backup mode is supported overnight or in the absence of sunlight. Battery-backed SAPF compensates for reactive power and harmonics. Battery backup mode operates via ZSI to effectively manage compensation continuity. Figure V.6 shows the current flowchart for battery backup mode.

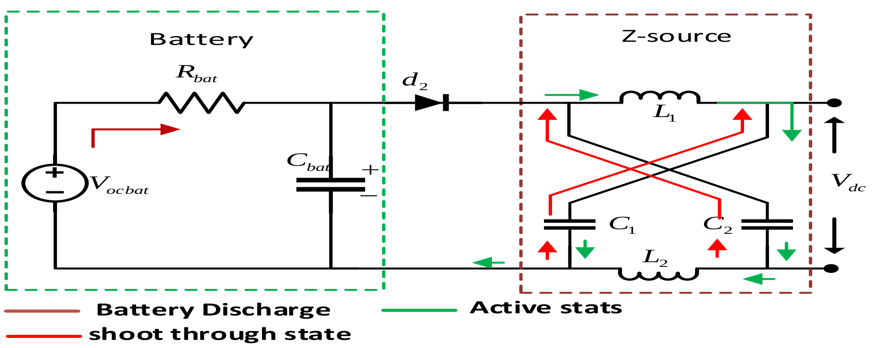

Figure V.6 Current flowchart for battery backup mode.

V.2.4 Continuous supply mode

In the period of voltage interruption, the PV-SAPF model provides a continuous supply of essential and sensitive loads. In these cases, the solar PV power generation unit or battery supplies the power source to the connected load. Semiconductor switches separate the power supply from the distribution network.

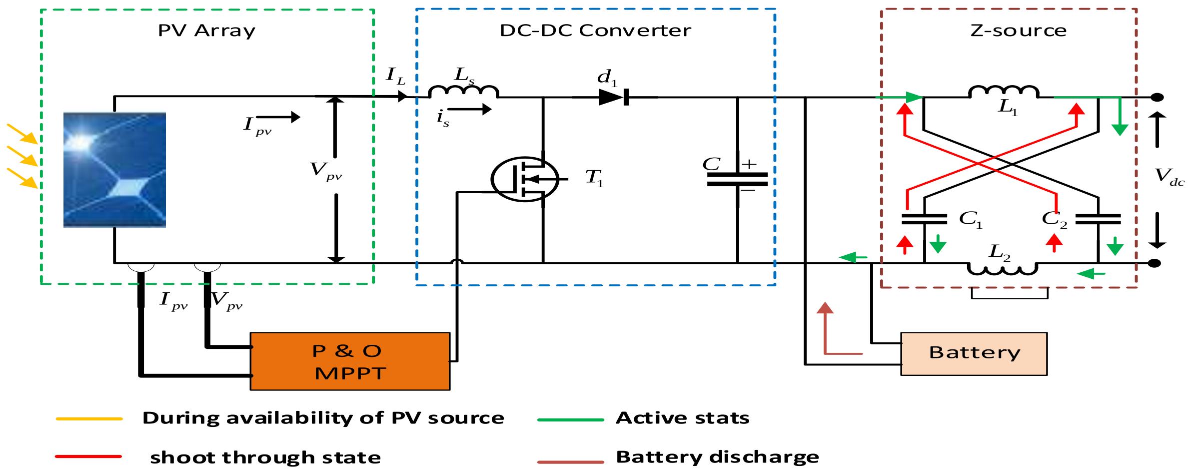

Figure V.7 Current flow chart for continuous supply mode.

V.3 PV-SAPF Control Scheme

To provide current compensation, the control scheme based on instantaneous reactive power theory for 3-phase PV-SAPF is used. This is one of the most popular theories that has been used, not only in theory but also in practice, can be considered as the first successfully implemented method based on the use of static converters [70].calcul des courants de reference du filtre

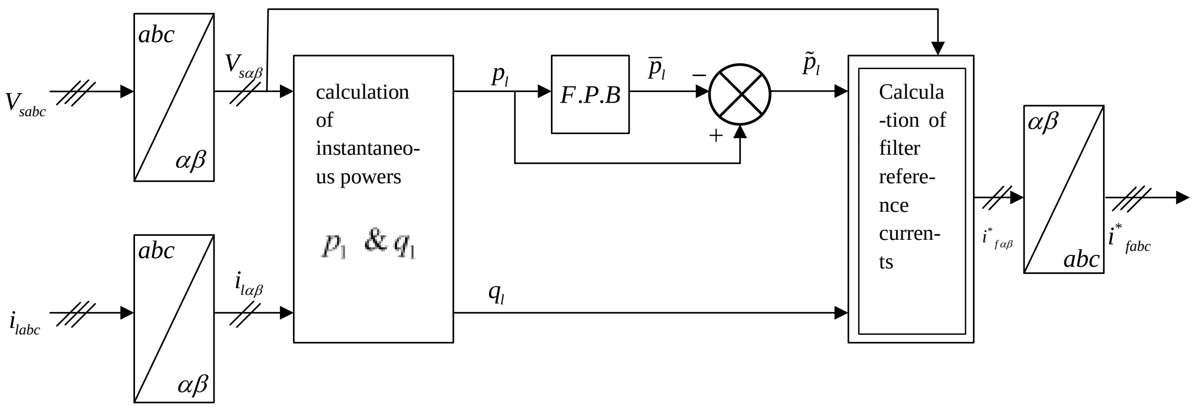

Figure V.8 Schematic diagram of the instantaneous power method.

V.3.1 Hysteresis control

The principle of hysteresis current control is to keep each of the generated currents within a band surrounding the reference currents. Any violation of this band gives a commutation command to stay within the band.

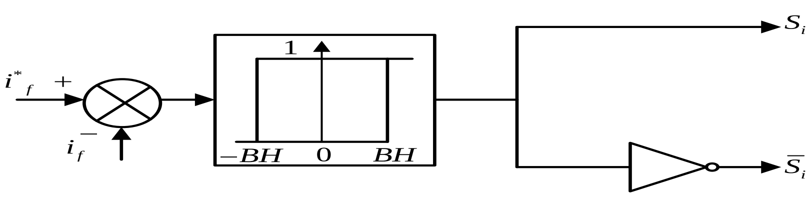

Figure V.9 Hysteresis band current controller.

V.3.2 Fixed band hysteresis control

With this type of current control, the switching frequency essentially depends on the derivation of the target current. The latter depends on the size of the decoupling inductance and the voltage drop across it. The filter affects the switching frequency and the dynamic behaviour of the active filter. The main advantage of this method is the simplicity of implementation, while the variable switching frequency, which cannot be properly controlled, can become its main disadvantage [71].

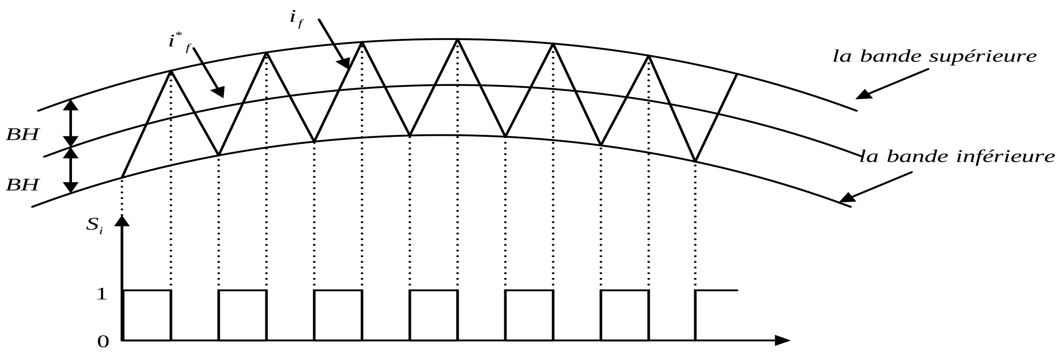

Figure V.10 Control of switches by fixed band hysteresis.

V.4 Simulation Results

The parameters of the PV-SAPF system are presented in Table V.1. Simulations are carried out using MATLAB/Simulink. The results of the simulation study are presented before and after connecting the PV-SAPF system. It is noted that the initial state of the capacitors' voltage in the system is zero.

Table V.1 Parameters of system.

Parameters	**symbol**	**Value**
System voltages (line to line) Vrms	V_s	$57V$
Frequency	f	$50Hz$
Filter (series SAPF)	L_s, R_s	$0.45\Omega, 2.5mH$
Battery voltage		$30V$
Battery capacity		$33Ah$
Filter (shunt SAPF)	L_f, R_f	$0.9\Omega, 4mH$
DC-DC converter		
Inductor	$L_{z-source}$	$5mH$
Capacitance	$C_{z-source}$	$1100\mu F$
Switching frequency	$f_{z-source}$	$1KH$
Proportional gain	K_p	6.8
Integral gain	K_i	1.1
Sample time	t	$1e^{-4}$
Non-linear load	R_C	17Ω
	L_C	$3\ mH$

V.4.1 DC Voltage Variation

First, the performance of a conventional PI controller and its response to a stepwise change of the DC bus voltage from 160 to 140 V is verified in Fig. 11. Obviously, the traditional PI controller gives very satisfactory results.

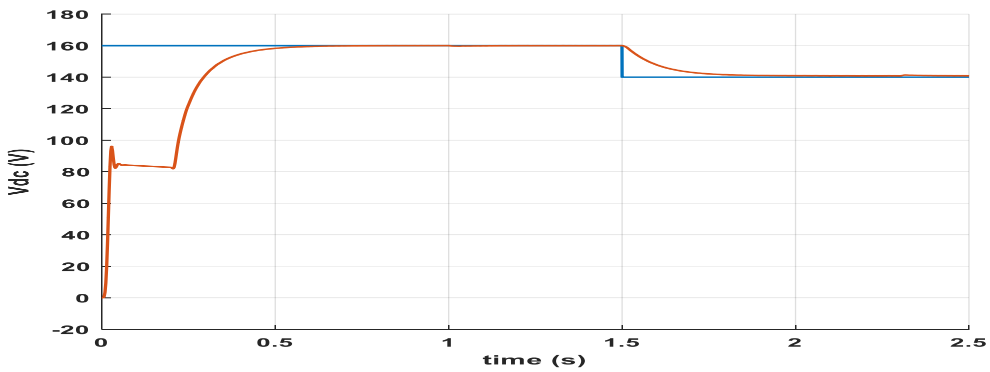

Figure V.11 Simulation results of DC bus voltage response with conventional PI-based reference DC voltage variation.

V.4.2 Continuous operation

The results of the state of the system before and after connecting of the filter are depicted as shown in Figure V.12 to 14. PV compliant ZSI-SAPF performance is tested under balanced voltage and load currents. Figure V.12 shows the source current before connecting the ZSI-based SAPF. Figure V.13 illustrates source current, and filter current after connecting the filter, as well as DC bus voltage. It can be clearly seen that the source current has a pure sinusoidal waveform after connecting the filter.

The current source was analyzed using the Fast Fourier Transform (FFT) analysis tool. Simulation results are shown in Figure V.14. The stream before filtering is heavily distorted, and the spectral analysis graph shows the order of harmonics present in the signal that are the odd harmonics except multiples of the third harmonic. It can be seen that the current obtained after filtering has a sinusoidal waveform. In addition, the harmonic components are effectively suppressed and only the fundamental component appears in the spectral display.

As a result, the measured THDi of the source current is successfully reduced to 0.72% after compensation in the simulation. However, these results meet the requirements of the international standard IEEE-519 [72].

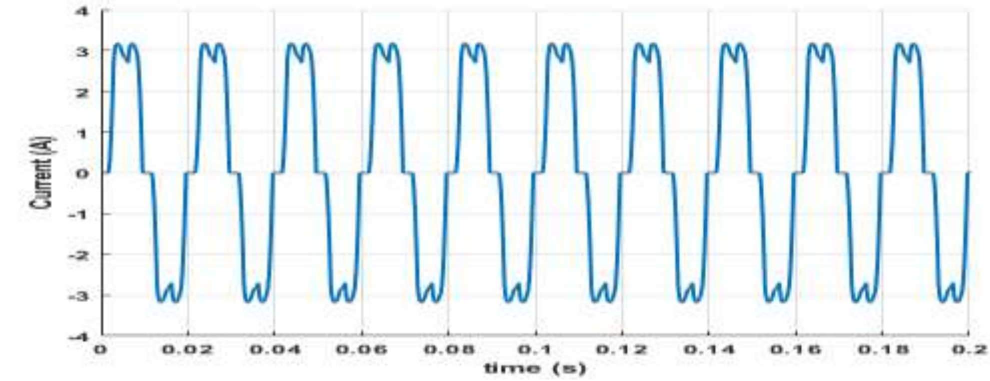

Figure V.12 Simulation results of source current I_{sa} before connecting the filter.

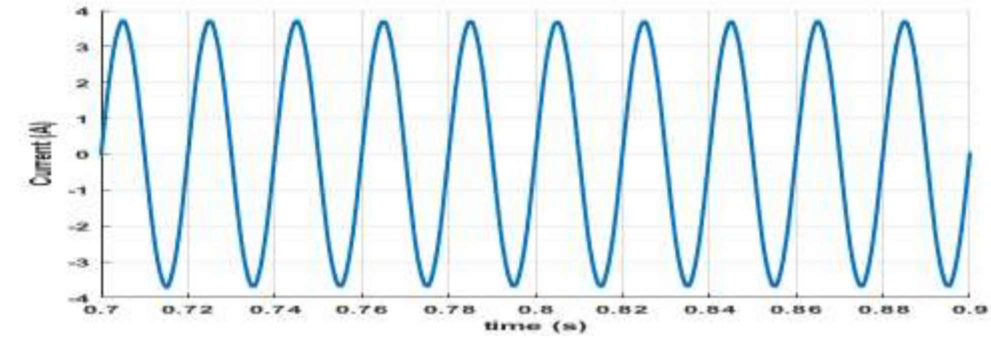

(a)

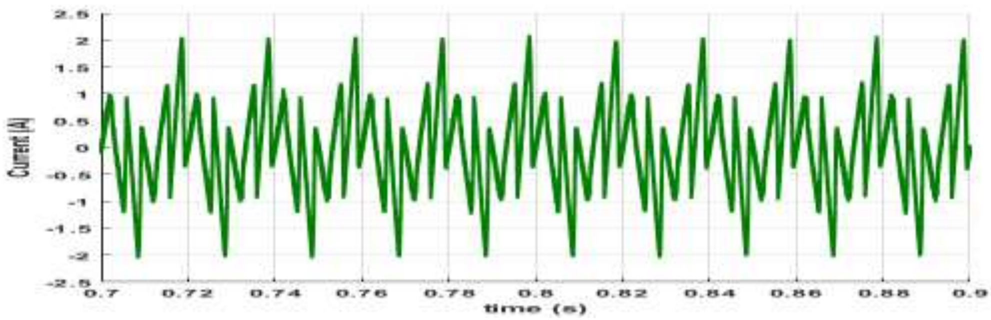

(b)

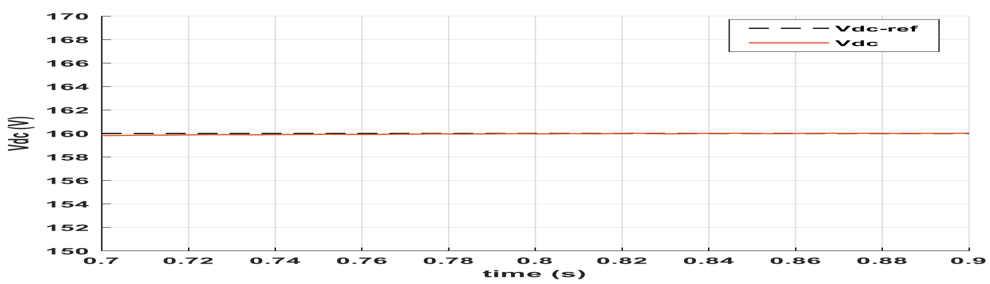

(c)

Figure V.13 Simulation results of (a) source current I_{sa}, (b) filter current I_{fa}, and (c) DC bus voltage V_{dc}, after the implementation of ZSI-SAPF.

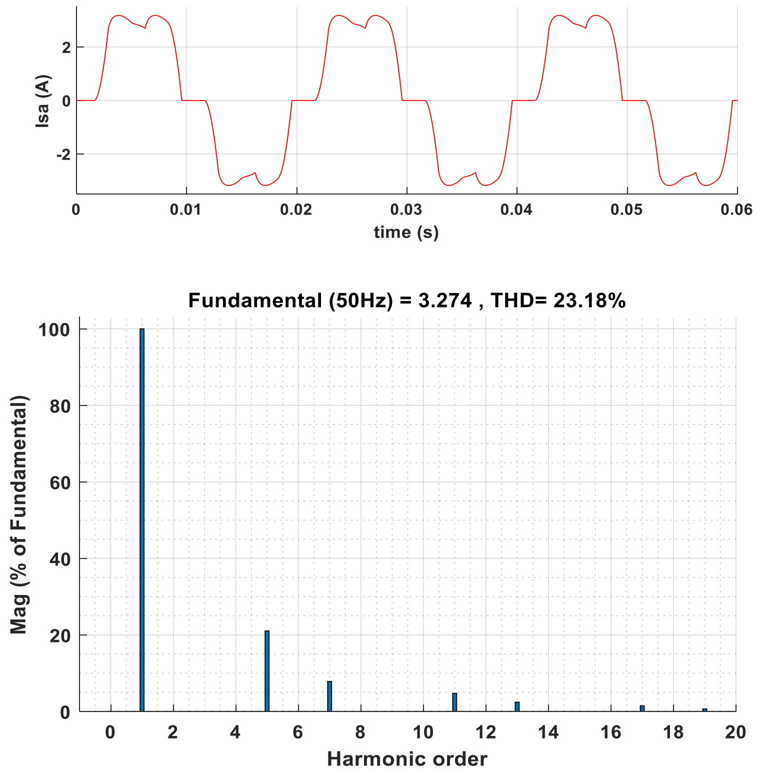

(a)

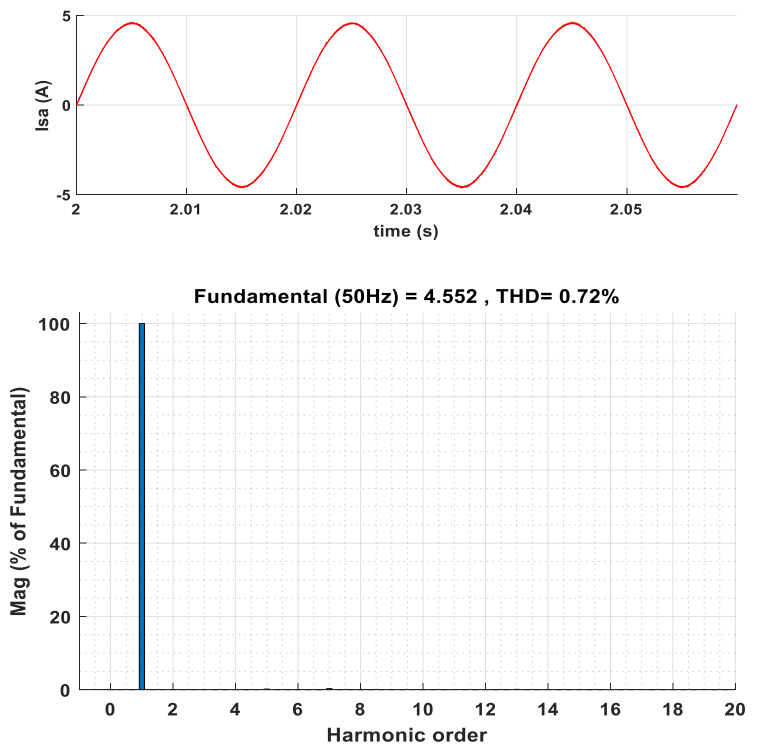

(b)

Figure V.14 Simulation results of the harmonics spectrum of source current before (a) and after (b) the implementation of ZSI-SAPF.

Figure V.15 shows the source current, filter current and DC bus voltage, respectively, which are the results obtained with the filter connected. Before the filter is connected, the load current is fully supplied from the network. The capacitors in the Z-source network are charged from the battery bank, which in turn is charged by the SPV, until the capacitors reach the line voltage level $Vdc = 160\ volts$.

Once connected, the SPV compliant ZSI-SAPF starts injecting the electric current needed to make the source current free from harmonics. The PI controller keeps the voltage level at the reference value. Where we notice the elimination of ripple in the active and reactive powers after connecting the filter, and thus the reactive power were successfully compensated.

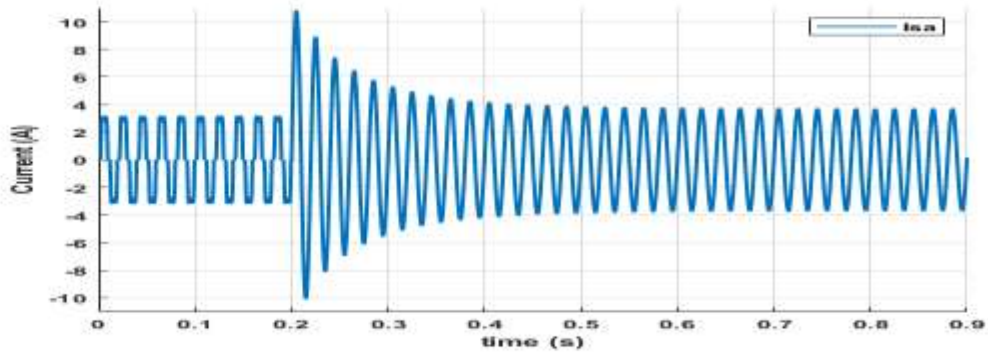

(a)

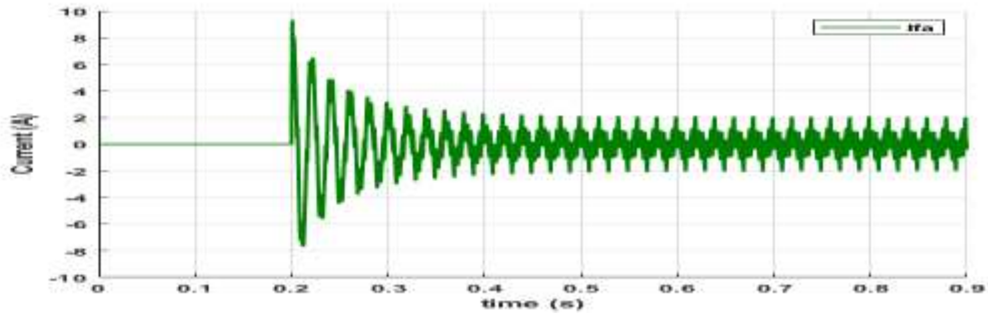

(b)

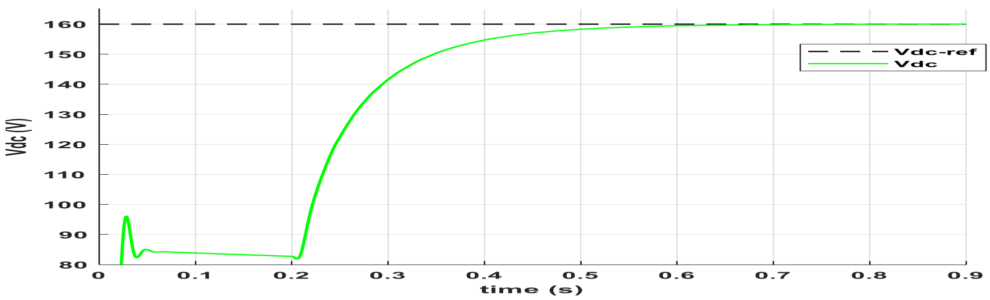

(c)

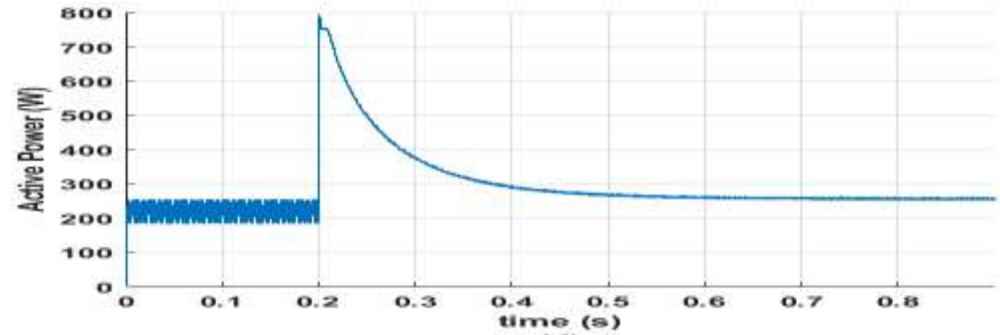

(d)

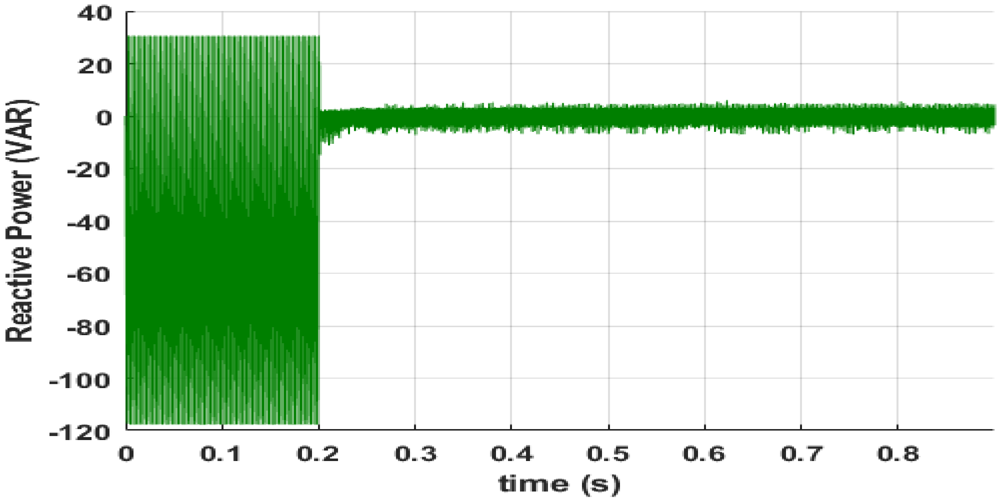

(e)

Figure V.15 Waveforms of the system parameters under ZSI-SAPF switched.

V.4.3 DC pus Variation

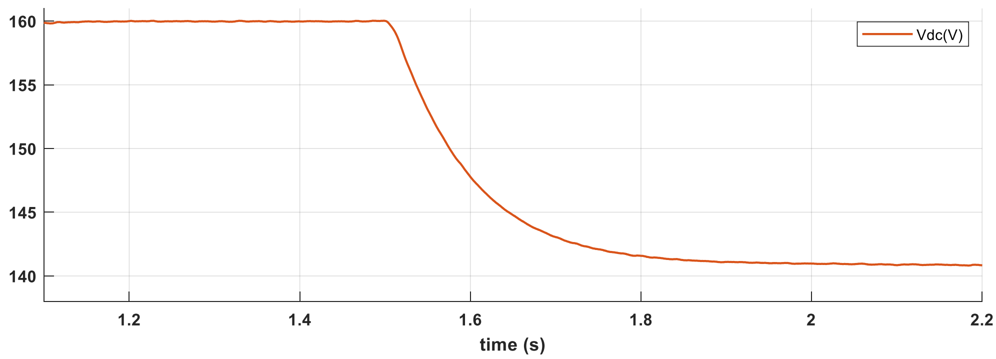

(a)

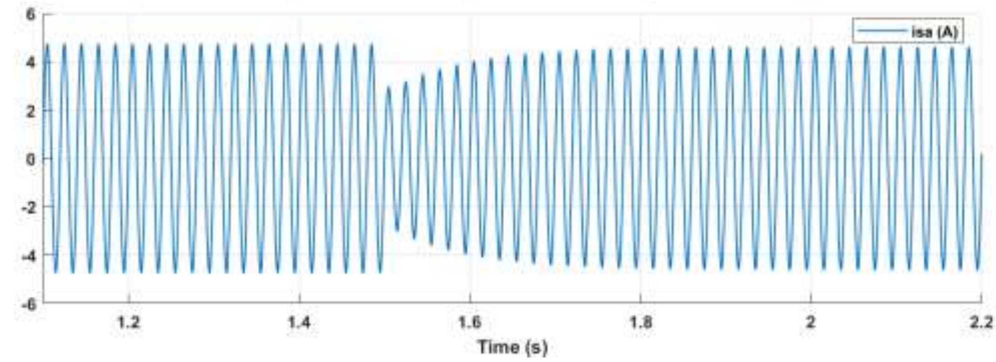

(b)

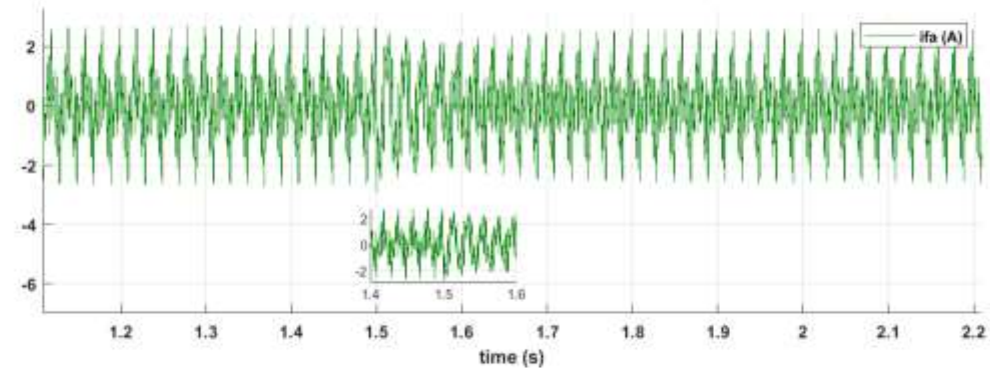

(c)

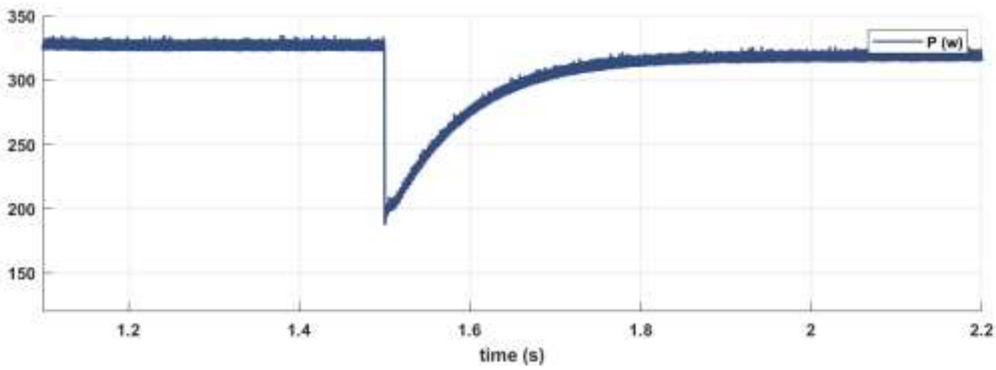

(d)

Figure V.16 Waveforms of the system parameters under DC bus variation.

V.4.4 Load Variation

The dynamic behaviour of the entire system was examined under load changes. In this test, the load is suddenly increased from $R_1 = 16\Omega$ to $R_2 = 24\Omega$ (with a variation of 33%). The results obtained in Figure V.17 show a good transient behaviour of the system in addition to a smooth change in the source current. During this phase, the load consumes additional energy from the Z-source inverter to meet its demand. However, this reduction is quickly corrected with the PI controller. To demonstrate the effectiveness of the DC bus controller, a two-stage non-linear load change was applied and established, the value of the non-linear load shows a variation of 33%. Very satisfactory results are obtained as shown in Figure V.17.

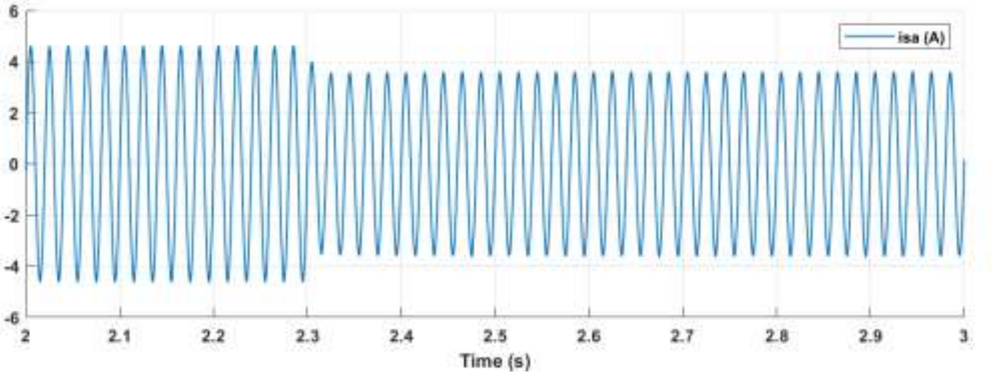

(a)

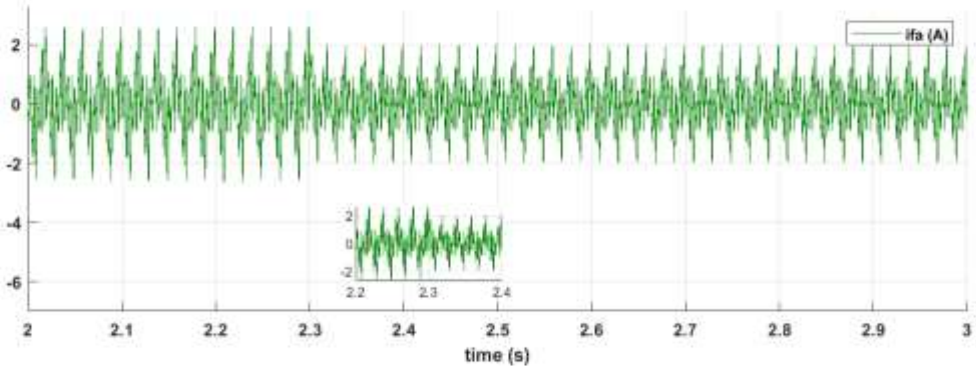

(b)

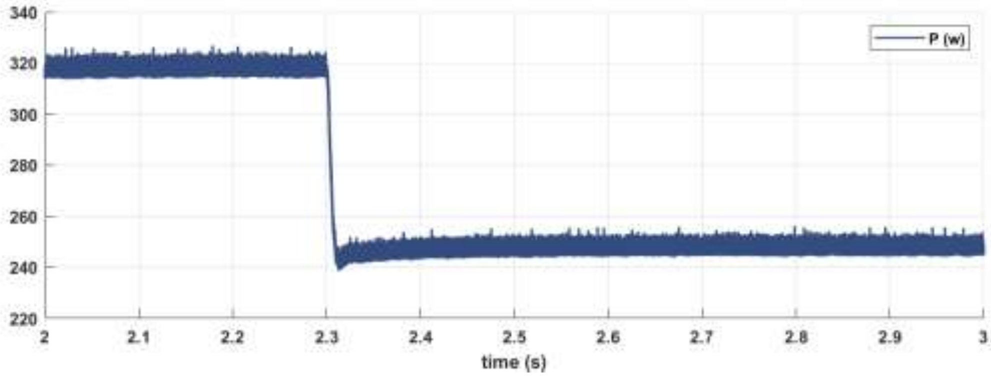

(c)

Figure V.17 Waveforms of the system parameters under load variation.

The proposed SPV-compliant ZSI-SAPF system with PI controller is comparable to some recently published systems for SAPF in terms of reliability, simplicity and effectiveness in improving power quality. The results of the comparison, as given in Table V.2, show the superiority of the proposed system compared to other methods.

Table V.2 Comparison results between the proposed and different control strategies.

Topology	**Control strategy**	**Simulation results of THD of source current**	
		before connecting SAPF	**after connecting SAPF**
SAPF	(p–q) method proposed in [57]	20.03%	1.78%
ZSI-SAPF	system proposed in this thesis	23.18%	0.72%

V.5 Conclusion

A design of a three-phase shunt active power filter based on Z-source inverter controlled by instantaneous reactive power theory and PI hysteresis control algorithm is proposed in this paper. The proposed structure is applied to compensate harmonic components caused by nonlinear loads. The performance of the proposed structure was evaluated under different operating conditions with a non-linear load. Simulation results using MATLAB/Simulink show satisfactory performance. Besides, to underscore the performance of the proposed structure, an improvement in efficiency was obtained as compared to the conventional structure. On the other hand, it is evident that the proposed structure achieves the best THDi (harmonic of current) in the simulation test by 0.72%. Furthermore, the system performance can be improved by extending the control algorithm to optimize the parameters of the PI controller. In addition, the unit power factor operation is ensured since the reactive power is almost zero.

Some inferences can be summarized from this work:

- The proposed shunt active power filter based on Z-Source inverter was able to restore the distorted current source to its original sine waveform.
- Investigations show that the proposed filter was able to minimize current harmonics well below the limits of the IEEE standard.
- The FFT spectrum analyses reveal that by employing the proposed ZSI-SAPF, the THDs were reduced from 23% to 0.72%.
- The proposed shunt active power filter based on Z-Source inverter can effectively mitigate the harmonic current under various operating conditions was evaluated. However, the comparative study emphasized that the system performance surpassed the other states of art in the literature which are applied to under various operating conditions were evaluated.
- This system can be experimentally established and verified through the development of a prototype model, and the control algorithm can be extended to optimizing the PI controller parameters.

GENERAL CONCLUSION

Power converter systems are increasingly prevalent in applications such as alternative energy sources and hybrid electric vehicles (HEVs). For power electronics designers, achieving efficiency, low cost, and reliability are primary objectives. Traditional power converter designs still deliver satisfactory results, and their performance is enhanced through advanced control techniques. Additionally, new power conversion topologies are emerging, offering improved performance in specific applications.

The Z-source converter (ZSC) is one such innovative power conversion topology, showing great promise in conditioning power from alternative energy sources and in applications like HEVs and utility interfacing. The unique buck and boost capability of the ZSC enables a broader input voltage range, eliminating the need for a separate DC/DC boost stage, thereby enhancing overall efficiency. Furthermore, the ZSC allows for the shoot-through state, improving system reliability.

This research is a continuation of the effort on modelling and control of the ZSC that has been achieved so far in the literature

A design of a three-phase shunt active power filter based on Z-source inverter controlled by instantaneous reactive power theory and PI hysteresis control algorithm is proposed. The proposed structure is applied to compensate harmonic components caused by nonlinear loads. The performance of the proposed structure was evaluated under different operating conditions with a non-linear load. Simulation results using MATLAB/Simulink show satisfactory performance. Besides, to underscore the performance of the proposed structure, an improvement in efficiency was obtained as compared to the conventional structure. On the other hand, it is evident that the proposed structure achieves the best THDi in the simulation test by 0.72%. Furthermore, the system performance can be improved by extending the control algorithm to optimize the parameters of the PI controller. In addition, the unit power factor operation is ensured since the reactive power is almost zero.

Appendix (A): Identify the basic input parameters of the circuit z-source

Fundamental Relationships in Z-Source

Key Equations:

- Output voltage:

$$V_{out} = B \cdot V_{in}$$

- Boost ratio, which depends on the shoot-through time (T_0) and the switching period(T_S)

$$B = \frac{1}{1-2 \cdot D} \quad ; \text{D: is } \frac{T_0}{T_s} \text{ (is the duty cycle)}$$

Capacitor Voltage (V_c):

$$V_C = \frac{V_{in}}{1-D}$$

Inductor Current (I_L):

$$I_L = \frac{P}{V_{in}}$$

Capacitor (C) Calculation

The capacitors in the Z-Source are designed to stabilize the voltage and minimize ripple.

- The capacitor value depends on the allowable voltage ripple $\left(\Delta V_C\right)$:

$$C = \frac{I_L \cdot D}{f_s \cdot \Delta V_C}$$

Where:

- ΔV_C: The allowed ripple in the capacitor voltage.
- f_s: The switching frequency.

Inductor (L) Calculation

Inductors are designed to minimize current ripple and store energy during switching cycles.

- The inductor value depends on the allowable current ripple (ΔI_L)

$$L = \frac{V_C \cdot D}{f_s \cdot \Delta I_L}$$

References

[1] M. M. Abdusalam, “Structures et stratégies de commande des filtres actifs parallèle et hybride avec validations expérimentales,” Thèse de doctorat, Université *Henri Poincaré-Nancy-I-France*, 2008.

[2] T. A. Kasmieh and H. S. Omran, “Active power filter dimensioning using a hysteresis current controller,” *resonance*, vol. 1, p. 2, 2009.

[3] Y. Pal, A. Swarup, and B. Singh, “A review of compensating type custom power devices for power quality improvement,” *2008 Jt. Int. Conf. Power Syst. Technol. POWERCON IEEE Power India Conf. POWERCON 2008*, 2008, doi: 10.1109/ICPST.2008.4745338.

[4] J. C. Das, “Passive filters-potentialities and limitations,” *IEEE Trans. Ind. Appl.*, vol. 40, no. 1, pp. 232–241, 2004.

[5] O. Vodyakho and C. C. Mi, “Three-level inverter-based shunt active power filter in three-phase three-wire and four-wire systems,” *IEEE Trans. power Electron.*, vol. 24, no. 5, pp. 1350–1363, 2009.

[6] A. Hamadi, S. Rahmani, and K. Al-Haddad, “Sliding mode control of three-phase shunt hybrid power filter for current harmonics compensation,” in *2010 IEEE International Symposium on Industrial Electronics*, IEEE, 2010, pp. 1076–1082.

[7] N.-K. Nguyen, “Approche neuromimétique pour l’identification et la commande des systèmes électriques: application au filtrage actif et aux actionneurs synchrones.” Université de Haute Alsace-Mulhouse, 2010.

[8] M. I. B. A. Bakar, “Active power filter with automatic control circuit for neutral current harmonic minimization technique.” june, 2007.

[9] F. Defaÿ, “Commande prédictive directe d’un convertisseur multicellulaire triphasé pour une application de filtrage actif.” 2008.

[10] S. Prusty, “FPGA Based Active Power Filter for Harmonics Mitigation.” 2011.

[11] K. H. Sueker, *Power electronics design: a practitioner’s guide*. Elsevier, 2005.

[12] M. Magraoui, “Validation de techniques de commande d’un filtre actif parallèle.” École de technologie supérieure, 2007.

[13] A. Hamadi, “Amélioration des performances du filtre actif: application du régulateur proportionnel intégral et du régulateur flou.” École de technologie supérieure, 2004.

[14] J. M. Sadeq, “Comparative Study Of Passive, Series And Shunt Active Power Filters With Hybrid Filters On Nonlinear Loads.” Nicosia, 2014.

[15] N. Mendalek, “Qualité de l’onde électrique et moyens de mitigation.” École de technologie supérieure, 2003.

[16] A. Javadi, “Modeling, Simulation and Real-time Control of Active Filters.” Ecole Polytechnique de Montréal, 2009.

[17] T. P. Cheng, “A single-phase hybrid active power filter with photovoltaic application,” *University. Teknol. Malaysia*, 2006.

[18] Q. Chen, Z. Chen, M. McCormick, and A. Dinu, “The application and optimization of C-type filter in a combined harmonic power filter the 35th IEEE Power Electronics Specialists,” in *Conference PESC*, 2004, pp. 20–25.

[19] M. Kale and E. Ozdemir, “An adaptive hysteresis band current controller for shunt active power filter,” *Electr. power Syst. Res.*, vol. 73, no. 2, pp. 113–119, 2005.

[20] S. Hussain, K. Satyanarayana, and B. K. V Prasad, “Power Quality Improvement by Using Active Power Filters,” *Int. J. Eng. Sci. Adv. Technol.*, vol. 1, no. 1, pp. 1–7, 2011.

[21] J. Xu, “Filtrage actif parallèle des harmoniques des réseaux de distribution d’électricité.” Institut National Polytechnique de Lorraine, 1994.

[22] Q. Zeng, L. Chang, and P. Song, “SVPWM-based current controller with grid harmonic compensation for three-phase grid-connected VSI,” *PESC Rec. - IEEE Annu. Power Electron. Spec. Conf.*, vol. 4, pp. 2494–2500, 2004, doi: 10.1109/PESC.2004.1355221.

[23] S. Karimi, “Continuité de service des convertisseurs triphasés de puissance et prototypage" FPGA in the loop": application au filtre actif parallèle,” *H. Poincaré, Nancy-I*, 2009.

[24] Sr. Bowes and M. J. Mount, “Microprocessor control of PWM inverters,” in *IEE*

Proceedings B (Electric Power Applications), IET, 1981, pp. 293–305.

[25] B. Mokrytzki, “Pulse width modulated inverters for ac motor drives,” *IEEE Trans. Ind. Gen. Appl.*, no. 6, pp. 493–503, 1967.

[26] M. P. Kazmierkowski and L. Malesani, “Current control techniques for three-phase voltage-source PWM converters: A survey,” *IEEE Trans. Ind. Electron.*, vol. 45, no. 5, pp. 691–703, 1998.

[27] S. R. Bowes, “New sinusoidal pulsewidth-modulated invertor,” in *Proceedings of the Institution of Electrical Engineers*, IET, 1975, pp. 1279–1285.

[28] F. G. Turnbull, “Selected harmonic reduction in static DC—AC inverters,” *IEEE Trans. Commun. Electron.*, vol. 83, no. 73, pp. 374–378, 1964.

[29] J. B. Casteel and R. G. Hoft, “Optimum PWM waveforms of a microprocessor controlled inverter,” in *1978 IEEE Power Electronics Specialists Conference*, IEEE, 1978, pp. 243–250.

[30] S. R. Bowes and B. M. Bird, “Novel approach to the analysis and synthesis of modulation processes in power convertors,” in *Proceedings of the Institution of Electrical Engineers*, IET, 1975, pp. 507–513.

[31] S. R. Bowes and R. R. Clements, “Computer-aided design of PWM inverter systems,” in *IEE Proceedings B (Electric Power Applications)*, IET, 1982, pp. 1–17.

[32] M. Mohapatra and B. C. Babu, “Fixed and sinusoidal-band hysteresis current controller for PWM voltage source inverter with LC filter,” in *2010 IEEE Students Technology Symposium (TechSym)*, IEEE, 2010, pp. 88–93.

[33] K. M. Rahman, M. R. Khan, and M. A. Choudhury, “Implementation of programmed modulated carrier HCC based on analytical solution for uniform switching of voltage source inverters,” *IEEE Trans. Power Electron.*, vol. 18, no. 1, pp. 188–197, 2003.

[34] M. A.-S. Nejad, S. Pierfederici, J.-P. Martin, and F. Meibody-Tabar, “Study of an hybrid current controller suitable for DC–DC or DC–AC applications,” *IEEE Trans. Power Electron.*, vol. 22, no. 6, pp. 2176–2186, 2007.

[35] G. H. Bode and D. G. Holmes, “Load independent hysteresis current control of a three

level single phase inverter with constant switching frequency," in *2001 IEEE 32nd Annual Power Electronics Specialists Conference (IEEE Cat. No. 01CH37230)*, IEEE, 2001, pp. 14–19.

[36] F. Z. Peng, "Application issues of active power filters," *IEEE Ind. Appl. Mag.*, vol. 4, no. 5, pp. 21–30, 1998.

[37] L. Asiminoaei, F. Blaabjerg, and S. Hansen, "Evaluation of harmonic detection methods for active power filter applications," in *Twentieth Annual IEEE Applied Power Electronics Conference and Exposition, 2005. APEC 2005.*, IEEE, 2005, pp. 635–641.

[38] S. Rahmani, A. Hamadi, and K. Al-Haddad, "A comprehensive analysis of hybrid active power filter for power quality enhancement," in *IECON 2012-38th Annual Conference on IEEE Industrial Electronics Society*, IEEE, 2012, pp. 6258–6267.

[39] F. Z. Peng, G. W. Ott, and D. J. Adams, "Harmonic and reactive power compensation based on the generalized instantaneous reactive power theory for 3-phase 4-wire systems," *PESC Rec. - IEEE Annu. Power Electron. Spec. Conf.*, vol. 2, pp. 1089–1095, 1997, doi: 10.1109/pesc.1997.616880.

[40] T. Tanaka, N. Koshio, H. Akagi, and A. Nabae, "Reducing supply current harmonics," *IEEE Ind. Appl. Mag.*, vol. 4, no. 5, pp. 31–37, 1998.

[41] S. Bhattacharya and D. Divan, "Synchronous frame based controller implementation for a hybrid series active filter system," in *IAS'95. Conference Record of the 1995 IEEE Industry Applications Conference Thirtieth IAS Annual Meeting*, IEEE, 1995, pp. 2531–2540.

[42] R. R. Errabelli, Y. Y. Kolhatkar, and S. P. Das, "Experimental investigation of sliding mode control of inverter for custom power applications," in *2006 IEEE Power Engineering Society General Meeting*, IEEE, 2006, pp. 8-pp.

[43] D. O. Abdeslam, P. Wira, J. Mercklé, Y.-A. Chapuis, and D. Flieller, "Stratégie neuromimétique d'identification et de commande d'un filtre actif parallèle," *Rev. Int. du Génie Electrique,(RS-RIGE) p*, pp. 35–64, 2006.

[44] A. L. de Heredia Bermeo, "Commandes avancées des systèmes dédiés à l'amélioration de la qualité de l'énergie: de la basse tension à la montée en tension." Institut National

Polytechnique de Grenoble-INPG, 2006.

[45] H. Akagi, Y. Kanazawa, and A. Nabae, “Instantaneous reactive power compensators comprising switching devices without energy storage components,” *IEEE Trans. Ind. Appl.*, no. 3, pp. 625–630, 1984.

[46] P. Santiprapan and K. L. Areerak, “Performance improvement of harmonic detection using synchronous reference frame method,” in *2010 International Conference on Advances in Energy Engineering*, IEEE, 2010, pp. 52–55.

[47] A. Abdelkarim, B. Youcef, L. Zellouma, D. Toumi, A. Ibrahim, and R. Aboelsaud, “Improved space vector modulation algorithm of 5-level three-phase z-source based cascaded inverter,” *Int. J. Power Electron. Drive Syst.*, vol. 13, no. 4, p. 2286, 2022.

[48] F. Z. Peng, “Z-source inverter,” *IEEE Trans. Ind. Appl.*, vol. 39, no. 2, pp. 504–510, 2003.

[49] X. Ding, Z. Qian, Y. Xie, and F. Z. Peng, “A novel ZVS Z-source rectifier,” in *Twenty-First Annual IEEE Applied Power Electronics Conference and Exposition, 2006. APEC’06.*, IEEE, 2006, pp. 5-pp.

[50] F. Zhang, X. Fang, F. Z. Peng, and Z. Qian, “A new three-phase ac-ac Z-source converter,” in *Twenty-First Annual IEEE Applied Power Electronics Conference and Exposition, 2006. APEC’06.*, IEEE, 2006, pp. 4-pp.

[51] P. C. Loh, D. M. Vilathgamuwa, Y. Sen Lai, G. T. Chua, and Y. Li, “Pulse-width modulation of Z-source inverters,” in *Conference Record of the 2004 IEEE Industry Applications Conference, 2004. 39th IAS Annual Meeting.*, IEEE, 2004.

[52] D. G. Holmes, “The significance of zero space vector placement for carrier-based PWM schemes,” *IEEE Trans. Ind. Appl.*, vol. 32, no. 5, pp. 1122–1129, 1996.

[53] F. Z. Peng, M. Shen, and Z. Qian, “Maximum boost control of the Z-source inverter,” *IEEE Trans. power Electron.*, vol. 20, no. 4, pp. 833–838, 2005.

[54] M. Shen, J. Wang, A. Joseph, F. Z. Peng, L. M. Tolbert, and D. J. Adams, “Constant boost control of the Z-source inverter to minimize current ripple and voltage stress,” *IEEE Trans. Ind. Appl.*, vol. 42, no. 3, pp. 770–778, 2006.

[55] B. Mansour, B. Abdelkader, and B. Said, “Application of backstepping to the virtual flux

direct power control of five-level three-phase shunt active power filter," *Int. J. Power Electron. Drive Syst.*, vol. 4, no. 2, p. 173, 2014.

[56] H. Akagi, "Modern active filters and traditional passive filters," *Bull. Polish Acad. Sci. Tech. Sci.*, vol. 54, no. 3, pp. 255–269, 2006.

[57] A. Krama, L. Zellouma, A. Benaissa, B. Rabhi, M. Bouzidi, and M. F. Benkhoris, "Design and Experimental Investigation of Predictive Direct Power Control of Three-Phase Shunt Active Filter with Space Vector Modulation using Anti-windup PI Controller Optimized by PSO," *Arab. J. Sci. Eng.*, vol. 44, no. 8, pp. 6741–6755, 2019, doi: 10.1007/s13369-018-3611-6.

[58] V. Mahajan, P. Agarwal, and H. O. Gupta, "Implementation of high-voltage multilevel harmonic filter based on rotated carrier modulation and artificial intelligence-based controllers," *Arab. J. Sci. Eng.*, vol. 39, pp. 7127–7143, 2014.

[59] F.-Z. Peng, H. Akagi, and A. Nabae, "A study of active power filters using quad-series voltage-source PWM converters for harmonic compensation," *IEEE Trans. Power Electron.*, vol. 5, no. 1, pp. 9–15, 1990.

[60] H. Sasaki and T. Machida, "A new method to eliminate AC harmonic currents by magnetic flux compensation — Considerations on basic design," *IEEE Trans. Power Appar. Syst.*, vol. PAS-90, no. 5, pp. 2009–2019, 1971, doi: 10.1109/TPAS.1971.292996.

[61] B. Mokhtar, B. Mokhtar, and B. Mokhtar, "Revue Synthèse N° 17, Janvier 2008 L. Zellouma et al.," pp. 64–72, 2008.

[62] A. Chebabhi, M. K. Fellah, A. Kessal, and M. F. Benkhoris, "Comparative study of reference currents and DC bus voltage control for Three-Phase Four-Wire Four-Leg SAPF to compensate harmonics and reactive power with 3D SVM," *ISA Trans.*, vol. 57, pp. 360–372, 2015.

[63] S. Saidi, R. Abbassi, and S. Chebbi, "Quality improvement of shunt active power filter with direct instantaneous power estimator based on Virtual Flux," *Int. J. Control. Autom. Syst.*, vol. 14, pp. 1309–1321, 2016.

[64] V. K. A. Shankar and N. S. Kumar, "Implementation of shunt active filter for harmonic compensation in a 3 phase 3 wire distribution network," *Energy Procedia*, vol. 117, pp.

172–179, 2017.

[65] S. Parthiban and V. Madhaiyan, “Experimental validation of solar PV sustained ZSI based unified active power filter for enrichment of power quality,” *Automatika*, vol. 62, no. 1, pp. 137–153, 2021.

[66] V. Madhaiyan and V. Subramaniam, “Extended reference signal generation scheme for integration of unified power quality conditioner in grid-connected photovoltaic system,” *Electr. Power Components Syst.*, vol. 43, no. 8–10, pp. 914–927, 2015.

[67] M. A. Mansor, K. Hasan, M. M. Othman, S. Z. B. M. Noor, and I. Musirin, “Construction and performance investigation of three-phase solar PV and battery energy storage system integrated UPQC,” *Ieee Access*, vol. 8, pp. 103511–103538, 2020.

[68] J. M. Kwon, K. H. Nam, and B. H. Kwon, “Photovoltaic power conditioning system with line connection,” *IEEE Trans. Ind. Electron.*, vol. 53, no. 4, pp. 1048–1054, 2006, doi: 10.1109/TIE.2006.878329.

[69] J. Abbasi Bolaghi, A. Taheri, and M. H. Babaei, “Switched-capacitor inductor Z-source inverter with an impedance network,” *Int. Trans. Electr. Energy Syst.*, vol. 31, no. 5, 2021, doi: 10.1002/2050-7038.12529.

[70] R. S. Herrera, P. Salmerón, and H. Kim, “Instantaneous reactive power theory applied to active power filter compensation: Different approaches, assessment, and experimental results,” *IEEE Trans. Ind. Electron.*, vol. 55, no. 1, pp. 184–196, 2008.

[71] A. Tripathi and P. C. Sen, “Comparative analysis of fixed and sinusoidal band hysteresis current controllers for voltage source inverters,” *IEEE Trans. Ind. Electron.*, vol. 39, no. 1, pp. 63–73, 1992.

[72] I. of E. and E. Engineers, *IEEE recommended practice and requirements for harmonic control in electric power systems*. IEEE, 2014.

[73] A. Pigazo, V. M. Moreno, and E. J. Estebanez, “A recursive park transformation to improve the performance of synchronous reference frame controllers in shunt active power filters,” *IEEE Trans. Power Electron.*, vol. 24, no. 9, pp. 2065–2075, 2009.

Abstract

This thesis aims to design a three-phase shunt active power filter utilizing a Z-source inverter controlled by the instantaneous reactive power theory and a PI hysteresis control algorithm. The proposed structure is intended to mitigate harmonic components induced by nonlinear loads. Evaluation of the proposed structure's performance under various operating conditions with a nonlinear load was conducted. Simulation results using MATLAB/Simulink demonstrate satisfactory performance. Additionally, the proposed structure exhibited improved efficiency compared to conventional designs, highlighting its potential effectiveness.

Keywords: shunt active power filter; instantaneous reactive power theory; Z-source inverter; total harmonic distortion.

ملخص

تهدف هذه الأطروحة إلى تصميم مرشح طاقة نشط ثلاثي الطور باستخدام عاكس مصدر Z يتم التحكم فيه بواسطة نظرية الطاقة التفاعلية اللحظية وخوارزمية التحكم في التباطؤ PI. يهدف الهيكل المقترح إلى تخفيف المكونات التوافقية الناتجة عن الأحمال غير الخطية. تم إجراء تقييم لأداء الهيكل المقترح في ظل ظروف التشغيل المختلفة مع الحمل غير الخطي. أظهرت نتائج المحاكاة باستخدام MATLAB/Simulink أداءً مرضيًا. بالإضافة إلى ذلك، أظهر الهيكل المقترح كفاءة محسنة مقارنة بالتصاميم التقليدية، مما يسلط الضوء على فعاليته المحتملة.

الكلمات الرئيسية: تحويلة مرشح الطاقة النشط. نظرية القوة التفاعلية اللحظية؛ عاكس مصدر Z؛ التشوه التوافقي الكلي.

Résumé

Cette thèse vise à concevoir un filtre de puissance active shunt triphasé utilisant un onduleur à source Z contrôlé par la théorie de la puissance réactive instantanée et un algorithme de contrôle d'hystérésis PI. La structure proposée vise à atténuer les composantes harmoniques induites par les charges non linéaires. L'évaluation des performances de la structure proposée dans diverses conditions de fonctionnement avec une charge non linéaire a été réalisée. Les résultats de simulation utilisant MATLAB/Simulink démontrent des performances satisfaisantes. De plus, la structure proposée présentait une efficacité améliorée par rapport aux conceptions conventionnelles, soulignant son efficacité potentielle.

Mots-clés : filtre de puissance active shunt ; théorie de la puissance réactive instantanée ; Onduleur source Z ; distorsion harmonique totale.